Kobe University Repository : Kernel

PDF issue: 2024-09-28

Evaluation Method and Behavior of Buried Flexible Pipe under External and Internal Pressure

Ariyoshi, Mitsuru

(Degree)
博士（農学）

(Date of Degree)
2018-09-25

(Date of Publication)
2019-09-01

(Resource Type)
doctoral thesis

(Report Number)
甲第7312号

(URL)
https://hdl.handle.net/20.500.14094/D1007312

※ 当コンテンツは神戸大学の学術成果です。無断複製・不正使用等を禁じます。著作権法で認められている範囲内で、適切にご利用ください。

Doctoral Dissertation

Evaluation Method and Behavior of Buried Flexible Pipe under External and Internal Pressure
(埋設たわみ性パイプの内外圧作用時の挙動と評価手法)

September 2018

Graduate School of Agricultural Science,
Kobe University

Mitsuru ARIYOSHI

Acknowledgements

Firstly, I would like to express my deep gratitude to my advisor Professor Toshinori KAWABATA, Dean of Faculty of Agriculture at Kobe University, for his guidance, encouragement and endless generosity. He provided me with the opportunity to work on the structural mechanics of buried pipes throughout my undergraduate and graduate studies. I could not have imagined having a better advisor for my study.

I would also like to express sincere gratitude to vice chairs of the doctoral dissertation: Professor Tsutomu TANAKA and Associate Professor Kazuya INOUE, for their insightful comments that broadened this research with various perspectives.

My sincere thanks also go to Dr. Kazunori UCHIDA, Director at Kobe University, who provided me with the opportunity to start my research career in the university laboratory.

I sincerely thank to all members of the Laboratory of Geotechnical Engineering for Agriculture at Kobe University, particularly Assistant Professor Yutaka SAWADA. They welcomed into their laboratory and gave valuable comments on my work.

I would like to express my deep appreciations to Professor Yoshiyuki MOHRI, professor in the Department of Regional and Comprehensive Agriculture at Ibaraki University. His guidance helped me immensely, and this dissertation would have been impossible to complete without him.

Special thanks to Dr. Susumu MASUKAWA, Director of the Division of Facilities and Geotechnical Engineering at the National Institute for Rural Engineering (NIRE), and Dr. Toshikazu HORI, Leader of the Soil Mechanics Unit, for their patience,

motivation and support that helped me attend Kobe University. My special thanks extended to the other members of NIRE; Dr. Yoshikazu TANAKA, Dr. Kenichi MATSUSHIMA, Dr. Akira IZUMI and Miss Sawako KUBOTA for their extensive and generous support of my research. Dr. Kazuhiro UENO, Assistant Professor at Shimane University, gave valuable comments on this work.

I would like to express my special appreciation to Mr. Mitsuru SATO and Masayuki KANEMOTO of Teikoku Co., Ltd. for their great support of my experimental work. My experiments would not have been possible without their techniques.

My sincere appreciation extends to Mr. Masaya HAZAMA of Kurimoto, Ltd., Mr. Kenzo KUBOTA of Sekisui Chemical Co., Ltd., and Mr. Yukihiko KUDO of the Japan Pipe Rehabilitation Association. They cooperated in my experiments and held great discussions with me.

Finally, I would like to express heartfelt thanks to my family: my wife, my children, my mother and my brother for their spiritual support and giving me a fruitful life.

Contents

List of Tables

List of Figures

Notations

D	:	Pipe diameter
D_m	:	Mean diameter
E	:	Young's modulus
E_p	:	Young's modulus of the pipe
F	:	Deflection lag factor
H	:	Horizontal load actin on pipe side
H_s	:	Cover depth
I	:	Moment of inertia of area
K	:	Coefficient determined by the bedding angle
M	:	Moment
M_0	:	Moment at the pipe bottom
M_H	:	Moment generated by the vertical earth pressure
M_V	:	Moment generated by thr horizontal earth pressure
P	:	Load
P_i	:	Internal pressure
P_V	:	Horizontal earth pressure
R	:	Curvature radius
T_0	:	Radial load at the pipe bottom
U	:	Strain energy
W	:	Vertical earth pressure acting on pipe
W'	:	Vertical earth pressure acting on liner

Z	:	Section modulus
a	:	Distance from the end of the base to the center of the measurement range
b	:	Distance from the end of the base to the center of the measurement range
d	:	Measurement length
e	:	Modulus of passive resistance of soil
i	:	Rotation angle at pipe bottom
l	:	Base length
r	:	Mean radius of the pipe
r_a	:	Curvature radius of the pipe after deformation
r_b	:	Curvature radius of the pipe before deformation
t	:	Wall thickness
x	:	Angle counterclockwise from pipe bottom
Δx	:	Horizontal deflection
Δx_1	:	Horizontal displacement at pipe side
Δx_2	:	Horizontal displacement at pipe side on both sections
β	:	Coefficient determined by the bedding angle
γ	:	Unit weight of soil
δ	:	Deflection
δ_b	:	Horizontal movement of pipe bottom
ε	:	Strain
ε_a	:	Radial strains at pipe sides
ε_b	:	Radial strains at pipe bottom
ε_t	:	Circumferential strain
ε_{max}	:	Maximum bending strain
θ	:	Bedding angle or contact angle
σ	:	Stress

CHAPTER 1

Chapter 1

Introduction

1.1 Background

Buried pipelines have been used widely throughout Japan for irrigation since the 1950s to accommodate the postwar enhancement of agricultural production. Irrigation pipelines are either rigid or flexible and can be made from steel, ductile iron, fiberglass-reinforced plastic mortar (FRPM), or polyvinyl chloride (PVC). Recently, since flexible pipes have been adapted for irrigation pipelines, rigid pipes have hardly been adapted.

According to Yamaguchi (2017a), the number of failures of irrigation pipelines increases every year. Joints are the main sites of failures in rigid pipes, whereas the pipe bodies usually fail in FRPM and PVC pipes. Steel and ductile-iron pipes fail mainly due to corrosions.

FRPM pipes occasionally fail if stress concentrations occur on the pipes because of differential settlements of the surrounding grounds. In such cases, because the pipes deform locally, pipes may fail even if the deflection ratios are less than the acceptable value of 5%. The deflection ratio is typically used as an indicator of structural performance. Thus, a new method is required to evaluate the local

deformations of FRPM pipes.

On the other hand, PVC pipe is durable against local deformations because it does not fail even if it deflects more than 50%. Failures of the PVC pipes are likely to occur due to fatigues, which, in Japan, are generally not considered in the design of irrigation pipeline. In the research reported in this thesis, *in situ* and laboratory tests of PVC pipes were conducted to investigate how PVC pipes fail in fields.

In irrigation applications, rigid pipes are installed for long periods, and the average service life of reinforced concrete (RC) pipes is 42.7 years. The service life of FRPM and PVC pipes, on the other hand, is less than 20 years (Yamaguchi, 2017b). The service life of rigid pipelines is sometimes extended with the cured-in-place pipe (CIPP) method, in which a resin-saturated liner is inserted along a damaged existing pipe. The liner is then inflated to fit it with the existing pipe. Unlike conventional flexible pipes, the design of CIPP liners should consider the existing pipe because the behavior of the liner is affected by the existing pipe along with the surrounding soil.

1.2 Literature Review

The literature on the behavior of buried pipes is extensive. This section reviews the literature on the structural designs of buried pipes, FRPM, PVC and CIPP.

Research on the structural performance of buried pipeline began with Anson Marston (1913, 1917 and 1930), who was Dean of Engineering at Iowa State University. The formula he devised for calculating the vertical earth pressure on a buried pipe is recognized worldwide as the Marston load equation. The equation models how settlement of backfill material and the pipe generates friction between the backfill material and the original ground. M.G. Spangler (1941), a student of Marston, studied the behavior of flexible pipes to develop a design specifically for flexible pipes, which behave differently from rigid pipes. He found that flexible pipes deflect under vertical earth pressure so that the sides of the pipes are supported horizontally by the soil. His formula considers this soil support as a modulus of passive resistance when determining the horizontal deflection of the pipe. Reynold K. Watkins (1958), a graduate student of

Spangler, investigated the modulus of passive resistance in Spangler's formula. Watkins corrected the modulus for passive resistance, and the modified formula is known as Spangler's equation or the Iowa formula. Many design standards for buried pipeline, including irrigation pipelines in Japan, are based on their research.

Some researchers have found that the earth pressure on pipe modeled by Marston and Spangler is not realistic. In Japan, Kawabata (1993) investigated the behavior of buried low stiffness pipe through field testing and finite element method (FEM) analysis. He showed that the pipe deforms greatly during construction. For instance, the pipe deform elliptically with the vertical deflection as material is backfilled to the top of the pipe. He also qualitatively evaluated the compaction process with FEM analysis. Mohri (1987) studied the behavior of large flexible pipes at the extraction point of steel sheet pile in field tests. He showed that the soil deforms greatly in this situation, and this deformation results in a large deflection of the pipeline at the extraction of the steel sheet pile. He also developed a novel method for installing shallow buried pipeline (1997), which is now used widely in Japan. Gravel around the pipe are bundled together with the pipe by geosynthetic material to counteract the pipe's buoyancy. Tohda (1986) studied the earth pressure on buried pipes using the theory of elasticity and conducted centrifuge-model tests. He found that the earth pressure on buried pipe is affected by the boundary conditions separating the pipe and soil, the lateral boundary conditions of the ground extending infinitely, and the ratio of the elastic modulus of the soil and the stiffness of the pipe. He also proposed a new design for buried pipe that uses elastic FEM analysis (1999).

FRPM pipes have been available in Japan since 1970 and have met the design standards for irrigation pipelines since 1977 (MAFF, 1977). FRPM pipes are now used widely for irrigation pipeline because of its durability and corrosion resistance. FRPM pipes account for 12% of irrigation pipeline installed by government projects, and an even greater percentage large-diameter pipes are made of FRPM (Yamaguchi, 2017b). FRPM pipes for irrigation pipeline are conventionally monitored using the vertical and horizontal deflection (MAFF, 2009). Ueno et al. (2014) and Okuda et al. (2013) developed a survey method to evaluate the structural safety of FRPM pipes using

microwaves. They have found that defects on the inner pipe surface alter microwave propagation characteristics, though they have not quantified the relationship.

PVC pipes were developed in the 1930s and were first used in earnest in Germany during the Second World War (PVC pipe association, 2012a). PVC pipes are now used widely all over the world. In Japanese irrigation pipeline, PVC pipes were first installed at Aichiyosui River, which was completed in 1961 and has 415 km of PVC pipe installed (Miyamoto, 2002). PVC pipes are used mainly in small-diameter applications and account for 27% of the irrigation pipeline installed by the Japanese government. Fatigue is a performance limit on PVC pipes (PVC pipe association, 2012b), but Japanese design standard for irrigation pipeline do not consider fatigue. Studies on fatigue have led to several methods for predicting fatigue failures. Vinson (1981) ran tests on 6 inch PVC pipes that were exposed to large repetitive pressure surges until fatigue failure occurred. He then developed an equation to predict fatigue failure as a function of peak stress. Jared et al. (2004) also performed fatigue tests on 6 inch pipes under four different pressure-cycling conditions and proposed an equation that includes the average stress and stress amplitude. The equation that they devised has adapted for the design of PVC pipe in North America by the American Water Works Association. In Japan, Hyakutake et al. (1988) conducted internal pressure cycle testing with PVC pipes. He found that the fatigue strength in the circumferential direction was much lower than that in the longitudinal direction and that the failure pattern varies depending on the temperature and number of pressure cycles. When researching the behavior of VU pipe, which is a thin PVC pipe used for irrigation and sewer pipelines, the Japan Institute of Agriculture and Engineering (1980) conducted traffic load tests. Traffic loads of 8-12 tons were applied to ϕ500 VU pipes buried at cover depths of 1-5 m. These tests showed that the deflection and strain caused by external pressure on the VU pipes are less than predicted by the Iowa equations. Nakajima and Kawaguchi (1988) measured the deflections and earth pressures of ϕ200 and ϕ500 VU pipes buried under a cover depth of 2 m to investigate how construction methods and ground conditions affect the modulus of soil reaction.

CIPP, developed in the UK in 1971, is now used widely to renew deteriorated

pipes. If the existing pipes are stable under the surrounding earth pressures, liners are only required to resist external groundwater pressure, according to UK standards. On the other hand, in CIPP design standards in many other countries including the US and Japan, liners must be able to resist soil pressure and external groundwater pressure because the existing pipes may continue to deteriorate. Liner thicknesses are determined in almost the same way as conventionally buried flexible pipes. Gumbel (1998) pointed out, however, that the deteriorated existing pipes cannot completely transfer soil and traffic loads to liners because cracked existing pipes deform to generate horizontal soil support, like flexible pipes do. An ASCE report (2007) also describes that the CIPP design standards in the US are overly conservative because they do not consider the load-bearing capacity of the deteriorated existing pipes. This ASCE report also pointed out that the Lushcer soil buckling theory, which is adapted for design of liner in the United States, is inappropriate because the soil pressure on the liners does not cause radial stress in the liner.

CIPP was introduced in Japan in the 1980s and has been used to restore sewer and water supply pipelines. Several studies have focused on the behavior of rehabilitated pipes, including liners subjected to external load. Takahashi et al. (2002) conducted scale model tests using ϕ250 high-density polyethylene pipe surrounded by damaged pottery pipe, and they conducted centrifuge tests using ϕ40 PVC pipe surrounded by damaged aluminum pipe. These tests showed that the deteriorated existing pipes reduce the strains and deflections of rehabilitated pipes. Mohri et al. (2005) conducted scale model tests to examine how the thickness of the filling material and the conditions of the existing pipes affect the behaviors of rehabilitated pipes. They found that rehabilitated pipes with thin filling material deform more if the existing pipes are more deteriorated and that pipes with thick filling material deform less regardless of the conditions of the existing pipes. Inoue (2008) conducted loading tests for ϕ300 liner surrounded by concrete pipe buried at 600 mm cover depth. His results showed that the strain on the liner induced by a T-25 truck load was much smaller than the failure limit of the liner, even when the concrete pipe had cracks at the top, bottom, and sides of the pipe. He also proposed the liner design of buckling induced by soil and water pressure.

Sawada et al. (2014) conducted loading tests with ϕ300 PVC pipes surrounded by broken up steel pipes buried in sand. They showed that the positions of the breaks in the surrounding pipes affect the behaviors of the rehabilitated pipes. Large strains occured when the cracks were at the top, bottom, or sides of the pipe. Ono et al. (2015) conducted centrifuge-model tests and varied the extent of damage in the existing pipes, the ring stiffness of the liners, the positions of the surcharge loads, and the stiffness of the backfill material. They showed that stress concentrations occur at the liners because of the contact between the existing pipes and the liners. Higher ring stiffness of the liners may reduce the stress concentrations, and existing pipes cracked at either four or eight positions reduce the overall deflections of the liners.

1.3 Objectives

As mentioned in Section 1.2, many researches have been devoted to the structural characteristics of flexible pipes. The basic behaviors of conventional flexible pipes are well understood, and design standards for flexible pipe are well established. However, the flexible pipes used for irrigation have been buried for many years in agricultural fields, and they occasionally fail by unknown causes. Clarifying the causes of these failures to propose a new evaluation method for flexible pipes in agricultural contexts is necessary to prevent similar failures in the future. The designs of CIPP liners are still new, and more-rational standards are needed for irrigation pipelines. This thesis focuses on the following goals to address these research needs.

- The development of an evaluation method that measures bending strain to evaluate local deformation of flexible pipes, especially those of FRPM pipe.
- Clarification of the causes of PVC pipe failure in irrigation systems.
- Clarification of the behavior of liners subjected to internal and external pressures.
- Development of liner design standards that consider the deteriorated existing pipe.

1.4 Thesis Organization

The rest of this thesis consists of seven chapters. Chapters 2 and 3 introduce an evaluation method that uses bending strains to measure local deformation of flexible pipe. Chapter 2 introduces the method and discusses validation tests performed with steel pipes. Chapter 3 discusses the validation of the method with FRPM pipe.

Chapters 4 and 5 describe the behavior of CIPP liners subjected to external and internal pressures. Chapter 4 focuses on internal pressure. The influences of the filling material in the annular gap between liner and existing pipe on the behavior of the liner are investigated in tests with ϕ1,000 pipe specimens. Chapter 5 describes tests of the behavior of liners subjected to external loads with ϕ300 pipe specimens and proposes a design standard for liners that considers the deteriorated existing pipe.

Chapter 6 discusses the behavior of low stiffness flexible pipe such as VU, which is a flexible PVC pipe used widely in irrigation pipelines. Chapter 7 discusses an investigation of PVC pipe failures in fields using field measurements and cyclic load testing for excavated pipes. Finally, Chapter 8 concludes the thesis with an interpretation of the main results.

References

American Society of Civil Engineers: Emerging Concepts for the Design of Pipel ine Renewal Systems. *Committee report*, 2007. Available from https://www.u ta.edu/ce/cuire/Emerging%20Concepts%20in%20Pipeline_Renewal_Design%20F inal%20Version.pdf

Gumbel, J. E.: Structural Design of Pipe Linings 1998-Review of Principles, Practice and Current Developments Worldwide, *Paper presented at the 4th ASTT conference,* Brisbane, Australia, 1998.

Hyakutake, H.: Fatigue Strength of PVC Pipes, *Journal of the society of materials*

science, Japan , No.37, pp.1381-1385, 1988. (in Japanese)

Inoue, Y.: A Study on the Structural Behavior and Design of CIPP Liner for Sewerage, Osaka City University, Ph.D. thesis, 2007. (in Japanese)

Japan Institute of Agriculture and Engineering: Report of the Behavior of PVC Pipe for Sewerage Subjected to Traffic Load, 1-95. 1980 (in Japanese)

Jeffrey, J. D., Moser, A. P., Folkman, S.: New Design Guidelines for Fatigue Failure in PVC Pipe, *Plastics Pipes XII Conference Proceedings*, Milan, Italy, 2004

Kawabata, T., Mohri, Y. and Kondo, T.: Behavior of Buried Large Thin Wall Flexible Pipe –Field Test and Numerical Analysis Considered with Stage of Construction of Buried Flexible Pipe, *Transactions of the Japanese Society of Irrigation, Drainage and Reclamation Engineering*, JSIDRE, No.167, pp.19-27, 1993. (in Japanese)

Marston, A.: The Theory of External Loads on Closed Conduits in the Light of the Latest Experiments, Bulletin 96, Iowa Engineering Experiment Station. 1930.

Marston, A. and Anderson, A.O.: The Theory of Loads on Pipes in Ditches and Tests of Cement and Clay Drain Tile and Sewer Pipe, Bulletin 31, Iowa Engineering Experiment Station, 1913.

Marston, A., Schlick, W. J. and Clemmer, H. F.: The Supporting Strength of Sewer Pipe in Ditches and Methods of Testing Sewer Pipe in Laboratories to Determine Their Ordinary Supporting Strength, Bulletin 47, Iowa Engineering Experiment Station, 1917.

Ministry of Agriculture, Forestry and Fisheries: Design Standard for Water Channel Work, 1977. (in Japanese)

Ministry of Agriculture, Forestry and Fisheries; Manual of Functional Maintenance for Irrigation Pipeline. 2009. (in Japanese)

Miyamoto, M: An Outline of the Development of Poly Vinyl Chloride Technolog y in Japan, including a description of historical materials (2), National Mus eum of Nature and Science, 2002. (in Japanese) Available from http://sts.ka haku.go.jp/diversity/document/system/pdf/007.pdf

Mohri, Y., Hazama, M., Makino, T. and Inoue K.: Mechanical Behavior for Renewal

pipe, Proceedings of Japan National Conference on Geotechnical Engineering, 40th, pp.1911-1912, 2005. (in Japanese)

Mohri, Y. and Kawabata, T.: Behavior of Large Diameter Flexible Pipe Buried in Ground. Case of sheet piling. *Water and Land*, Japanese Association for the Study of Irrigation, Drainage and Reclamation Engineering, No.69, pp.7-14, 1987. (in Japanese)

Mohri.Y., Kawabata, T. , Fujita N. and Ling, H.I.: Large-Scale Experiment Related to Effects of Geogrid on Flotation of Buried Pipeline, *Geosynthetics Engineering Journal*, No.12, pp.98-106.1997. (in Japanese)

Nakajima, K. and Kawaguchi, N.: Results of Test to Ascertain Actual Properties of Pipe Made of Hard Vinyl Chloride by Laying it Underground, *Water and Land*, No.72, pp.57-70, 1988. (in Japanese)

Okuda, T., Mamiya, S., Murata, H., Okamura, Y. and Hazama, M.; Nondestructive Measurement for Fiberglass Reinforced Plastic Mortar Pipes, Proceedings of FRP con-ex, No.58, pp.19-21, 2013. (in Japanese)

Ono, K., Sonoda, Y., Sawada, Y., Ling, H.I. and Kawabata, T.: Centrifuge Modeling for Mechanical Behavior of Liners in Damaged Host Pipes, *Transportation Infrastructure Geotechnology*, No.3, pp.139-154. 2015.

PVC pipe association: The Handbook of PVC Pipe Design and Construction, fifth edition, Industrial press, INC. pp.1.5. (2012a)

PVC pipe association: The Handbook of PVC Pipe Design and Construction, fifth edition, Industrial press, INC. pp.7.34. (2012b)

Sawada, Y., Sonoda, Y., Ono, K., Inoue, K., Mohri, Y., Ariyoshi, M. and Kawabata, T: Influence of Damage Levels of Outer Aging Pipes on Mechanical Behavior of Rehabilitated Pipes, *Irrigation, Drainage and Rural Engineering Journal*, No.291, pp.157-163. 2014 (in Japanese)

Spangler, M.G.: The Structural Design of Flexible Pipe Culverts, Bulletin 153, Iowa Engineering Experiment Station, 1941.

Takahashi, Y., Li, L., Deguchi, T., Yamada, K. : A Study on the Bedding Effects of the Deteriorated Existing Pipe on the Flexible Rehabilitated Pipe and its Mechanism,

Journal of Japan Sewage Works Association Research journal, No471, pp.103-113, 2002. (in Japanese)

Tohda, J. and Mikasa, M.:A Study of Earth Pressure on Underground Pipes Based on Theory of Elasticity, *Proceedings of Japan Society of Civil Engineerings*, No.376, pp.181-190, 1986. (in Japanese)

Tohda J. and Yoshimura H.: Proposal of a Rational Design Method for Buried Flexible Pipes, *Proceedings of Japan Society of Civil Engineerings*, No.617, pp.49-63, 1999. (in Japanese)

Ueno, F., Murata, H., Okamura, Y., Okuda, T. and Hazama, M; New Nondestructive Measurement for Fiberglass Reinforced Pastic Mortar Pipes Using Microwave and Photonic Techniques, *Proceedings of electronics society institute of electronics, information, and communication engineers*, pp.199, 2014. (in Japanese)

Yamaguchi, Y.: Example Analysis about Accident Factors and Measures of Irrigation Pipeline, *Water, Land and Environmental Engineering*, Vol.85, No.8, pp.767-769, 2017a. (in Japanese)

Yamaguchi, Y.: A Study on Maintenance Situation and Risk Management of Irrigation Pipeline, *Water, Land and Environmental Engineering*, Vol.85, No.10, 945-948, 2017b. (in Japanese)

Vinson, H. W.: Response of PVC Pipe to Large, Repetitive Pressure Surges. *Proceedings of the international conference on underground plastic pipe*, ASCE, New York, USA, 485-494. 1981.

Watkins, R. K. and Spangler, M. G.: Some Characteristics of the Modulus of Passive Resistance of Soil - A Sudy in Similitude, *Proceedings of Highway research*, pp.576-583, Logan, Utah, 1958.

CHAPTER 2

The contents of this chapter are based on

Ariyoshi, M., Mohri, Y., Hori T., Matsushima K., Ueno, K.: Bend strain estimation method to verify the structural safety of buried pipeline, *Irrigation, drainage and rural engineering journal*, 286, pp.349–357 (2013) (in Japanese with English Summary)

Chapter 2

Bending Strain Estimation Method to Verify the Structural Safety of Buried Pipelines

2.1 Introduction

The number of irrigation pipelines used beyond their useful life is increasing year by year because they have been used since the 1950s due to the enhancement of agricultural production. Upgrading all the facilities to work beyond their useful life is a critical issue in terms of budget; thus, managing the maintenance and monitoring of the pipelines is crucial (MAFF, 2011). Structural and hydraulic performance of the pipelines must be investigated to evaluate their safety (MAFF, 2007; MAFF, 2009a); in particular, a proper control of the structural deterioration is necessary because it may lead to leakage.

Deflections is generally measured to estimate the structural safety of flexible pipes and a deflection ratio (deflection/mean diameter) of 5% is referred to as the maximum allowable value; however, in some cases, pipes break even at lower ratios. Idomoto et al. (2001 and 2002) pointed out that the allowable deflection ratio has no meaning as performance limit because it is not determined by the leakage performance of the joints or the failure of the pipes. Thus, more appropriate investigation methods are required to

determine the structural performance of the pipelines.

The Japanese design standards for irrigation pipelines are based on the works of Marston (1913, 1917 and 1930) and Spangler (1941). They determined the distribution of the earth pressures acting on the pipes and calculated the resulting stress and deflections. Howard (1972) conducted large model tests and showed that the deformation of a buried pipe depends on the stiffness of both soil and pipe (1972). Highly and poorly stiff pipes deform into elliptical and rectangular shapes, respectively. Thus, predicting pipe failure using the deflection ratio is quite difficult.

Therefore, we developed a method to measure the bending strains related to the pipe failure. We measured the curvature radius of buried pipes and calculated the bending strains based on their change. We conducted a model test on a steel pipes to validate the method.

2.2 Bending Strain Estimation Method

Buried flexible pipes deform due to the moments generated by earth pressures. In the design standard, the bending stress at the pipe bottom is calculated from the moment and used as an index to evaluate the structural safety. Hence, measuring the bending strain, which is proportional to the stress, can help evaluating the structural safety.

When a moment is applied to a buried pipe, the curvature radius changes shown in **Figure 2.1** and, contemporarily, bending strain occurs. The bending strains are calculated from the changes in the curvature radius using the following expression of relationship

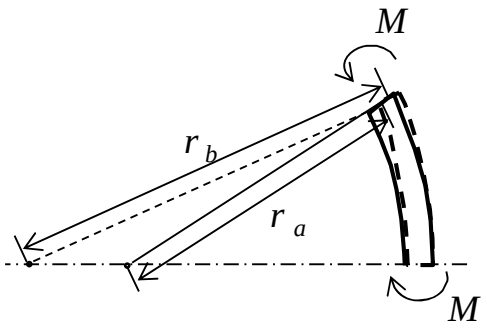

Figure 2.1 Change in the curvature radius of a pipe subjected to a moment *M*.

between loads and displacements of a bending beam.

$$\varepsilon_{max} = \frac{t}{2}\left(\frac{1}{r_a} - \frac{1}{r_b}\right) \tag{2.1}$$

where

ε_{max} maximum bending stress

t wall thickness

r_a curvature radius of the pipe after deformation

r_b curvature radius of the pipe before deformation

In equation 2.1, the wall thickness is assumed as sufficiently small compared to the curvature radius. The steel pipes used in the test satisfy this assumption because the wall thickness is about 1–2% of the curvature radius.

According to the method proposed, we measured the curvature radius with a depth gauge shown in **Figure 2.2** purchased from Nakamura Seisakusyo Co., Ltd., (model number E-TH15B); only the base was remodeled into a longer one for the purpose of our experiment. As shown in **Figure 2.3**, the strain is measured by press the base against the pipe and measuring the distance d from the base bottom to the inner surface of the pipe in the region of interest. The curvature radius of the orange part in **Figure 2.3** is equal to that of the circumcircle of ΔABC plus half of the wall thickness and can be calculated by the following equations.

$$r = \frac{abl}{\sqrt{(a+b+l)(-a+b+l)(a-b+l)(a+b-l)}} + \frac{t}{2} \tag{2.2}$$

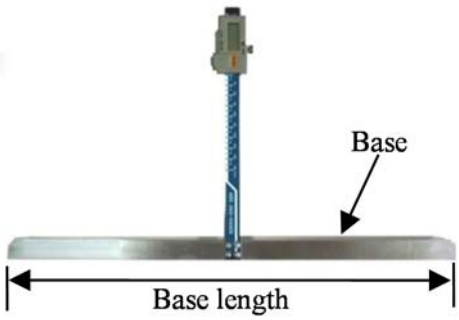

Figure 2.2 Layout of the device (a depth gauge) used to measure of curvature radius.

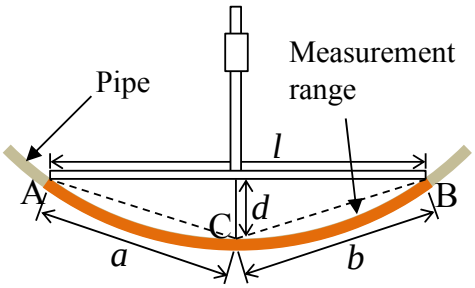

Figure 2.3 Measurement method of the curvature radius.

$$a = b = \sqrt{d^2 + \left(\frac{l}{2}\right)^2} \tag{2.3}$$

where

r mean radius of the pipe

a or b distance from the end of the base to the center of the measurement range

l base length

d measurement length

Equation 2.3 is substituted into equation 2.2, giving

$$r = \frac{l^2 + 4d^2}{8d} + \frac{t}{2} \tag{2.4}$$

As shown by equation 2.4, the bending strain could be easily estimated by just measuring d.

2.3. Experimental Method

2.3.1 Outline

The pipe specimens were deformed in air and sand, and the resulting strains were measured by both strain gauges and the proposed method, for validation purposes. The test of the pipe in sand is conducted to reproduce the loading conditions of pipelines installed in fields. In the bending strain estimation method, two long bases were used to examine how the base length affects the accuracy of the method.

2.3.2 Pipe Specimens

Table 2.1 Characteristics of the testing steel pipes.

Wall thickness (mm)	4.5
Inside diameter (mm)	800
Length（mm）	1,980
Young's modulus（GPa）	206
Ring stiffness (EI/r^3) （kPa）	24

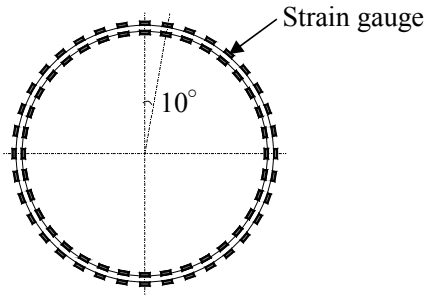

Figure 2.4 Strain gauges attached to the inner and outer surfaces of the pipe specimen.

Steel pipes SS400, with the characteristics shown in **Table 2.1**, were used for all tests. The circumferential strains of both inner and outer surfaces of the pipes were measured every 10° using 72 strain gauges shown in **Figure 2.4**. For the bending strain estimation method, two bases with different length (200 and 400 mm) were used to examine how the base length affects the accuracy of the method, and a displacement transducer was attached to the pipe for measuring the vertical deflection.

The r_b value is needed for this method. Hence, it was measured by placing the pipe with the longitudinal direction perpendicular to the floor because this prevents the deformation due to its own weight. Then, we measured the curvature radius at the same position of the strain gauges.

Figure 2.5 shows that the curvature radius before deformation was not the same for all positions; especially, near the welded part (30°–70°), the difference among the curvature radii was relatively large. **Figure 2.5** shows that the curvature radius differs also depending on the base length; the difference was larger near the welded part whose

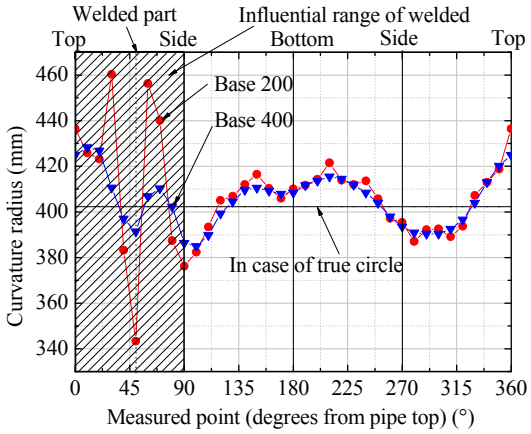

Figure 2.5 Curvature radius before deformation measured at different positions using the bending strain estimation method.

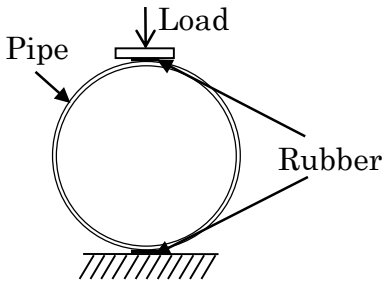

Figure 2.6 Parallel-plate loading test.

shape is distorted. On the other hand, far from the welded part (100°–350°) , the curvature radii measured with the two bases were almost the same. The influence of the difference in the curvature radius before deformation on the accuracy of the method is discussed in 2.5.1.

2.3.3 Test Case

(a) Parallel-Plate Loading Test

A pipe was deformed to a 5% of vertical deflection ratio in the parallel-plate loading test shown in **Figure 2.6** and the circumferential strains of the inner and outer surfaces were measured using the strain gauges. The radial strains were calculated to average the circumferential strains of inner and outer surfaces. The bending strains of the inner surface were calculated by subtracting the radial strains from the circumferential strains of inner surface. The bending strains were measured also with the bending strain

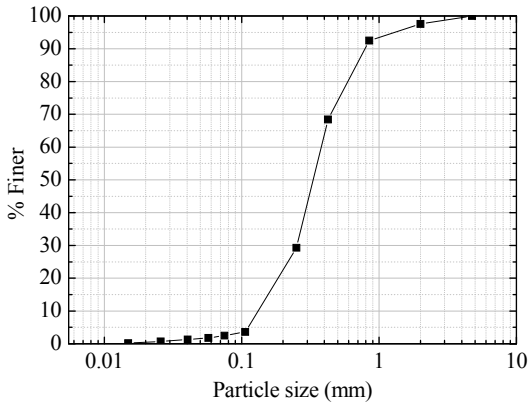

Figure 2.7 Grain size distribution of the backfill material (Kasumigaura sand) used for the loading test on buried pipe.

estimation method at the same position of the strain gauges. Then, the values obtained with the two methods were compared.

(b) Loading Test on Buried Pipe

The pipe specimen was buried in Kasumigaura sand, having the particle size distribution as shown in **Figure 2.7** and 9.2% of water content**.** The bedding part was compacted to 94% of the standard Proctor density and the remaining part to 79%. After backfilling the sand, a loading plate was placed on the ground surface to apply pressure with an actuator shown in **Figure 2.8**.

The ground surface pressure was applied to deflect pipe to 3% and the strains were measured with both the proposed method and the strain gauges at the deflection

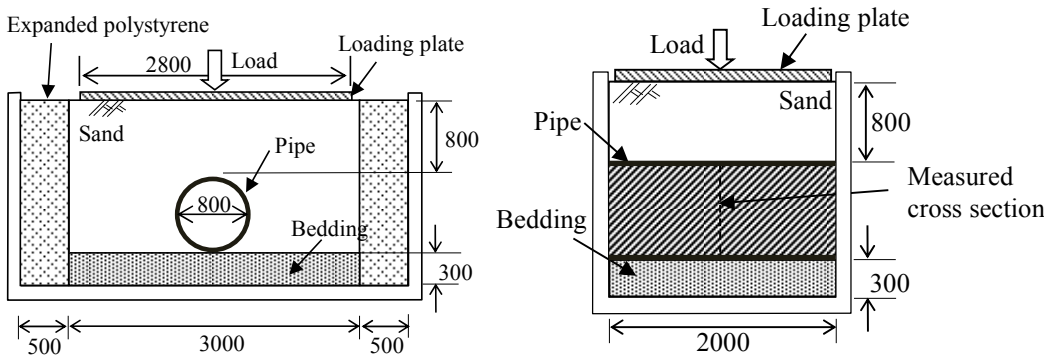

Figure 2.8 Schematic set-up of the loading test on the buried pipe.

stage. Then, the ground surface pressure was increased to deflect the pipe to 5% and the strains were measured again. After that, the two expanded polystyrene foams shown in the cross section (top) of **Figure 2.8** were pulled out to loosen the sand. Finally, the load was applied again to deflect the pipe to 7.5% and the resulting strains were measured.

2.4 Experimental Results

2.4.1 Measurement Results for the Bending Strains

Figures 2.9–2.12 show the distribution of the bending strains of the inner surface

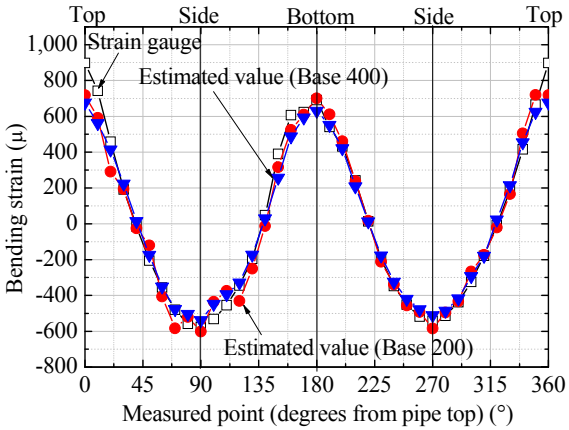

Figure 2.9 Bending strains distribution in the parallel plate test (5% deflection ratio).

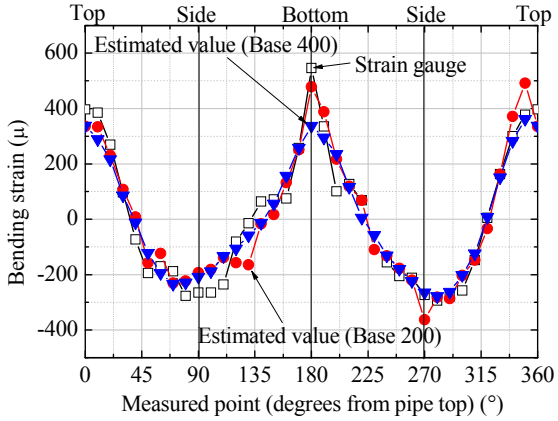

Figure 2.10 Bending strains distribution in the loading test on the buried pipe (3% deflection ratio).

of the pipes analyzed in the parallel-plate loading test and the loading test on the buried pipe. The tensile strains were defined as positive. The measurement points of the bending strains, which were the angles from the pipe top, are reported on the horizontal axis. **Table 2.2** compares the bending strains of the top, side, and bottom of the pipe obtained using strain gauges and the proposed method in both tests.

As shown in **Figure 2.9** and **Table 2.2, i**n the parallel-plate loading test, the strains obtained using our estimation method were almost the same as those obtained with the strain gauges, despite some differences for the pipe top. At the bottom and side of the pipe, the differences between the values obtained using the two methods were <10%,

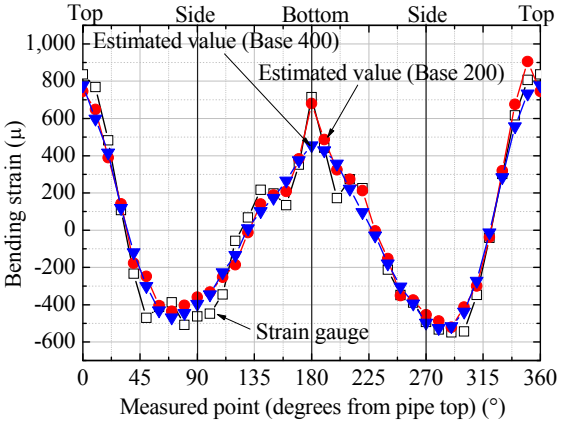

Figure 2.11 Bending strains distribution in the loading test on the buried pipe (5% deflection ratio).

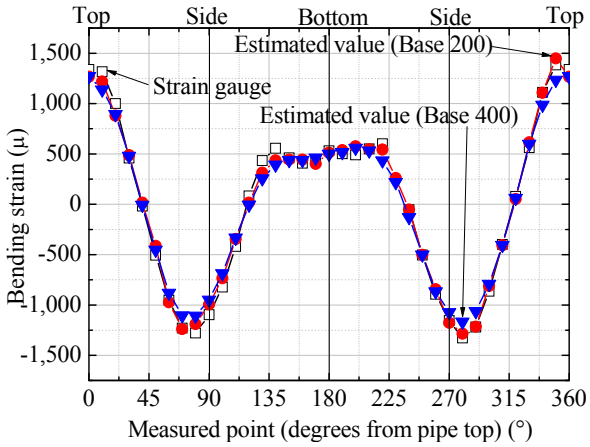

Figure 2.12 Bending strains distribution in the loading test on the buried pipe (7.5% deflection ratio).

Table 2.2 Bending strains at the top, side, and bottom of the pipe obtained using the strain gauges and the proposed estimation method.

Loading condition	Parallel-plate loading test			Loading test on buried pipe								
Deflection ratio (%)	5			3			5			7.5		
Measuring method	Strain gauges	Estimation method		Strain gauges	Estimation method		Strain gauges	Estimation method		Strain gauges	Estimation method	
Base length (mm)	—	200	400	—	200	400	—	200	400	—	200	400
Strains at pipe top (m)	898	719 (80)[*2]	676 (75)	397	335 (84)	338 (85)	837	745 (89)	777 (93)	1,339	1,266 (95)	1,270 (95)
Strains at pipe side*[1] (m)	-576	-602 (105)	-539 (94)	-277	-223 (81)	-229 (83)	-509	-404 (79)	-445 (87)	-1,278	-1,191 (93)	-1,108 (87)
Strains at pipe bottom (m)	691	701 (101)	630 (91)	546	478 (88)	337 (62)	714	680 (95)	455 (64)	532	512 (96)	500 (94)
Strains at pipe side*[1] (m)	-542	-585 (108)	-511 (94)	-294	-282 (96)	-278 (95)	-533	-487 (91)	-526 (99)	-1,329	-1,286 (97)	-1,167 (88)

*[1] Strains at the pipe sides were measured at 0° and 270° in the parallel-plate loading test, and at 80° and 280° in the loading test on the buried pipe

*[2] ( ) is the ratio of the bending strains obtained using the estimation method and those given by the strain gauges

which implies that the proposed estimation method can be effectively used for measuring the bending strains.

Similar to the parallel-plate loading test, in the loading test on the buried pipe, the strains determined with the bending strain estimation method were almost the same as those obtained using the strain gauges, regardless of the base length shown in **Figures 2.10–2.12**. However, in the tests with 3% and 5% deflection ratios, the strain at the pipe bottom obtained using the 400 mm base was far from that given by the strain gauges although that obtained using the 200 mm base was close to that given by the strain gauges

(See the **Figures 2.10** and **2.11**, **Table 2.2**). The shorter the base length, the narrower the measurement range; thus, a shorter base would be better because it could allow the measurement of more local deformations.

Figure 2.12 shows that the distribution of the bending strains changed greatly at the 7.5% vertical deflection ratio because the soil was loosed by pulling out the expanded polystyrene foams, changing the distribution of the earth pressures acting on the pipe. **Figure 2.12** and **Table 2.2** show that the strains obtained with the two method were almost same overall; even if the pipe deformed considerably, exceeding the maximum allowable deflection ratio, the method could be still used to measure the bending strains.

As shown in **Figure 2.13**, the accuracy of the method was high when the strains were large. Some of the bending strains estimated with the proposed method were less than 50% of the absolute values given by the strain gauges, which were <300 μ. However, for bending strains >1000 μ, all the results obtained with the bending strain estimation method were in the range of 87–105% of the absolute values given by the strain gauges.

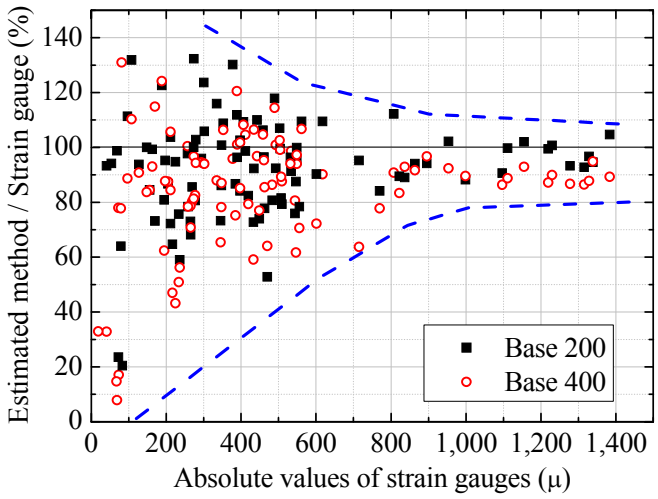

Figure 2.13 Ratios between the bending strains given by the estimation method and by the strain gauges.

2.4.2 Bending Strains and Radial Strains

The distribution of the bending strains does not depend on the deflections. **Figure**

2.14 shows that the distribution at the upper part was symmetrical to that at the lower part in the parallel-plate loading test, although not in the loading test on the buried pipe, in which the pipe deformed locally at the bottom.

Figure 2.15 reveals that all the radial strains were in compression at the 5% deflection ratio in the loading test on the buried pipe. On the other hand, in the parallel-plate loading test and at the 7.5% deflection ratio in the loading test on the buried pipe, some of them were in tension. In particular, at the 7.5% deflection ratio in the loading test on the buried pipe, the radial strains increased in the tension direction at almost all measuring points due to the loosening of the soil. Regardless of being tensile or compressive, the radial strains were significantly smaller than the bending strains; they

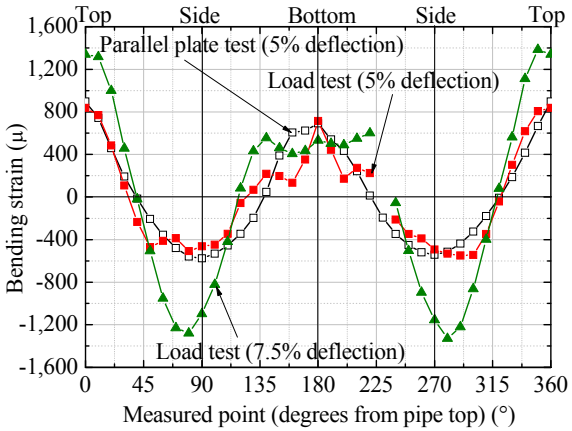

Figure 2.14 Bending strains distribution.

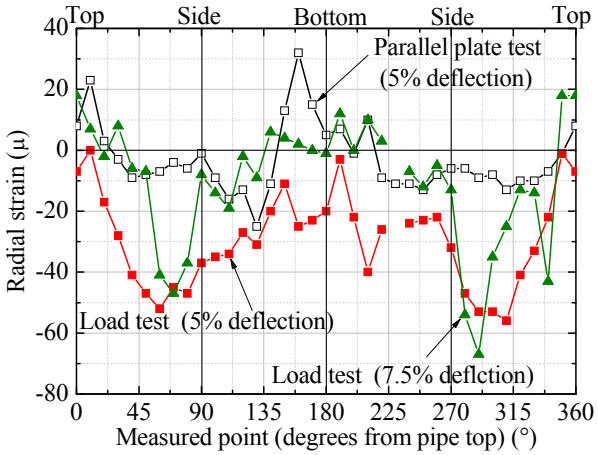

Figure 2.15 Radial strains distribution.

were <10% of the bending strains when these ones were >500 μ shown in **Figure 2.16**. This suggests that measuring the bending strains can evaluate the structural safety of buried pipes because their circumferential strains are generated mostly by moment (bending strains), not normal force (radial strains).

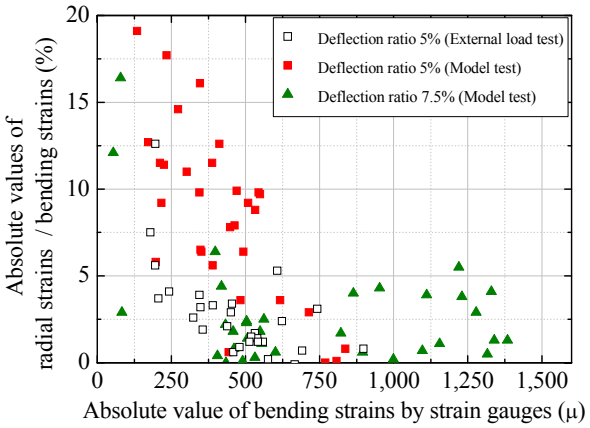

Figure 2.16 Ratios between the absolute values of the bending strains and the radial strains.

2.5 Discussion

In this section, we examine how the errors in the curvature radius before deformation and in the measurement length affect the accuracy of the method. We also propose the appropriate base length for each pipe diameter because the accuracy of the method depends mainly on this parameter.

2.5.1 Errors in the Curvature Radius Before Deformation

Curvature radius before deformation r_b, defined in equation 2.1, could not be measured in fields because the buried pipes have already been deformed by earth pressures, but it can be calculated from the diameter and wall thickness of the pipe. This may generate some errors in the bending strains obtained using the estimation method, if the pipe section before deformation is not a true circle.

In fact, welded steel pipes have not a true circular section. **Figure 2.17** and **Table**

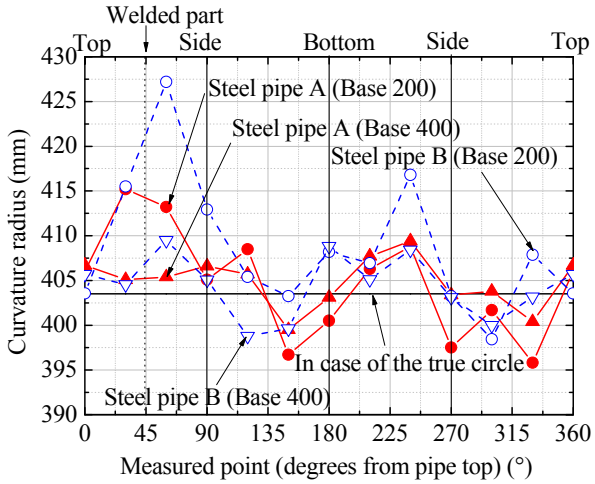

Figure 2.17 Curvature radius of the welded steel pipes before deformation.

Table 2.3 Average and maximum values of the difference between the curvature radiuses obtained using the proposed method and that calculated from the wall thickness and diameter of the pipes.

	Mean diameter calculated from wall thickness and inside diameter (r_{cal}) (mm)	Mean curvature radius			
		Base length (mm)	Average of absolute values of the difference (r_{dif}) between r_{cal} and the curvature radiuses obtained by the method (mm)	Maximum of r_{dif} (Except influential range of welded)*1 (mm)	Maximum of r_{dif} (Including influential range of welded) (mm)
Steel pipe A	403	200	5.3	-7.7	11.7
		400	2.5	5.9	5.9
Steel pipe B	403	200	6.5	13.3	23.7
		400	3.0	5.3	6.0

*1 Influential range of the welded pipe was within 20 degrees from the welded point.

2.3 show the r_b values obtained with the proposed method for two welded steel pipes, which had a wall thickness of 6 mm and an inside diameter of 400 mm, and had never been loaded. The curvature radii were measured when the longitudinal direction of the pipes was perpendicular to the floor to prevent deformation due to their own weight and at every 30° with the estimation method, using both the 200 mm and the 400 mm bases. The r_b values varied depending on the measuring position, and the average differences

between the curvature radii obtained using the estimation method and those calculated from the diameter and wall thickness of the pipes are in the range of 2.5–6.5 mm as shown in **Table 2.3**.

A longer base is more suitable for the pipe sections that are not true circles, such as the welded parts, even when not loaded. **Table 2.3** shows that the maximum difference (r_{dif}), including the influential range of the welded part when using the 200 mm base, was more than twice that obtained using the 400 mm base. Such differences affect the accuracy of the bending strain estimation method, as shown in **Figure 2.18** in terms of the relationship between the r_{dif} in r_b and the errors in the bending strains obtained with the proposed method when the strain is around the yield point (1183 μ). The maximum difference (23.7 mm) obtained when using the 400 mm base on the steel pipe B led to errors below 10% in the estimation of the bending strains with the proposed method, although that obtained with the 200 mm base (6.0 mm) led to errors higher than 30%.

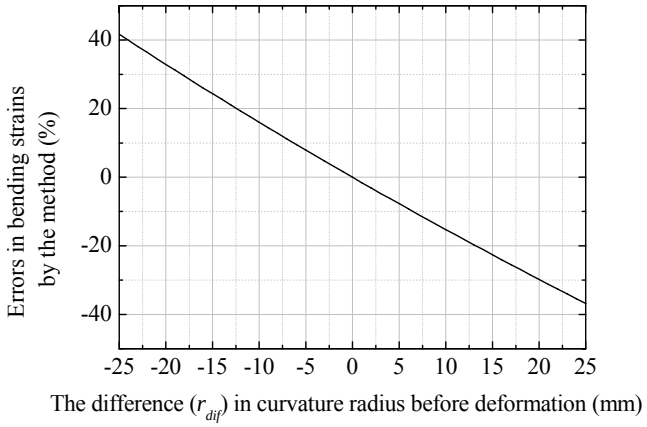

Figure 2.18 Influence of the errors in curvature radius before deformation on the bending strains estimated with the proposed method.

2.5.2 Errors in the Measurement Length

Errors also may occur in the measurement length *d* when using the proposed method for fields, although the error was within 0.1 mm when we measured the measurement length *d* 10 times at the same point in the test. When we tried the method in some fields, the error was within 0.5 mm.

Longer bases are better if the errors in the measurement length are large. The errors in the measurement length affect the accuracy of the bending strain estimation method as shown in **Figure 2.19** in terms of the relationship between the base lengths and the errors in the bending strains obtained with the proposed method when the strain is around the yield point (1183 μ). Errors within 0.5 mm in the measurement length when using the 400 mm base led to only 3% errors in the bending strains estimated with the proposed method, although when using the 200 mm base they induced 17% errors.

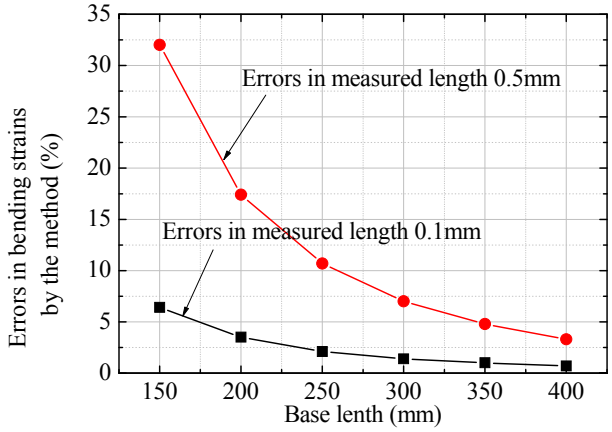

Figure 2.19 Influence of the base lengths on the estimated values.

2.5.3 The Appropriate Base Length

The base length should be determined based on two viewpoints: 1. influence of the errors in curvature radius before deformation and in measurement length on the accuracy of the estimated bending strains, and 2. local deformation of the pipe. Longer bases are better for the former, while shorter ones are better for the latter.

Figure 2.20 shows that the base lengths so that a 0.5 mm error in the measurement length would lead to a 10% error in the bending strains estimated with the proposed method when the strain is around the yield point (1183 μ). The 0.5mm error was used in the calculations because the error in the measurement length was within 0.5 mm when using the method in some fields. The base lengths for diameters in **Figure 2.20** are recommended when you use the method in fields. The appropriate base length could be

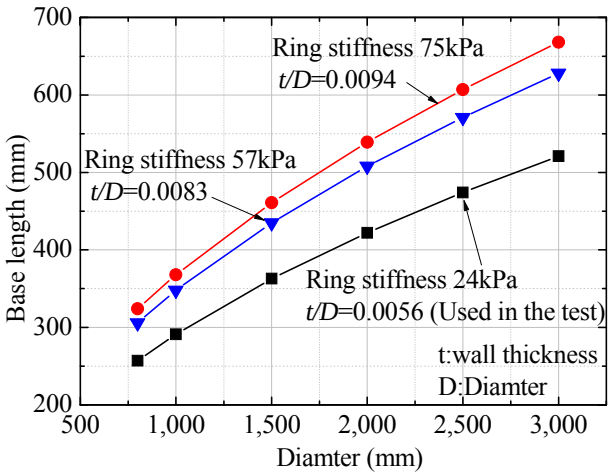

Figure 2.20 Relationship between the diameters and the base lengths when 0.5 mm errors in the measured length correspond to 10% errors in the estimated values.

determined by making such calculations.

2.6 Conclusions

We developed a method to estimate the bending strains by measuring the curvature radius of buried pipes and verified its applicability for steel pipes. The results led to the following conclusions:

1. Bending strains could be estimated by measuring the change in the curvature radius of buried pipes.
2. The larger the bending strains, the better the accuracy of their values estimated with the proposed method. All the bending strains measured using our method were in the range of 87–105% of their absolute values for bending strains >1000 μ.
3. Longer bases are better if the pipes sections are not true circle, such as the welded parts, even when not loaded because the influence of the error in curvature radius before deformation on the accuracy of the method decreases.
4. Longer bases are better for the accuracy of the method if the errors in the measurement length are large.
5. The appropriate base length should be determined from the two viewpoints: 1.

influence of the errors in curvature radius before deformation and measurement length on the accuracy of the bending strains estimated using the proposed method, and 2. local deformation of the pipe.

References

Howard, A.K.: Laboratory Load Tests on Buried Flexible Pipe, American water works association, 64(10), 655-662. 1972.

Idomoto, Y., Sasaki Y., Tsujioka S., Nakajima, K. and Nakamura H.: Design of Pipeline Based on Reliability, *Research reports of JIID*, No.22, pp.91-100, 2001. (in Japanese)

Idomoto, Y. and Nakajima K.: Example of Performance Based Code of Design Standard for Irrigation Pipeline, *Research Reports of JIID*, No.23, pp.81-96. 2002. (in Japanese)

Marston, A.: The Theory of External Loads on Closed Conduits in the Light of the Latest Experiments, Bulletin 96, Iowa Engineering Experiment Station. 1930.

Marston, A. and Anderson, A.O.: The Theory of Loads on Pipes in Ditches and Tests of Cement and Clay Drain Tile and Sewer Pipe, Bulletin 31, Iowa Engineering Experiment Station, 1913.

Marston, A., Schlick, W. J. and Clemmer, H. F.: The Supporting Strength of Sewer Pipe in Ditches and Methods of Testing Sewer Pipe in Laboratories to Determine Their Ordinary Supporting Strength, Bulletin 47, Iowa Engineering Experiment Station, 1917.

Ministry of Agriculture, Forestry and Fisheries: Annual Report on Food, Agriculture and Rural Areas in Japan FY2010, pp.288-290. 2010. (in Japanese)

Ministry of Agriculture, Forestry and Fisheries: Manual of Stock Management for Irrigation Facilities. 2007. (in Japanese)

Ministry of Agriculture, Forestry and Fisheries: Manual of Functional Maintenance for Irrigation Pipeline. 2009a. (in Japanese)

Ministry of Agriculture, Forestry and Fisheries; Design standard for irrigation pipeline. 2009b. (in Japanese)

Spangler, M.G.: The Structural Design of Flexible Pipe Culverts, Bulletin 153, Iowa Engineering Experiment Station, 1941.

CHAPTER 3

The contents of this chapter are based on:

Ariyoshi, M., Mohri, Y., Hazama M., Kubota K.: Vertification of Bending Strain Estimation Method for Fiberglass Reinforced Plastic Mortar Pipe, *Irrigation, drainage and rural engineering journal*, 303, pp.I_381-I_389 (2016) (in Japanese with English Summary)

Chapter 3

Bending Strain Estimation Method for Fiberglass Reinforced Plastic Mortar Pipes

3.1 Introduction

Fiberglass reinforced plastic mortar (FRPM) pipes have been sold since 1970; nowadays, they are widely used for irrigation pipelines throughout Japan. These pipes have been adapted for the Japanese design standard for irrigation pipelines since 1977 (MAFF, 1977) and the Japan Standard JIS A 5350 “Fiberglass reinforce plastic mortar pipes” was enacted in 1984.

Buried pipes, including FRPM ones, occasionally fail resulting in leakages because of the stress concentration on them due to differential settlements of ground. In such cases, the failure may occur even if the deflection ratios are below the allowable value (5%) because pipes deform locally.

Measuring of vertical and horizontal deflection ratio is the conventional method to evaluate the deformation of buried pipes. However, this method could evaluate the overall deformation but not the local deformation, which is the responsible for the failure. Thus, a new method to evaluate local deformation is required.

Okuda et al. (2013) and Ueno et al. (2014) are developing a survey method to evaluate the structural safety of FRPM pipes using microwaves. They stated that the defects on the inner surface of the pipe change its propagation characteristics, although it has not been quantitative evaluated. Tsuchida et al. (2010) conducted a parallel-plate loading test and an internal pressure test on excavated FRPM pipes, which were used for 11 and 12 years in the field, respectively. They revealed that the strength of a FRPM pipe decreases after a long-term burial. Idomoto et al. (2007) and Otsuka et al. (2013) conducted long-term tests based on ISO standards 10471 and 7509, and determined the long-term ultimate strains.

Ariyoshi et al. (2013) developed a new method to estimate bending strains, which can evaluate the local deformations of buried pipes, by measuring the curvature radius of the pipe and applied it on ϕ 800 steel pipes for validation. We demonstrated that the bending strains of buried steel pipes could be estimated with high accuracy by using the appropriate base length.

In this chapter, we examine the applicability of this method for FRPM pipes. Unlike steel pipes, FRPM pipes are not made of a single material but consist mainly of glass fiber reinforced plastic and resin mortar. Actual diameters and wall thicknesses are not the same as the nominal values, which may lead to errors in the bending strains estimated with the proposed method. We conducted model tests on FRPM pipes with four different diameters to examine how the difference between the actual and nominal values of diameter and wall thickness affect the bending strains obtained with the proposed method. In addition, we propose the most appropriate base length for each diameter of the analyzed FRPM pipes.

3.2 Experimental Method

3.2.1 Outline

Bending strains of deformed FRPM pipes were measured by strain gauges and by the bending strain estimation method. In the proposed method, we used five different length bases for four different diameter FRPM pipes. The bending strains obtained in the

two ways were compared to examine the accuracy of the proposed method and determine the most appropriate base length for each pipe diameter.

When using the proposed method in fields, the wall thickness and the curvature radius before deformation may not be measured. However, the nominal values of wall thickness and diameter could also be used to calculate the bending strains. Thus, we examined the errors in bending strains obtained with the proposed method by using these nominal values instead of the actual values.

3.2.2 Pipe Specimens

FRPM pipes with a length of 300 mm and different diameters (ϕ 800, ϕ 1200, ϕ 2000, and ϕ 2400) were used in the tests. The differences between nominal values and measured values for the diameter were within 0.2%, although those for the wall thickness were 3–14% shown in **Table 3.1**.

As shown in **Figure 3.1**, the strain gauges were attached at every 15° on the inner and outer surfaces of the ϕ 1200, ϕ 2000, and ϕ 2400 pipes, which were used for the parallel-plate loading test. The strain gauges were attached at every 10° on the inner and outer surfaces of the lower part of the ϕ 800 pipes shown in **Figure 3.2**, which were used for the three-point loading test and the parallel-plate loading test, because the bottom of the pipe is assumed to deform locally in the three-point loading test.

Table 3.1 Characteristics of the testing FRPM pipes.

Internal diameter (mm)		Wall thickness (mm)		Classif-ication	Experiment case
Nominal value	Measur-ed value	Nominal value	Measur-ed value		
800	799.0	16	18.3	Type 3	Parallel-plate loading test
800	800.7	16	17.9	Type 3	Three-point loading test
1,200	1,199.2	24	26.2	Type 3	Parallel-plate loading test
2,000	2,003.0	40	41.4	Type 3	Parallel-plate loading test
2,400	2,401	48	50.1	Type 4	Parallel-plate loading test

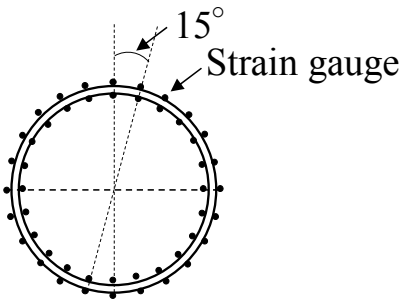

Figure 3.1 Strain gauges attached to testing pipes. (except ϕ800)

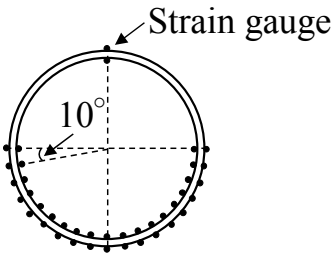

Figure 3.2 Strain gauges attached to the testing pipe. (ϕ800)

3.2.3 Test Case

(a) Measurement of the Curvature Radius

We investigated how the errors in the curvature radius before deformation affect the bending strains estimated with the proposed method. In case of buried FRPM pipes in the field, the curvature radius before deformation r_b (equation 2.4) may be calculated from the nominal values of wall thickness and diameter of the pipe. However, as shown in **Table 3.1**, the actual values are not exactly the same as the nominal values, and the FRPM pipe section may be not a true circle even when not loaded.

To measure the curvature radius before deformation, the pipe specimens were placed so that the longitudinal direction was perpendicular to the floor because this prevents the deformation due to their own weight. Then, we measured the curvature radius at the same position of the strain gauges using five different length bases for four different diameter pipes shown in **Table 3.2**.

(b) Parallel-Plate Loading Test

As shown in **Figure 3.3**, loads were applied at the top of the pipes to obtain a

Table 3.2 Base lengths used in the experiments.

Inside diameter（mm）	Base length（mm）
800	200，300
1,200	200，300，400
2,000	300，400，500
2,400	400，500，600

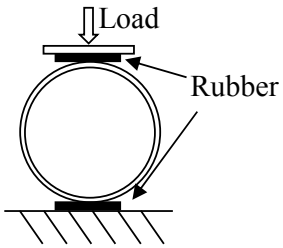

Figure 3.3 Parallel-plate loading test.

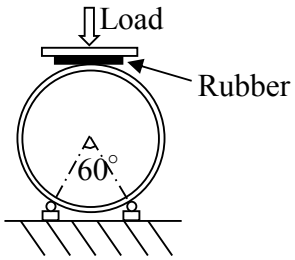

Figure 3.4 Three-point loading test.

deflection ratio of 5%. Then, the bending strains were measured using the strain gauges and the proposed method at the same points. As shown **Tables 3.1** and **3.2**, four different diameter pipes and five different length bases were used. In addition, only, for the ϕ 2400 pipe, different operators measures curvature radius twice at the same point to examine also the personal errors.

(c) Three-Point Loading Test

Unlike the parallel-plate loading test, the pipes were placed on a pair of smaller iron pipes at 30° from the pipe bottom shown in **Figure 3.4**. A load was applied to the top of the pipes to obtain a deflection ratio of 5%. Then, the bending strains were measured

using the strain gauges and the proposed method at the same points. For this test, we assumed that some stiff objects such as trees could also be in contact with the pipes in the fields. The ϕ 800 FRPM pipe, and 200 mm and 300 mm length bases were used for this test.

3.3. Results and Discussion

3.3.1 Curvature Radius of the FRPM Pipe

The curvature radius measured with the proposed method is dependent on base lengths. For the ϕ 1200 FRPM pipe, the curvature radii measured using the 300 mm and the 400 mm bases were almost the same and close to the nominal values shown in **Figure 3.5**. On the other hand, the curvature radii measured with the 200 mm base varied depending on the measurement positions and were quite different from the nominal values. The maximum difference between measured and nominal values, when using the 200 mm base, was observed at 300° and was higher than 50 mm. **Table 3.3** shows that the standard deviation of the curvature radius measured with the 200 mm base was more than twice those measured with the 300 mm and 400 mm ones.

These differences between nominal and measured values generate errors in the bending strains. **Figure 3.6** are obtained from substituting curvature radius measured with

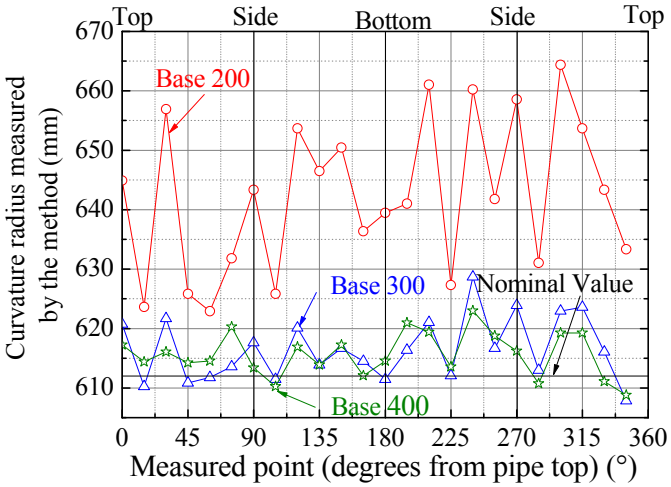

Figure 3.5 Curvature radius of the ϕ1200 pipe measured with the bending strain estimation method.

Table 3.3 Average values and standard deviations of the curvature radius measured with the bending strain estimation method.

Diameter (mm)	800		1,200			2,000		
Base length (mm)	200	300	200	300	400	300	400	500
Average* (mm)	412.5	410.6	642.4	616.5	615.7	1,042.9	1,027.3	1,032.4
Standard deviation (mm)	11.8	5.6	12.6	5.2	3.6	8.1	4.6	4.0

Diameter (mm)	2,400		
Base length (mm)	400	500	600
Average* (mm)	1,245.1	1,238.1	1,236.9
Standard deviation (mm)	6.6	8.1	7.5

* Averages of the nominal values are 408mm in ϕ800, 612mm in ϕ 1,200, 1,020mm in ϕ 2,000 and 1,224mm in ϕ 2,400.

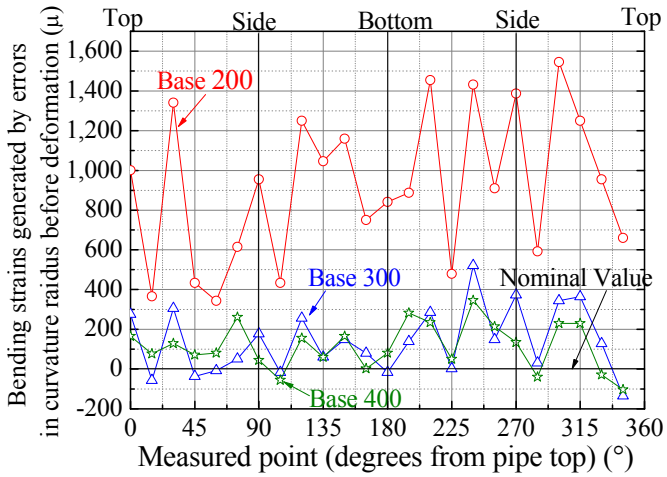

Figure 3.6 Maximum bending strains of the ϕ1200 pipe generated by errors in curvature radius before deformation.

the proposed method and that calculated from the nominal values into the curvature radius after deformation r_a and r_b in equation 2.1, respectively. The average and maximum bending strains obtained using the 200 mm base were 920 and 1550 μ, respectively, although even the maximum bending strain obtained with the 400 mm one was <400 μ. This happened because errors in the measurement length *d* lead to large errors in the bending strains when the base is too short; for example, an error of 0.5 mm in *d* led to 1127 μ when using the 200 mm base, but only to 264 μ when using the 400 mm one. Thus, short bases should be avoided in this type of measurements.

The longer the base, the smaller the standard deviation of the bending strains as shown in **Table 3.3**. For the ϕ 800 and ϕ 1200 pipes, the standard deviations obtained using the 300 mm base were much smaller than those given by the 200 mm one; similarly, for the ϕ 2000 pipe, the standard deviations obtained using the 400 mm base were much smaller than those given by the 300 mm one. If the base length is longer than certain length, the difference in standard deviation is sufficiently small. For the ϕ2400 pipe, the standard deviations obtained using base longer than 400mm are almost the same.

3.3.2 Parallel-Plate Loading Test

In the parallel-plate loading test, the strains were calculated from the loads and deflections theoretically based on the thin-walled assumption, according to the following equations (Timoshenko, 1957).

$$M = 0.318Pr \tag{3.1}$$

$$E = 0.149\frac{Pr^3}{\delta I_z} \tag{3.2}$$

$$\sigma = \frac{M}{Z} \tag{3.3}$$

$$\varepsilon = \frac{\sigma}{E} \tag{3.4}$$

where

M moment

P load

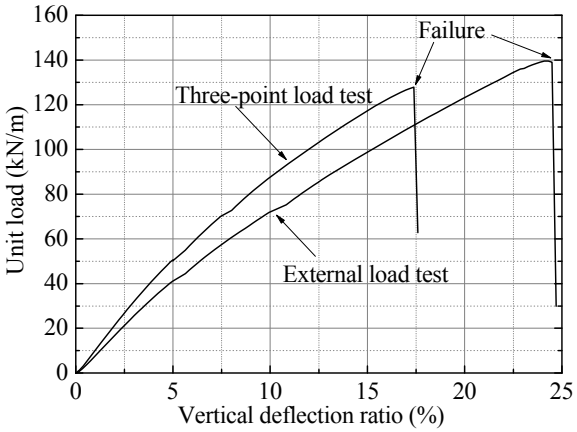

Figure 3.7 Relationship between load and vertical deflection.

Table 3.4 Strains calculated and measured with the strain gauges at 5% of vertical deflection.

Nominal diameter（mm）	Calculation (μ)	Strain gauge (μ)
800	4,759	4,311
1,200	4,524	4,024
2,000	4,362	4,686
2,400	4,350	4,241

r mean radius

E Young's modulus

δ deflection

I_z moment of inertia of area

σ stress

Z section modulus

ε strain

As shown in **Figure 3.7**, the load was 41.1 kN/m when the vertical deflection rate was 5% in the parallel-plate loading test for the ϕ 800 pipe. Substituting these values in the equations 3.1-3.4, the strain was calculated to be 4760 μ. This calculated strain was close to those measured with the strain gauges in the parallel-plate loading test (pipe top: 4160 μ, pipe bottom: 4460 μ). In a similar way, for the other diameter pipes, the strains calculated from load and deflection were close to the measured ones (**Table 3.4**). This

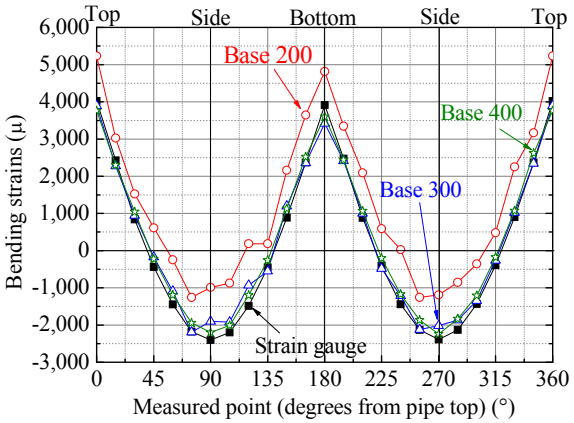

Figure 3.8 Bending strains distribution at 5% of vertical deflection (ϕ1200 diameter pipe; wall thickness and curvature radius before deformation were nominal values).

implies that the method based on the thin-walled assumption may be useful for FRPM pipes although they are not made of a single material.

In this section, the bending strains are calculated in three ways: (1) using the nominal values of wall thickness and curvature radius before deformation, (2) using the nominal value of wall thickness and the measured one of curvature radius before deformation, and (3) using the measured values of both.

(1) The nominal values of both parameters were used to calculate the bending strains for the ϕ 1200 pipe shown in **Figure 3.8**. The bending strains obtained using the strain gauges were calculated from the circumferential strains of the inner and outer surfaces of the pipe. The bending strains measured with the proposed method using the 300 and 400 mm bases were almost the same at all positions and close to those obtained with the strain gauges. **Figure 3.9** shows that the differences between the bending strains given by the strain gauges and those obtained using the proposed method with the 300 and 400 mm bases were <300 μ at most points and the maximum difference was 550 μ. On the other hand, the differences between the bending strains given by the strain gauges and those obtained using the proposed method with the 200 mm base were clearly large, with an average value of 1090 μ and a maximum of 1670 μ.

High accuracy is required for the proposed method in case of large strains because they cause pipe failures. **Table 3.5** shows that the strains at the top, side, and

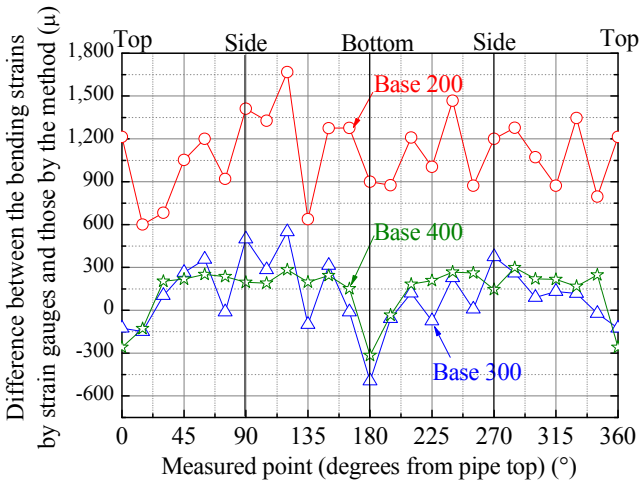

Figure 3.9 Difference between the bending strains obtained using the strain gauges and those given using our method at 5% of vertical deflection (ϕ1200 model pipe; wall thickness and curvature radius before deformation were nominal values).

bottom of the pipe where large strains occur. Except when using the 200 mm base for the ϕ 1200 pipe, the accuracies at the pipe top and bottom, where the maximum strains generally occur, were >80%; in particular, for the ϕ 2000 and ϕ 2400 pipes, these accuracies were almost >90%. This suggests that we may effectively use the nominal values to calculate the bending strains.

(2) The nominal values of wall thickness and the measured ones of curvature radius were used to calculate the bending strains. **Figure 3.10** shows that the differences between the bending strains given by the strain gauges and those obtained with the proposed method using the 200 mm base decreased greatly. This happened because the nominal values were significantly different from the measured ones for the curvature radius before deformation mentioned in Section 3.3.1.

(3) The measured values of wall thickness and curvature radius were used to calculate the bending strains shown in **Table 3.6**. At all points, the absolute values of the bending strains shown in **Figure 3.11** were a bit larger than those in **Figure 3.10** because the measured values of wall thickness were larger than the nominal ones. As shown by equation 2.1, the bending strains are proportional to the pipe thickness. Comparing **Tables**

Table 3.5 Strains at the top, side, and bottom of the pipe (wall thickness and curvature radius were nominal values).

Diameter (mm)	800			1,200			
Measuring method	Strain gauge	Estimation method		Strain gauge	Estimation method		
Base length (mm)	-	200	300	-	200	300	400
Strains at pipe top (μ)	4,181	3,833 (0.92)*	3,482 (0.83)	4,019	5,232 (1.30)	3,893 (0.97)	3,760 (0.94)
Strains at pipe side (90°) (μ)	−2,556	−2,279 (0.89)	−2,032 (0.79)	-2,398	−987 (0.41)	−1,899 (0.79)	−2,202 (0.92)
Strains at pipe bottom (μ)	4,456	3,848 (0.86)	3,552 (0.80)	3,917	4,817 (1.23)	3,422 (0.87)	3,601 (0.92)
Strains at pipe side (270°) (μ)	−2,516	−2,293 (0.91)	−1,913 (0.76)	-2,389	−1,189 (0.50)	−2,014 (0.84)	−2,243 (0.94)

Diameter (mm)	2,000				2,400			
Measuring method	Strain gauge	Estimation method			Strain gauge	Estimation method		
Base length (mm)	-	300	400	500	-	400	500	600
Strains at pipe top (μ)	4,809	4,717 (0.98)	4,634 (0.96)	4,435 (0.92)	4,229	4,219 (1.00)	3,780 (0.89)	3,798 (0.90)
Strains at pipe side (90°) (μ)	-2,830	-2,451 (0.87)	-2,450 (0.87)	-2,558 (0.90)	-2,545	-2,142 (0.84)	-2,185 (0.86)	-2,183 (0.86)
Strains at pipe bottom (μ)	4,617	5,008 (1.08)	4,873 (1.06)	4,622 (1.00)	4,256	4,449 (1.05)	4,173 (0.98)	4,043 (0.95)
Strains at pipe side (270°) (μ)	-2,824	−2,617 (0.93)	−2,606 (0.92)	−2,707 (0.96)	−2,340	−2,131 (0.91)	−2,291 (0.98)	−2,226 (0.95)

*( ) is the ratio of the bending strains by the method and those by strain gauges

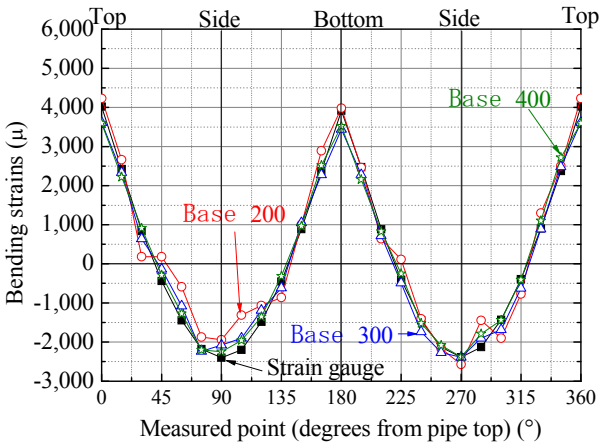

Figure 3.10 Bending strain distribution at 5% of vertical deflection (ϕ1200 pipe; the wall thicknesses were nominal values and the curvature radii before deformation were measured ones).

3.5 and **3.6**, some bending strains increased and other strains decreased because the curvature radii measured changed depending on the measuring points. However, the strains reported in the two tables did not greatly differed except when using the 200 mm base for the ϕ 1200 pipe. This also implies that the proposed method may be reliable even when using the nominal values of wall thickness and pipe diameter.

When different operators measured the curvature radius twice at the same point for ϕ 2400 pipe, there were almost no personal errors; the average difference in the measured length was 0.01 mm, with a maximum of 0.29 mm and a standard value of 0.11 mm.

3.3.3 Three-Point Loading Test

Relationships between deflections and loads depend on load conditions. In the three-point test, a load 1.2 times that used in the parallel-plate loading test was required to deflect the pipe at 5% shown in **Figure 3.7**. Similarly, the relationship between deflections and strains depend on the load conditions. **Figure 3.12** revealed that the strains distributions in the three-point test and in the parallel-plate loading test were clearly different, although the deflection ratio was the same. The bending strain (5930 μ) of the pipe top in the three-point test was 1.3 times larger than that (4460 μ) observed in the parallel-plate loading test.

Table 3.6 Strains at the top, side, and bottom of the pipe (wall thickness and curvature radius were measured values).

Diameter (mm)	800			1,200			
Measuring method	Strain gauge	Estimation method		Strain gauge	Estimation method		
Base length (mm)	-	200	300	-	200	300	400
Strains at pipe top (μ)	4,181	3,847 (0.92)*	3,479 (0.83)	4,019	4,605 (1.15)	3,936 (0.98)	3,910 (0.97)
Strains at pipe side (90°) (μ)	-2,556	-2,514 (0.98)	-2,550 (1.00)	-2,398	-2,113 (0.88)	-2,259 (0.94)	-2,443 (1.02)
Strains at pipe bottom (μ)	4,456	3,847 (0.86)	3,560 (0.80)	3,917	4,326 (1.10)	3,743 (0.96)	3,829 (0.98)
Strains at pipe side (270°) (μ)	-2,516	-2,664 (1.06)	-2,345 (0.93)	-2,389	-2,802 (1.17)	-2,598 (1.09)	-2,586 (1.08)

Diameter (mm)	2,000				2,400			
Measuring method	Strain gauge	Estimation method			Strain gauge	Estimation method		
Base length (mm)	-	300	400	500	-	400	500	600
Strains at pipe top (μ)	4,809	4,664 (0.97)	4,751 (0.99)	4,439 (0.92)	4,229	4,188 (0.99)	3,808 (0.90)	3,885 (0.92)
Strains at pipe side (90°) (μ)	-2,830	-2,959 (1.05)	-2,750 (0.97)	-2,884 (1.02)	-2,545	-2,458 (0.97)	-2,491 (0.98)	-2,417 (0.95)
Strains at pipe bottom (μ)	4,617	4,773 (1.03)	4,911 (1.06)	4,469 (0.97)	4,256	4,227 (0.99)	4,159 (0.98)	4,024 (0.95)
Strains at pipe side (270°) (μ)	-2,824	-3,009 (1.07)	-2,825 (1.00)	-3,008 (1.07)	-2,340	-2,482 (1.06)	-2,519 (1.08)	-2,477 (1.06)

*( ) is the ratio of the bending strains by the method and those by strain gauges

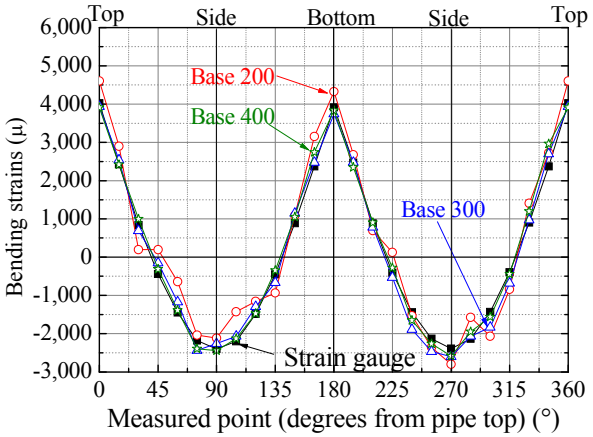

Figure 3.11 Bending strain distribution at 5% of vertical deflection (ϕ1200 pipe: wall thickness and curvature radius before deformation were the measured values).

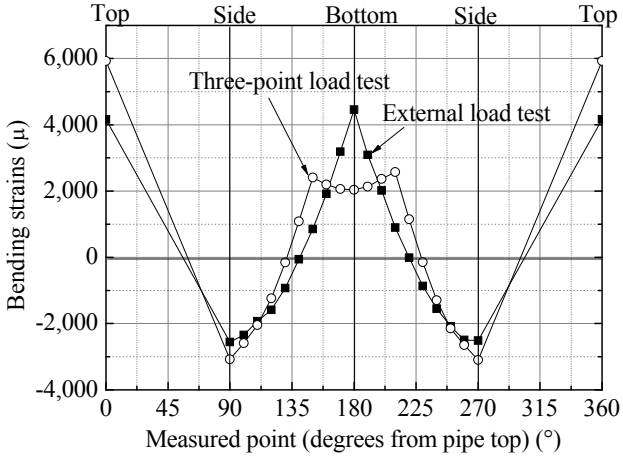

Figure 3.12 Bending strains distribution at 5% of vertical deflection in the parallel plate test and in the three-point loading test.

Figure 3.13 shows the distribution of the bending strains at a deflection ratio of 5%. The nominal values of wall thickness and diameter were used to calculate the bending strains. The values obtained using the proposed method and the strain gauges were almost the same in most positions including those of the iron pipes (150° and 210°). This implies that the method may be useful when the buried pipe deforms locally. When the measured values of the curvature radius were used to calculate the strains, the difference in the bending strains obtained at around 270° with the strain gauges and with the proposed

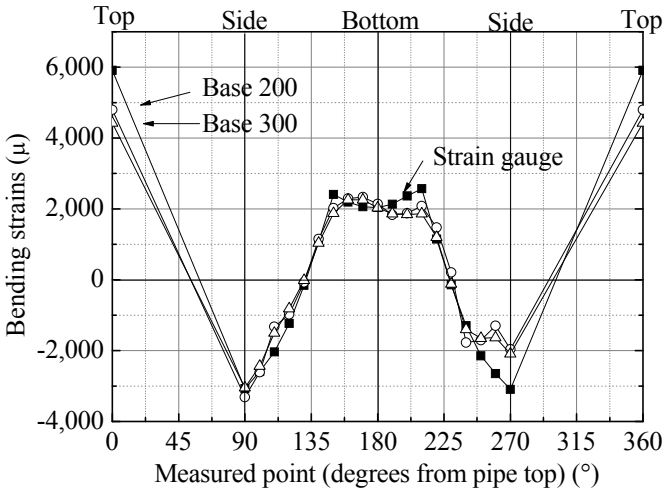

Figure 3.13 Bending strains distribution at 5% of vertical deflection (wall thickness and curvature radius before deformation was the nominal values).

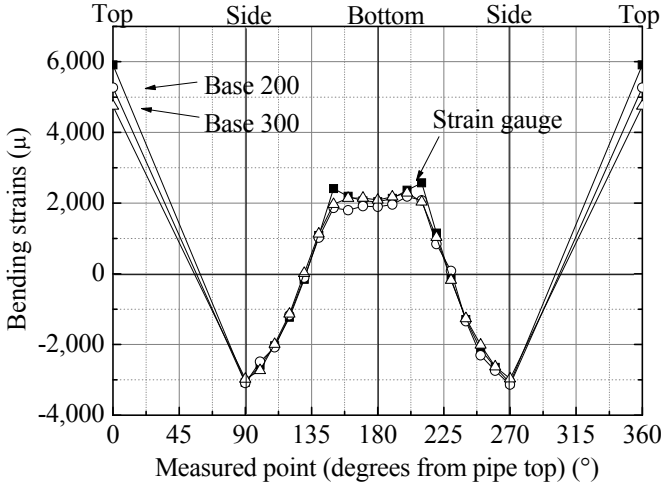

Figure 3.14 Bending strains distribution at 5% of vertical deflection (wall thickness

method decreased because the measured values of r_b were slightly different from the nominal ones as shown in **Figure 3.14**.

3.3.4 Base Length and Pipe Diameter

The base length should be selected according to the pipe diameter. As shown when using the 200 mm base for the ϕ 1200 pipe shown in **Figure3.8**, a too short base increases the errors in the bending strains. The shorter the base, the larger the influence of the errors in *d* on the bending strains.

We calculated how an error of 0.5 mm in *d*, which is assumed to be the typical error

when using the method in fields, affects the bending strains. **Figure 3.15** are obtained from substituting the nominal values and the curvature radius calculated from the 0.5-mm errors in d into r_b and r_a in equation 2.1, respectively. This shows that the errors in bending strains generated by a 0.5 mm error in d. By using **Figure 3.15**, the appropriate base lengths for each pipe diameter were determined in order to keep the error in bending strains below 500 μ (**Table 3.7**). These base lengths are recommended for FRPM pipes.

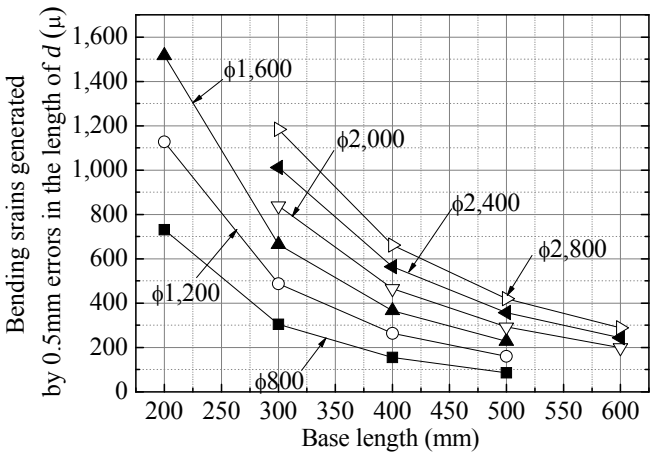

Figure 3.15 Relationship between base lengths and bending strains generated by a 0.5 mm error in the measurement length d.

Table 3.7 Appropriate base lengths for pipe diameters.

Diameter (mm)	Base length (mm)
800～1,100	300
1,200～2,400	400
2,600～3,000	500

3.4 Conclusions

The applicability of the bending strain estimation method for FRPM pipes was verified by conducting parallel-plate loading tests and three-point loading tests. The bending strains obtained with the proposed method were compared to those obtained

using strain gauges at a vertical deflection of 5%. We calculated the bending strains by using the nominal and/or actual values of wall thickness and diameter to examine how the difference between them would affect the accuracy in the estimation of the bending strains. In addition, we propose the appropriate base lengths according to the pipe diameter. The results led to the following conclusions:

1. The proposed method, which was based on the thin-walled assumption, could be applied for FRPM pipes because the relationship among load, deflection and strains observed in the parallel-plate loading test on the FRPM pipes was coherent with that of the thin-walled assumption.

2 When the nominal values of the curvature radius before deformation are used, too short bases increase the errors in the bending strains. Base length should be determined according to pipe diameters.

3 The nominal values of wall thickness were larger than the measured ones; thus, the bending strains calculated using the nominal values were larger than those obtained from the measured ones, which indicate the actual bending strains. However, the influence of such difference is limited, and the bending strains may be estimated with high accuracy even when using the nominal values.

4. The bending strains obtained with the proposed method are almost the same as those given by the strain gauges both in the parallel-plate loading test and the three-point loading one. This implies that the method may be applied even when the pipe deforms locally.

5. The appropriate base lengths for different pipe diameters are proposed based on the calculation of how errors in the measurement lengths affect the accuracy of the proposed method: 300 mm base for ϕ 800–1100 pipes, 400 mm base for ϕ 1200–2400 pipes, and 500 mm base for ϕ 2600–3000 pipes.

References

Ariyoshi, M., Mohri, Y., Hori, T., Matsushima K. and Ueno Kazuhiro: Bending Strain Estimation Method to Verify the Structural Safety of Buried Pipeline, *Irrigation,*

Drainage and Rural Engineering Journal, No.286, 67-75. 2013. (in Japanese)

Idomoto, Y., Miyazaki, T., Yano H. and Nakashima K.: Long-term Performance Tests of Filament Wound (FRPM) pipes, *Journal of the Japanese Society of Irrigaion, Drainage and Reclamation Engineering*, No.75(2), pp.121-124. 2007. (in Japanese)

Japanese Industrial Standards: JIS A 5350 Fiberglass Reinforced Plastic Mortar Pipes. 1984. (in Japanese)

Ministry of Agriculture, Forestry and Fisheries; Design Standard for Irrigation Pipeline. 1977. (in Japanese)

Ministry of Agriculture, Forestry and Fisheries: Manual of Functional Maintenance for Irrigation Pipeline. 2009. (in Japanese)

Okuda, T., Mamiya, S., Murata, H., Okamura, Y. and Hazama, M.; Nondestructive Measurement for Fiberglass Reinforced Plastic Mortar Pipes, Proceedings of FRP con-ex, No.58, pp.19-21, 2013. (in Japanese)

Otsuka, S., Mamiya, S., Mohri, Y. and Ariyoshi, M.: Evaluation of the FRPM Pipe by the Long-term Ultimate Bending Test, Japanese Society of Irrigation, *Drainage and Rural Engineering Conference*, pp.760-761, 2013. (in Japanese)

Timoshenko, S.: Strength of Materials, translated by Udoguchi, T. and Kunio, T., Tokyo Tosho Co., Ltd., pp.351-370. 1957.

Tsuchida, Y., Ito Y. and Utsunomiya J: Investigation of Damage Factors of Fiber Reinforced Plastic Mortar Pipes, Japanese Society of Irrigation, *Drainage and Rural Engineering Conference*, pp.432-433. 2010. (in Japanese)

Ueno, F., Murata, H., Okamura, Y., Okuda, T. and Hazama, M; New Nondestructive Measurement for Fiberglass Reinforced Pastic Mortar Pipes Using Microwave and Photonic Techniques, *Proceedings of electronics society institute of electronics, information, and communication engineers*, pp.199, 2014. (in Japanese)

CHAPTER 4

The contents of this chapter are based on:

Ariyoshi, M., Mohri, Y., Kudo. Y.: Behavior of Liner Applied to Agricultural Pipelines Under Internal Water Pressure and Effect of Filling the Annular, *Geosynthetics Engineering Journal*, 31, pp.143-148 (2016) (in Japanese with English Summary)

Chapter 4

Behavior of Liners Subjected to Internal Pressure and Effect of Filling the Gap Between Existing Pipe and Liner

4.1 Introduction

In Japan, many irrigation pipelines have been used since the 1950s and some of them are now deteriorating. The resulting water leakages cause not only the lacks of stable water supplies but also ground runoffs and traffic problems. However, not all the deteriorated pipelines could be replaced with new ones due to cost and land usage issues.

Recently, the cured-in-place pipe (CIPP) method has been used to renew the deteriorated irrigation pipes. CIPP was developed in the UK in 1971 and brought to our country in the 1980s, where it has been used for sewerages and water supplies. CIPP could be utilized for any land use because it does not need excavations. In the CIPP, a resin-saturated liner is inverted or pulled into an existing pipe and inflated with water to press it in the pipe. Once fully inflated, steam or hot water are filled into the liner to start the hardening of the resin. This technique may be cheaper than the replacing with new pipes.

For sewerage applications of CIPP, some manuals have been issued, such as “Guidelines for design and construction of renewal pipelines” and “Manual for design and construction of renewal pipelines” (JSWA, 2008; JSWA, 2011). However, these

manuals should not be applied to agricultural pipelines because, unlike sewerages, their pipes have many bends, a high water pressure, and little manholes. In some cases of irrigation pipelines, CIPP is expected to be useful for repairing only the joints causing leakages.

Previous researches revealed that the behavior of the liner depends on the soil properties and the existing pipes. Sawada et al. (2014) conducted model tests with polyvinyl chloride (PVC) pipes and steel divided pipes, which simulated the deteriorated existing pipe, and clarified how the divided pipes affect the behavior of the liner. Inoue (2008) conducted model tests with concrete pipes and liner, and showed that the strains of the liner generated by earth pressure were significantly smaller than the failure strains of the liner. He proposed a design of buckling liners as a result of earth pressure.

These researches aimed mainly at investigating the behavior of the liners subjected to external pressure, while the behavior of those subjected to internal pressure has been poorly investigated. Hence, clarifying this second behavior is necessary for an effective design of CIPP for irrigation pipelines.

Thus, we examined how the following three aspects affect the behavior of liners subjected to internal pressure; (1) fulfill of the gap between existing pipe and liner, (2) deterioration of the existing pipe, and (3) bend under thrust force caused by internal pressure. To investigate these three aspects, we conducted a model test by applying internal pressure to a liner inserted into a concrete pipe of a ϕ 1000 diameter.

4.2 Experimental Method

4.2.1 Outline

The cross section and overview of the model test are shown in **Figures 4.1** and **4.2**, respectively. Liner was inserted into ϕ 1000 diameter concrete pipes, which had a longitudinal length of about 11 m and three straight pipes in the middle part of the model test. The central pipe of these three straight ones was divided into four pieces to approximate a deteriorated pipe. The divisions were at the top, bottom, and sides of the pipe, where the concrete and reinforcing bars were completely cut off shown in **Figure**

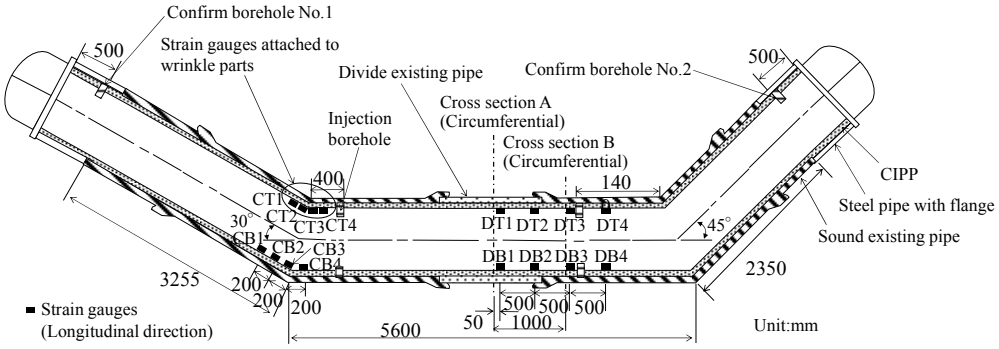

Figure 4.1 Cross section of the model test.

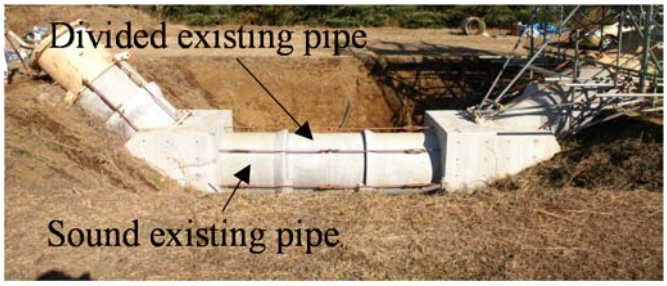

Figure 4.2 Overview of the model test.

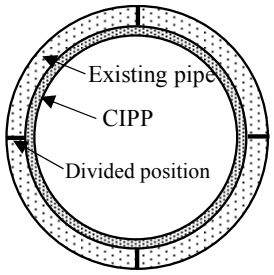

Figure 4.3 Divisions in the existing pipe.

4.3; generally, cracks are likely to occur at these positions due to aging (Serpente, 1994). The divided pipe was fixed with bands to prevent movements during the hardening of the liner shown in **Figure 4.4**, and these bands were loosen during the test applying internal pressure.

The behavior of 30° and 45° bends under thrust forces was examined. Concrete blocks were placed at the bends to prevent their movements. Steel pipes were connected at both ends to fix the lids with flanges.

The liner shrinking due to the temperature change after hardening results in a

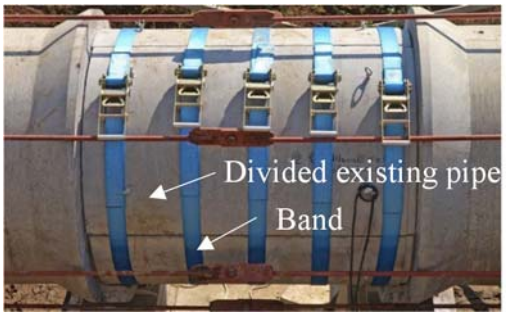

Figure 4.4 Divided existing pipe fixed with bands.

Table 4.1 Material properties of the liner.

Flexural strength	MPa	166
Flexural modulus of elasticity	MPa	9,694
Tensile strength	MPa	94
Tensile modulus of elasticity	MPa	9,682
Tensile breaking elongation	%	2.6
Wall thickness	mm	19.9 (Max 22.4, Min 6.3)
Coefficient of thermal expansion	$\times 10^{-5}$/K	3.0

gap between liner and existing pipe. In fields, the gap may be filled or not. Thus, we conducted tests by applying 1.0 MPa internal pressure under two conditions, one with the gap unfilled and the other with it filled. The pressure applied was gradually increased with a step of 0.1 MPa every 5 minutes.

4.2.2 Liner

The material properties of the liner are shown in **Table 4.1**. The flexural and tensile properties were obtained from JIS K 7171 and JIS K 7161, respectively. Wall thicknesses were measured at every 12° at the pipe end. At the bends, wrinkles occurred at the pipe top shown in **Figure 4.5** because the longitudinal length of the pipe top was shorter than that of the bottom. The maximum heights of the wrinkles at 30° and 45° bends were 80 and 90 mm, respectively.

Figure 4.5 Wrinkles at the bend.

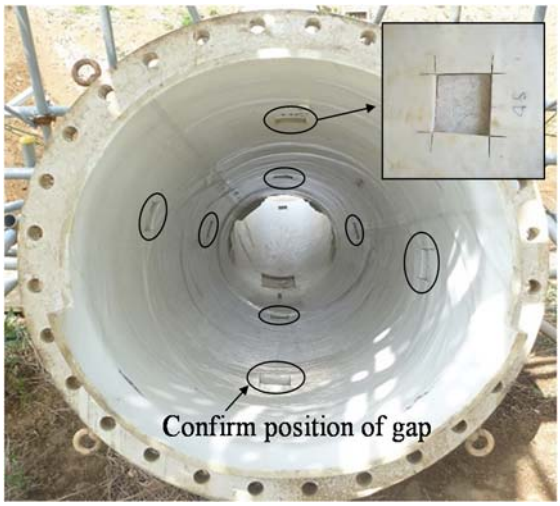

Figure 4.6 Confirm positions of the gaps.

4.2.3 Gap Between Liner and Existing Pipe

Prior to the test of applying internal pressure, another liner was inserted into the same concrete pipes and the gap between them was filled with air-mixed cement milk to examine the thickness of the gap and the possibility of filling it. This preliminary test revealed that the average thickness of the gaps at eight positions shown in **Figure 4.6** was 2 mm, with a maximum of 4 mm and a minimum < 1 mm, and confirmed the possibility of filling the gap with air-mixed cement milk shown in **Figure 4.7**. New liner were inserted for the test of applying internal pressure after removing the one used for this preliminary test.

The air-mixed cement milk consisted of cement (3,136 N), water (2,058 N), and foaming material (34.3 N), with a flow value of 141 mm. The milk was injected from the

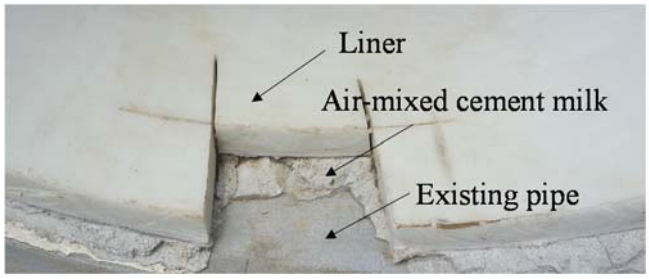

Figure 4.7 Filling the gap between liner and existing pipe.

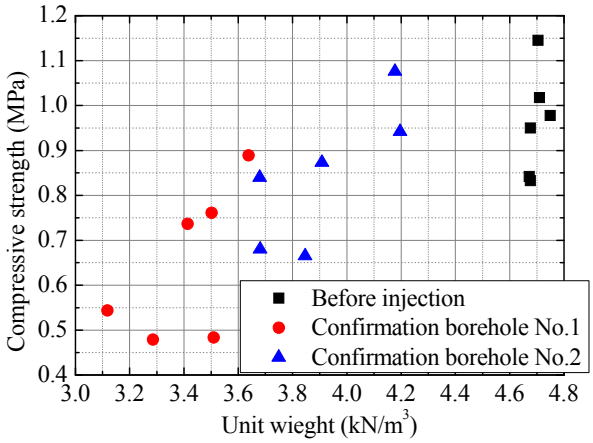

Figure 4.8 Uniaxial compression test results on the air-mixed cement milk.

injection boreholes, and its discharge was confirmed from the two confirm boreholes at 500 mm from the both ends of the liner as shown in **Figure 4.1**. The air-mixed cement milk before injection and that from the confirm boreholes were taken into molds with 500 mm diameter and 100 mm height. Uniaxial compression tests were conducted after hardening it for 10 days. **Figure 4.8** revealed that the air-mixed cement milk from the confirmation boreholes showed unit weights lighter and compression strength smaller than those of the mixture before injection. These results imply that the material separation of the milk may occur during the filling procedure.

4.2.4 Measurements

As shown in **Figure 4.1**, strain gauges were attached to the inner surface of the liner at every 30° from the pipe top at the cross sections A and B to measure the circumferential strains. The concrete pipe was divided at the cross section A, while it was sound at cross section B. Other strain gauges were attached to the inner surface of the

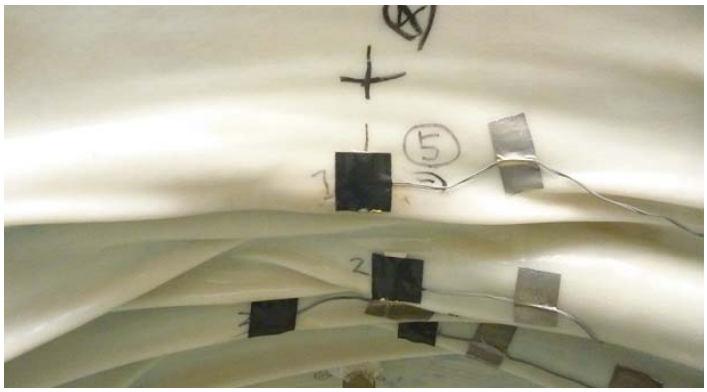

Figure 4.9 Strain gauges at the pipe top (strain gauges were attached under the black tapes).

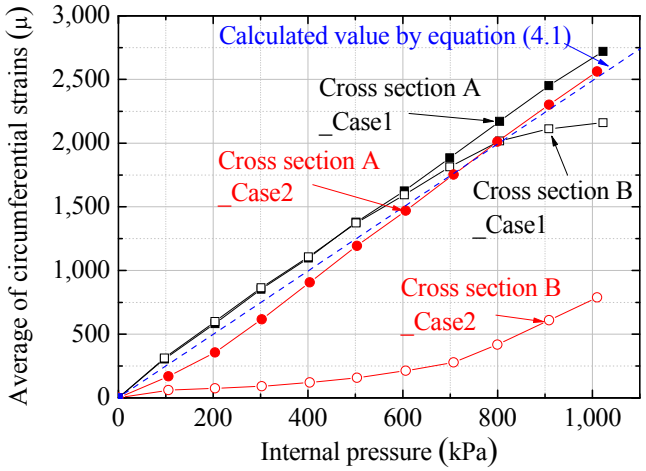

Figure 4.10 Relationship between internal pressure and average circumferential strains.

liner at both straight and bend parts to measure the longitudinal strains. The strain gauges were attached to the wrinkles at the pipe top in bends shown in **Figure 4.9** and at the straight parts both where the concrete pipe was sound and divided.

4.3 Experimental Results

4.3.1 Circumferential Strains

(a) Case1: Without Filling the Gap

Figure 4.10 shows the relationship between the internal pressure and the

average circumferential strains measured using 12 strain gauges attached to the liner at every 30°. The average values at the cross sections A and B increased proportionally with the internal pressure for pressures below 600 kPa. Similar to conventional pipelines, the relationship between strains of the liner and internal pressure can be described by the following equation.

$$\varepsilon = \frac{Hd}{2tE} \tag{4.1}$$

where

ε circumferential strain

H internal pressure

d internal diameter (0.96 m)

t wall thickness (19.9 mm)

E Young's modulus (9.68 GPa)

By using equation 4.1, the strains were calculated to be 1,495 μ at 600 kPa internal pressure, which was almost the same as the average values obtained using the strain gauges (cross section A: 1624 μ, cross section B: 1594 μ).

However, the average strains of cross section B increased only a little at internal pressures higher than 800 kPa. This is because the liner may contact the concrete pipe entirely, and thus, the concrete pipe restrains the liner. The average strain of cross section B was 2,161 μ at an internal pressure of 1 MPa, which corresponded to the compression strain of th liner (2100 μ) by heat shrink calculated from the temperature change (70 °C) after hardening and the linear expansion coefficient ($3.0 \times 10^{-5}K^{-1}$). This implies that the circumferential strains of the liner due to internal pressure may not become larger than the compression ones caused by heat shrink when the existing pipes are sound.

On the other hand, the average strain of cross section A was proportional to internal pressure until its end, meaning that the circumferential strains of the liner due to internal pressure may always follow equation 4.1 even after it contacts the concrete pipes when the existing pipes loose their strength.

As shown in **Figure 4.11** and **Table 4.2**, the circumferential strains due to

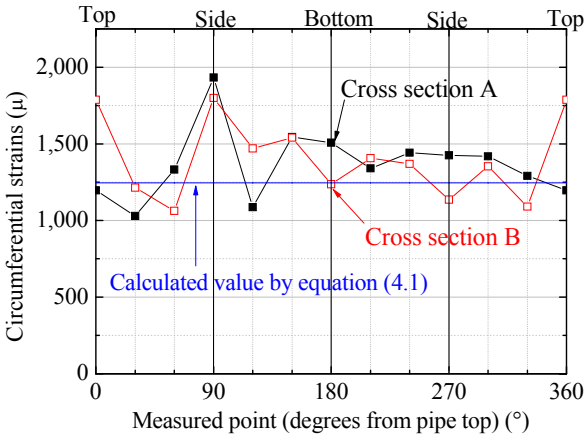

Figure 4.11 Circumferential strains distribution generated by a 500 kPa internal pressure (Case1).

Table 4.2 Average values and standard deviations of the circumferential strains generated by 500 kPa internal pressure.

	Case1		Case2	
	Cross section A	Cross section B	Cross section A	Cross section B
Average	1,379	1,372	1,194	158
Standard deviations	225	236	191	107
Maximum	1,932	1,800	1,560	430
Minimum	1,030	1,062	943	34

internal pressure varied depending on the measuring points. The standard deviations of the cross sections A and B were > 200 μ, and the maximum strain of cross section A was 1.9 times larger than the minimum one. This is because the wall thickness of the liner also differed depending on the measuring points. In addition, the pipe section was not a true circle, which cause not only radial strains but also bending strains due to internal pressure.

(b) Case2: Fulling the Gap

Filling the gap greatly reduces the circumferential strains when the existing pipe is sound. **Figure 4.10** shows that the average strain of cross section B at an internal pressure of 600 kPa in this case (213 μ) was only 13% of that observed in Case1 (1594

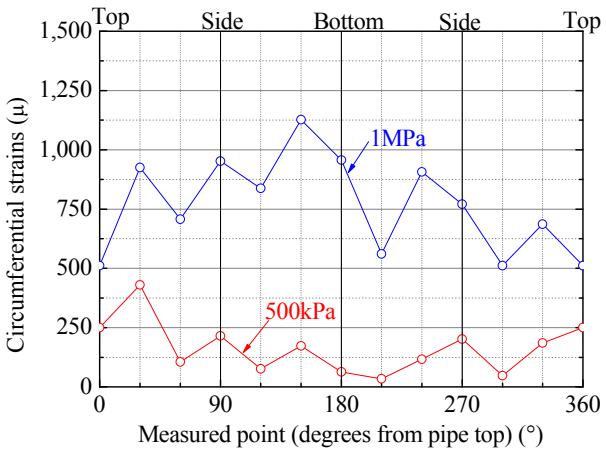

Figure 4.12 Distribution of circumferential strains of cross section B in Case2 (500 kPa and 1.0 MPa).

μ). However, when the internal pressure exceeded about 700 kPa, the strains of cross section B increased more than in Case1. **Figure 4.12** shows that the strains, except at the pipe top and 30°, increased more than three times although the internal pressure doubles. This implies that the behavior of the air-mixed cement milk may be nonlinear in case of compression.

The strains of cross section B greatly differed depending on the measuring points because the air-mixed cement milk may not be injected uniformly. The standard deviation (107 μ) was more than half of the average value (158 μ), and the maximum strain (430 μ) was 12 times larger than the minimum one (34 μ). Even with this variation, filling the gap was effective to reduce the circumferential strains of the liner because the maximum strain (430 μ) was clearly smaller than the minimum strain observed in Case1 (1062 μ).

However, filling the gap could not reduce circumferential strains when the existing pipe is divided. **Figure 4.10** shows that the average strain of cross section A in Case 2 was almost the same as that observed in Case1. Similar to the conventional pipelines, the relationship between strains and internal pressure of the liner always follows equation 4.1.

4.3.2 Longitudinal Strains of Bends

(a) Case1: Without Filling the Gap

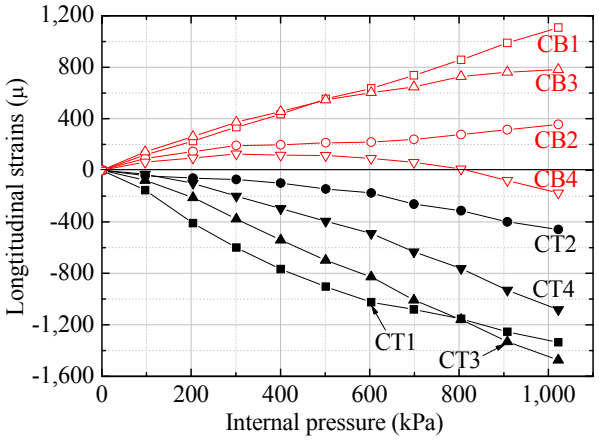

Figure 4.13 Longitudinal strains at the bends (Case1).

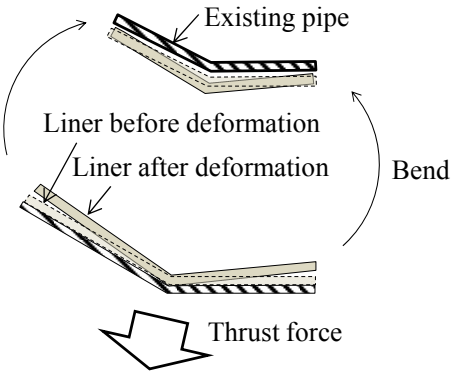

Figure 4.14 Thrust force and deformation of liner at the bend.

As shown in **Figure 4.13**, the longitudinal strains of the liner at the pipe top were in compression and those at pipe bottom were in tension, although these values had variations. At the bends, the thrust force generated by internal pressure was acting on the pipe bottom shown in **Figure 4.14**. The liner might bend as shown in **Figure 4.14** because a 375 kN thrust force, calculate based on the Japanese design standard for irrigation pipelines (MAFF, 2009), was acting on it at an internal pressure of 1.0 MPa. The longitudinal strength should be taken into consideration for the liners subjected to high internal pressures because longitudinal strains at the bends increase proportionally with the internal pressure. The absolute values of the strains at the wrinkles at the pipe top were about the same as those at the pipe bottom.

(b) Case2: Filling the Gap

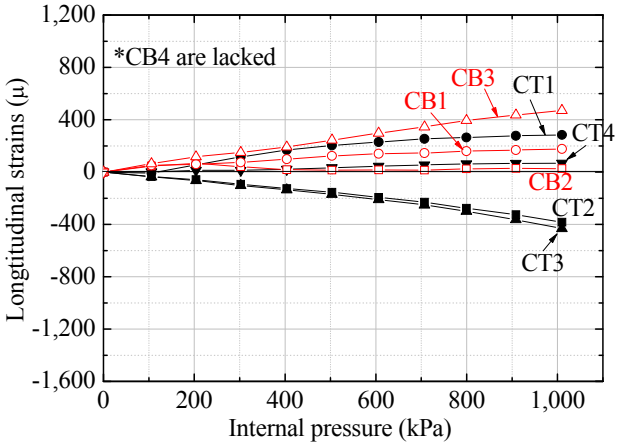

Figure 4.15 Longitudinal strains at the bends (Case2).

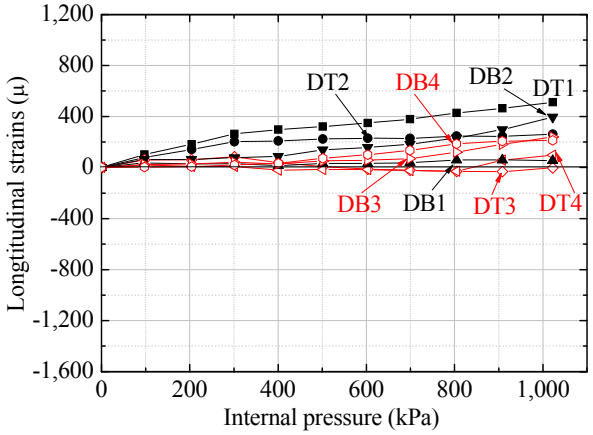

Figure 4.16 Longitudinal strains at the straight portion of the pipe (Case1).

Figure 4.15 revealed that filling the gap reduced the longitudinal strains. The maximum tensile strain (471 μ) was reduced to 42% of that (1109 μ) observed in Case1, and the maximum compression strain (-431 μ) was also reduced to 29% of that (-1474 μ) measured in Case1. Similar to the circumferential strains, filling the gap was effective to reduce the longitudinal strains at the bends because it decreased the space for bending the liner.

4.3.3 Longitudinal Strains of Straight Portion

(a) Case1: Without Filling the Gap

The longitudinal strains at the straight portion shown in **Figure 4.16** were

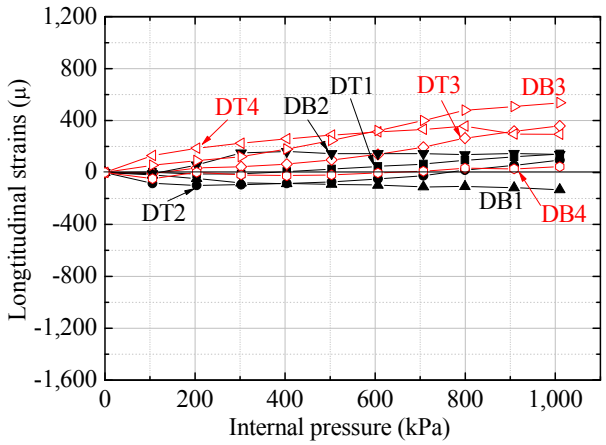

Figure 4.17 Longitudinal strains at the straight portion of the pipe (Case2).

small compared with those at the bends because large forces such as thrust force are not generated from internal pressure in straight portions. Some of the strains were less than 100 μ even when a 1-MPa internal pressure was applied to the liner, and the maximum strain (512 μ) was 35% of that (-1474 μ) observed at the bends. Almost all the strains were in tension because the bends, which may move toward outside due to the thrust force, were near the straight portion.

(b) Case2: Filling the Gap

Figure 4.17 indicated that filling the gap did not particularly change the longitudinal strains at the straight portion. Compared to Case1 shown in **Figure 4.16**, some of the strains increased and others decreases. The maximum strain was almost the same as that observed in Case1. Filling the gaps did not reduce the longitudinal strains at the straight portion because the air-mixed cement milk did not adhere to the liner although it might contact it.

4.4 Conclusions

We conducted a model test by applying internal pressure to a liner inserted into a ϕ1000 diameter concrete pipe to investigate the behavior of the liner. We clarified the influences of filling the gap, deterioration of the existing pipe, and thrust force generated

at the bends on the deformation of liners subjected to internal pressure. The results led to the following conclusions:

1. The circumferential strains of the liner generated by internal pressure follow the classic equation for circumferential stress on thin-wall pipes until the liner is in contact with the existing pipe, generally. After the liner contacts the existing pipe, the circumferential strains increase only a little. In addition, when the liner contact the existing pipe, the circumferential strains may be calculated from the heat shrink of the liner after hardening.

2 Filling the gap between liner and existing pipe greatly reduces the circumferential strains when the existing pipe is sound. However, it is not effective when the existing pipe is divided.

3. Large longitudinal strains may occur at the bends of liners subjected to high internal pressure because longitudinal strains at bends increase proportionally with the internal pressure. Filling the gap is effective to reduce the longitudinal strains at the bends because it decreases the space for bending the liner.

4. No local deformation could be found in the wrinkles at the bends. The absolute values of the longitudinal strains at the wrinkles, which were at the pipe top, were about the same as those at the pipe bottom.

5. Longitudinal strains at the straight portion were small compared with those at the bends. Filling the gaps does not reduce the longitudinal strains at the straight portion, because the air-mixed cement milk does not adhere to the liner although it may contact it.

References

Inoue, Y.: A Study on the Structural Behavior and Design of CIPP Liner for Sewerage, Osaka City University, Ph.D. thesis, 2007. (in Japanese)

Japan Sewage Works Association: Manual of Design and Construction Management for Pipe Rehabilitation, 2008. (in Japanese)

Japan Sewage Works Association: Guideline of Design and Construction Management for Pipe Rehabilitation, 2011. (in Japanese)

Ministry of Agriculture, Forestry and Fisheries; Design standard for irrigation pipeline. 2009. (in Japanese)

Sawada, Y., Sonoda, Y., Ono, K., Inoue, K., Mohri, Y., Ariyoshi, M. and Kawabata, T: Influence of Damage Levels of Outer Aging Pipes on Mechanical Behavior of Rehabilitated Pipes, *Irrigation, Drainage and Rural Engineering Journal*, No.291, pp.157-163. 2014 (in Japanese)

Serpente, R.,F.: Understanding the Modes of Failure for Sewers, *Urban Drainage Rehabilitation Programs and Techniques*, ASCE, 1994.

CHAPTER 5

The contents of this chapter are based on:

Ariyoshi, M., Mohri, Y.: Behavior of a Liner Subjected to Internal and External Pressures and the Design Method of a Liner Considering an Existing Pipe, *Irrigation, drainage and rural engineering journal*, 303, pp.I_209-I_221 (2016) (in Japanese with English Summary)

Chapter 5

Behavior of Liners Subjected to External and Internal Pressures and the Design Method of a Liner Considering an Existing Pipe

5.1 Introduction

The cured-in-place pipe (CIPP) method, which consists in inserting a resin-saturated liner into an existing pipe and hardening it by steam or hot water, has been recently used to renew deteriorated irrigation pipelines. Some manuals of rehabilitation methods, including CIPP, for deteriorated sewerages have been issued because CIPP has been used for this purpose since 1980s, prior to its use for irrigation pipelines. However, these manuals should not be simply applied to irrigation pipelines as mentioned in section 4.1.

CIPP has been used in water supply facilities to restore hydraulic performances such as water flow capacity and to prevent the generation of red water by rust. Thus, CIPP could be used for the existing pipes whose strength is sound (JWWA, 2012). On the other hand, CIPP could be used in irrigation pipelines to renew an existing pipe regardless of its strength because it improves not only hydraulic but also structural performances. Thus, dedicated manuals about liners considering the deteriorated existing pipes are required.

Some researches were carried out on the behavior of rehabilitation pipes, including liners subjected to external loads. Takahashi et al. (2002) conducted model tests using a ϕ250 diameter high-density polyethylene pipe surrounded by a damaged pottery pipe and centrifuge tests using a 40 diameter polyvinyl chloride (PVC) pipe surrounded by a damaged aluminum pipe. They showed that deteriorated existing pipes reduce the strains and deflections of the rehabilitation ones. Mohri et al. (2005) conducted model tests to examine how the thickness of the filling material and divisions number of the existing pipe affect the behavior of rehabilitation pipes. He showed that rehabilitation pipe, having a thin filling material deforms more with the increase of the divisions number, while those with a thick filling material deforms less and regardless of the divisions number. Inoue (2008) conducted loading tests using a 300 diameter liner surrounded by a concrete pipe buried at a cover depth of 600 mm. He found that the strains of the liner induced by a T-25 truck load are much smaller than the failure strains of the liner, even when the concrete pipe has cracks at the top, bottom, and sides. He also proposed a design of liner buckling by soil and water pressure. Sawada et al. (2014) conducted loading tests using ϕ300 diameter PVC pipes surrounded by divided steel pipes buried in sand. They demonstrated that the position of the divisions affects the behavior of the rehabilitation pipe and that large strains occur when there are cracks at the top, bottom, and sides of the pipe. In the previous researches, existing pipes may deform or not the rehabilitation ones because the behavior of the rehabilitation pipes may be sensitive to the conditions of the existing pipes. This suggests that existing pipes should be modeled carefully.

Thus, we conducted loading tests using true liners surrounded by concrete pipes, which reproduced deteriorated existing pipes, buried in sand to examine how a deteriorated existing pipe affect the behavior of the liner. We cracked the concrete pipes at the top, bottom, and sides, where cracks usually occur as pointed out by Serpente (1994) using parallel-plate loading tests or cut them from the outer surface to the reinforcing bars to reproduce the deterioration of existing pipes. The case of cutting the reinforcing bars assumes the worst scenario, in which the reinforcing bars break due to rust after cracks formation. We propose a structural design of liner that considers a deteriorated existing pipe based on the experiment results.

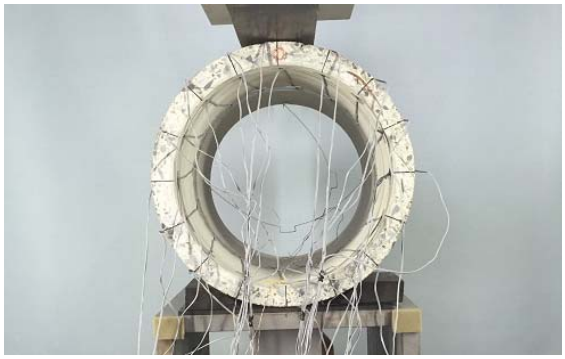

Figure 5.1 Parallel-plate loading test.

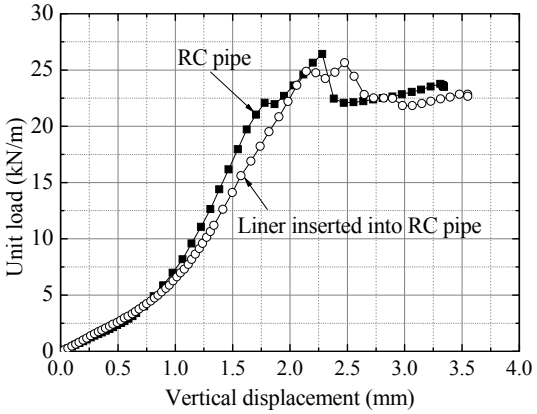

Figure 5.2 Results of the parallel-plate loading test

5.2 Experimental Method

5.2.1 Pipe Specimens

Reinforce concrete (RC) pipes, liners, and other liners inserted into the RC pipes were used as pipe specimens. The RC pipe had an inner diameter of 300 mm, a wall thickness of 30 mm, and reinforcing bars in the middle of the wall. The reinforcing bars were normal iron wires with a ϕ3.2 diameter, the main ones were placed at every 32 mm in the longitudinal direction and the distributing ones at every 36° in the circumferential direction. A parallel-plate loading test shown in **Figure 5.1** was conducted on the RC pipe and **Figure 5.2** shows its peak strength found to be 26.4 kN/m.

The liner had an outer diameter of 307 mm, a wall thickness of 6.2 mm, and and

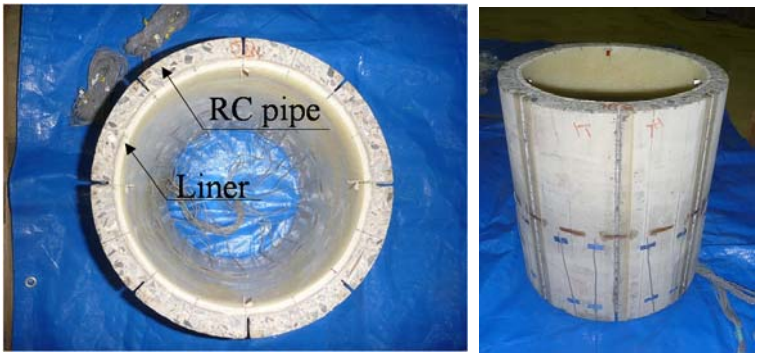

(a) Cross section (b) Longitudinal section

Figure 5.3 Pipe specimen with the reinforcing steel bars cut off.

Figure 5.4 Non-woven fabric between existing pipe and liner.

a Young's modulus of 9.0 GPa as obtained from the parallel-plate loading test. For the case of the liner inserted into the cracked RC pipe, a parallel-plate loading test with the load applied at 1 mm from the displacement at peak strength was conducted to crack the RC pipe shown in **Figure 5.2**. In the test, cracks occurred at top, bottom, and sides of the pipe. For the other cases of the liner inserted into the cracked RC pipe, we cut the RC pipe from the outer surface to the reinforcing bars at four or eight positions (See the ditches in **Figure 5.3**). These cases suppose that the reinforcing bars break due to rust after cracks formation.

In some cases, a non-woven fabric was placed between liner and RC pipe shown in **Figure 5.4** to examine how it would affect the behavior of the liner. The thickness of the non-woven fabric before and after being sandwiched between liner and RC pipe was 7 mm and 1–3mm, respectively.

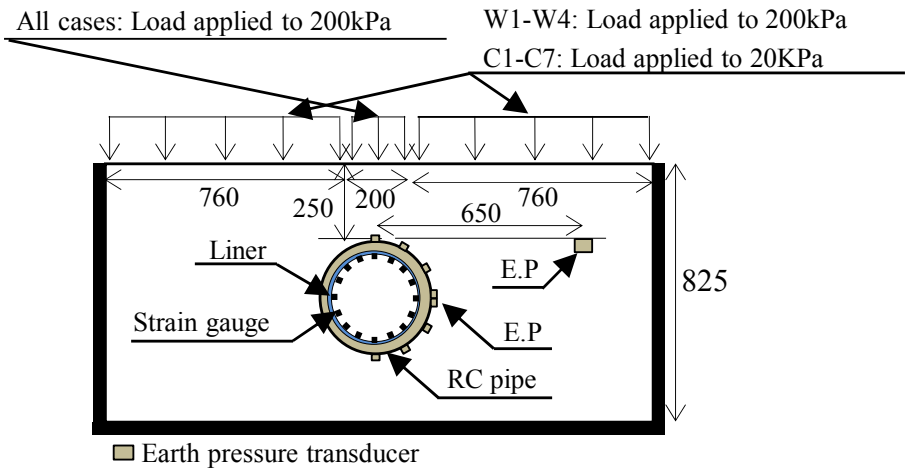

Figure 5.5 Cross section of the model test.

5.2.2 Model Test

As shown in **Figure 5.5**, the pipe specimens were buried at a cover depth of 250 mm in a steel soil tank having a length of 1720 mm, a height of 825 mm, and a width of 400 mm. Toyoura sand was used and it had a relative density of 35–39%, which was the same as the dry density of 1.46–1.47 g/cm^3 of sand, to reproduce the poor conditions of backfill materials.

5.2.3 Test Case

Table 5.1 shows the test cases. A uniformly distributed pressure of 200 kPa was applied on the whole ground surface for the W1–W4 cases. For the C1–C7 cases, locally distributed pressures of 200 kPa and 20 kPa were applied on the ground surface above the pipe and excluding it, respectively as shown in **Figure 5.5**. The distributed pressures, which were applied using airbags, were gradually increased of 10 kPa every 5 minutes.

An internal pressure of 100 kPa was also applied to the liner at the distributed loads of 0, 70 120, and 170 kPa. The internal pressure was applied with an airbag having a longitudinal length of 280 mm and being installed inside the middle of the liner. The internal pressure was gradually increased of 20 kPa every 3 minutes.

5.2.4 Measurements

Table 5.1 Experimental parameters.

Case	Loading condition	Pipe specimen	RC pipe condition	Nonwoven fabric
W1_L_N	Uniformly (W)*	Liner (L)*	-	Present (N)*
W2_R	Uniformly	RC (R)	Cracked	-
W3_LR	Uniformly	Liner, RC	Cracked	Absent
W4_LR8_N	Uniformly	Liner, RC	Cut off 8 rebar (8)*	Present
C1_L	Locally (C)*	Liner		-
C2_R4	Locally	RC	Cut off 4 rebar (4)*	-
C3_R8	Locally	RC	Cut off 8 rebar	-
C4_LR4	Locally	Liner, RC	Cut off 4 rebar	Absent
C5_LR4_N	Locally	Liner, RC	Cut off 4 rebar	Present
C6_LR8	Locally	Liner, RC	Cut off 8 rebar	Absent
C7_LR8_N	Locally	Liner, RC	Cut off 8 rebar	Present

* （） abbreviated expressions in the case name

Case	Residual wall thickness of existing pipe (mm)							
	0°	45°	90°	135°	180°	225°	270°	315°
W1_L_N								
W2_R								
W3_LR								
W4_LR8_N	9.6	8.3	10.0	9.9	11.0	11.3	10.7	11.9
C1_L								
C2_R4	13.2		10.8		10.3		14.1	
C3_R8	8.6	8.6	11.3	8.4	9.4	11.6	7.9	6.9
C4_LR4	11.0		11.0		9.8		6.7	
C5_LR4_N	10.9		9.0		10.3		12.1	
C6_LR8	9.5	10.4	9.5	12.8	8.3	12.4	9.8	9.7
C7_LR8_N	8.8	9.2	9.8	9.4	9.9	12.3	10.3	9.4

The vertical and horizontal deflections were measured using displacement transducers installed inside the pipe specimen at 50 mm from their end because the airbags were placed in the middle of the pipes. The deflections in W2, C2, and C3 cases were those of the RC pipe and in the other cases were those of the liner.

The circumferential strains were measured using strain gages attached to the inner surface of the liner at every 22.5° shown in **Figure 5.5**. Additional strain gages were attached to the outer surface of the liner only in the W1 and C1 cases because the RC pipe was not used for these ones.

In addition, normal earth pressures acting on the pipes were measured with earth pressure transducers attached to the outer surfaces of the pipe specimens at every 30° shown in **Figure 5.5**. In the cases using cracked or ditched RC pipes, two earth pressure transducers were attached at 5° except that at the pipe side because they could not be attached to cracked or ditched positions. Soil pressures were also measured at the same height of the cover depth in sand.

5.3 Experimental Results

5.3.1 Deflections

a) Uniformly Distributed Pressure

Cracked RC pipes hardly deflected, as shown in the cases W2 and W3 in **Figure 5.6**, when the ground surface pressure was 200 kPa. This implies that cracked RC pipes could carry earth pressures if the reinforcing bars are sounds. On the other hand, the RC pipe cracked at the top and bottom at ground surface pressures of just 70–80 kPa when the reinforcing bars were cut at eight positions (case W4). After the RC pipe was divided, the liner started to deflect. However, the divided RC pipe could carry the earth pressures, which were applied before the pipe was divided, because only a little deflection occurred right after its division. After being divided, when the ground surface pressure increased from 70 to 200 kPa, the deflection increased by 3.1 mm, which was almost the same as that of the case with only the liner (W1). The result suggests that the liner alone may carry the incremental pressure applied after the division of the RC pipe.

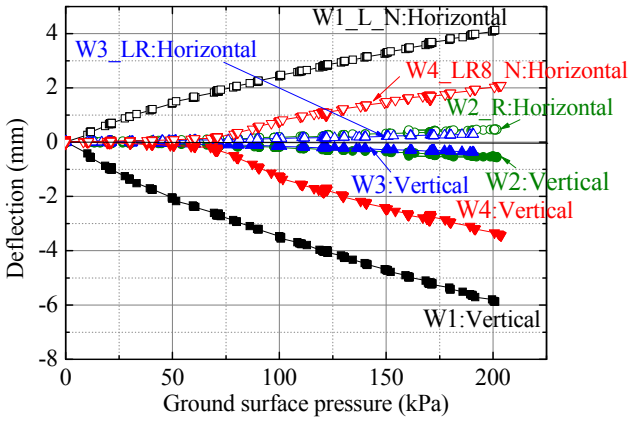

Figure 5.6 Relationship between ground surface pressures and deflections (uniformly distributed pressure).

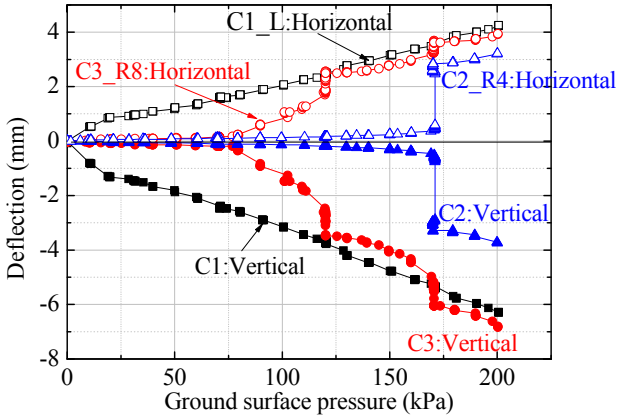

Figure 5.7 Relationship between ground surface pressures and deflections (locally distributed pressure, C1–C3 cases).

b) Locally Distributed Pressure

The RC pipes cracked and divided at the top, bottom, and sides at ground surface pressures of 170 and at 80 kPa in cases C2 and C3, respectively in **Figure 5.7**. Although the liners started to deflect after the RC pipes divided, the pipes did not collapse even at the 200-kPa ground surface pressure; the soil around the RC pipes could have prevented the collapse of the divided pipes. The increment of the deflection in case C3 was clearly larger than that in C1 when the ground surface load increased from 80 to 120 kPa. This implies that most of the earth pressure applied on the liner inserted into the

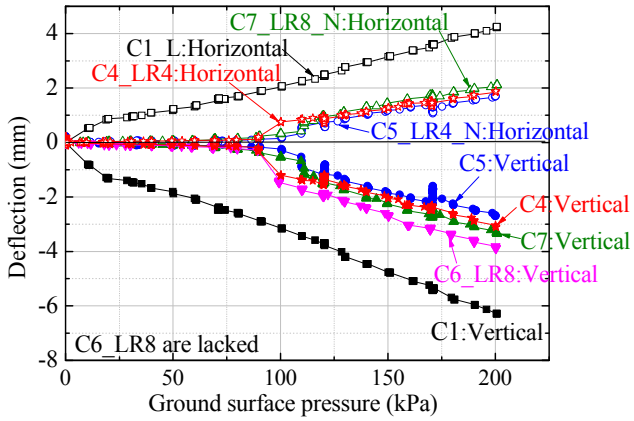

Figure 5.8 Relationship between ground surface pressures and deflections (locally distributed pressure, C1 and C4–C7 cases).

divided RC pipe may be carried by the liner itself because the divided RC pipe deflects more than liner.

Internal pressures increased deflections because the divided pipes could not withstand the hoop stresses generated by them. As shown in **Figure 5.7**, the deflections increased rapidly when internal pressures are applied at 170kPa and 120kPa in the Cases C2 and C3, respectively.

Figure 5.8 indicated that the RC pipes cracked and divided at the top, bottom, and sides at ground surface pressures of 90–110 kPa when the liner inserted into the RC pipes with the reinforcing bars cut (cases C4–C7). The divided RC pipes may carry most of the earth pressure, which was applied before their division, even after being divided because little deflections occurred at the time of their divisions. On the other hand, the liners may carry most of the earth pressure applied after its division because the increment of deflections after that in cases C4–C7 was almost the same as that in case C1.

In addition, the non-woven fabric did not affect the deflection of the liner, as there was no clear difference among the C4–C7 cases shown in **Figure 5.8**.

5.3.2 Earth Pressure Acting on Pipes

a) Uniformly Distributed Pressure

The vertical earth pressure acting on the pipe top in case W3 was clearly larger than that in case W1 because in the second case the liner deflected, the arch effect

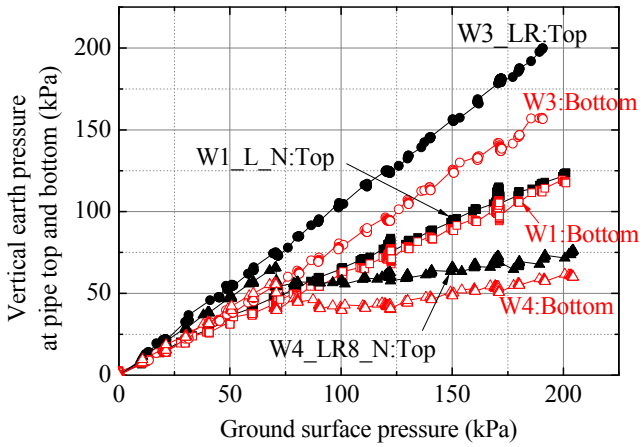

Figure 5.9 Relationship between ground surface pressures and vertical earth pressures (uniformly distributed pressure, pipe top and bottom).

occurred, and the vertical earth pressure acting on the pipe top decreased as shown in **Figure 5.9**. Before the RC pipe cracked (70 kPa) in case W4, the vertical earth pressure acting on its top was almost the same as that in case W3. After the RC pipe cracked, the vertical earth pressure acting on the pipe top increased less than that before the cracking because the stiffness of the RC pipe decreased rapidly due to the cracks. The vertical earth pressure in case W2, which was almost the same as that in case W3, was omitted.

Unlike the vertical earth pressure, **Figure 5.10** showed that the horizontal earth pressure acting on the pipe side in case W1 was clearly larger than that in case W3 because passive earth pressure was generated by the deflection of the pipe. In case W4, before the RC pipe cracked (70 kPa), the horizontal earth pressure acting on the pipe side was small But, after the cracking, it increased more than that before the cracking because the pipe started to deflect.

As shown in **Figure 5.11** Normal earth pressures acting on the pipe top in case W3 were much larger than those acting on the other parts because the RC pipe had a high stiffness. On the other hand, normal earth pressures acting on the pipe top in case W1 were smaller than those acting on the other parts because the deflection of the liner generated horizontal earth pressure due to a low stiffness. In case W4, the normal earth pressure distribution before the RC pipe cracked (70 kPa) was almost the same as that in case W3, while the distribution after the RC pipe cracked (170 kPa) was almost the same as that in case W1. This suggests that a liner inserted into a RC pipe behaves like a rigid

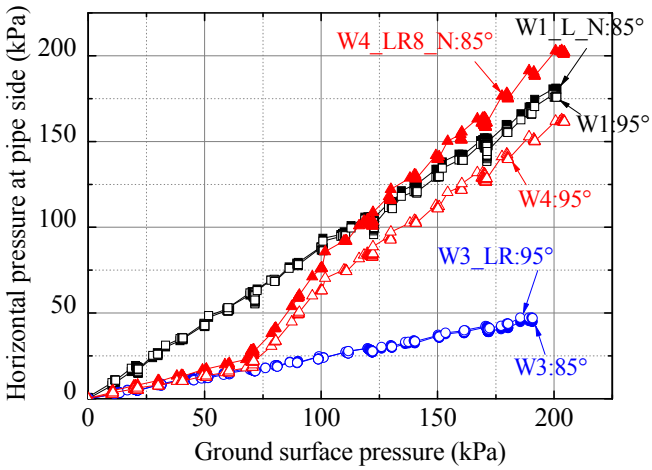

Figure 5.10 Relationship between ground surface pressures and horizontal earth pressures (uniformly distributed pressure, pipe side).

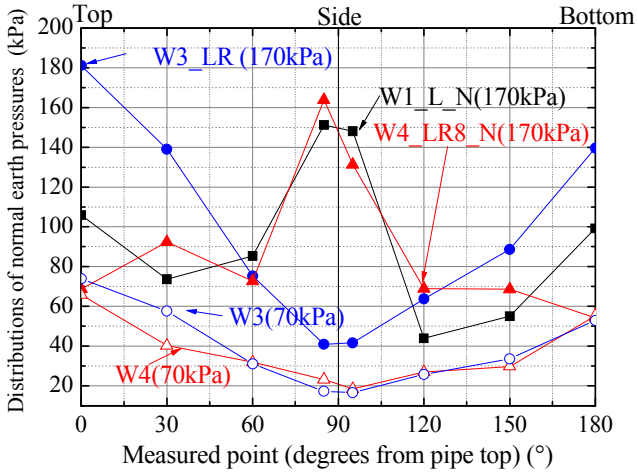

Figure 5.11 Normal earth pressures distribution (uniformly distributed pressure).

pipe when the RC pipe is not divided, and that it behaves like a flexible pipe when the RC pipe is divided.

b) Locally Distributed Pressure

After the RC pipe cracked (90–110 kPa) in cases C4, C5, and C6, the vertical earth pressure increased less than that before the cracking because the ring stiffness decreased rapidly as shown in **Figure 5.12**. On the other hand, the vertical earth pressure in case C7 did not clearly change after the RC pipe cracked. The soil pressure transducer

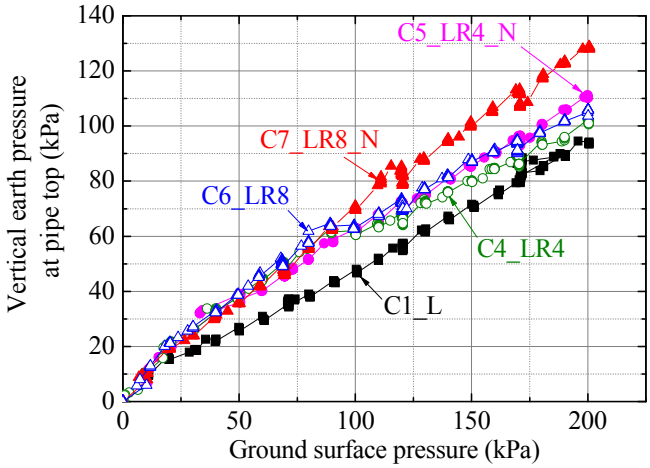

Figure 5.12 Relationship between ground surface pressures and vertical earth pressures (locally distributed pressure, pipe top).

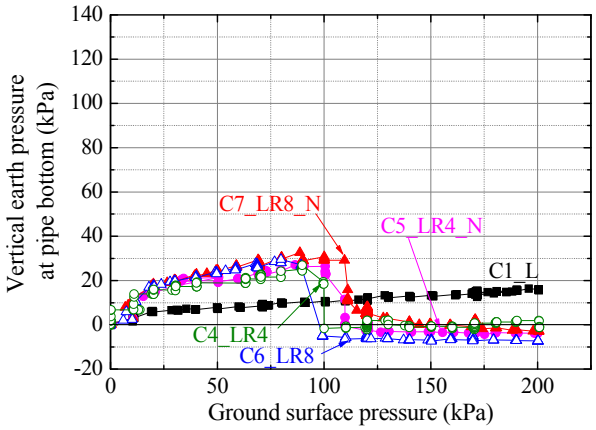

Figure 5.13 Relationship between ground surface pressures and vertical earth pressures (locally distributed pressure, pipe bottom).

may have not measured the real soil pressure on the pipe top because the deflection, the normal earth pressure at the pipe bottom and side, and the strains distribution in case C7 were similar to those in cases C4–C6.

Figure 5.13 shows that **t**he vertical earth pressure at the pipe bottom in cases C4–C7 decreased to about 0 kPa after the RC pipe cracked because the bottom of the RC pipe may have deformed in the convex toward the liner. Thus, the RC pipes and liners may have had strong contacts at the pipe bottom.

After the RC pipe cracked in cases C4–C7, the horizontal earth pressure

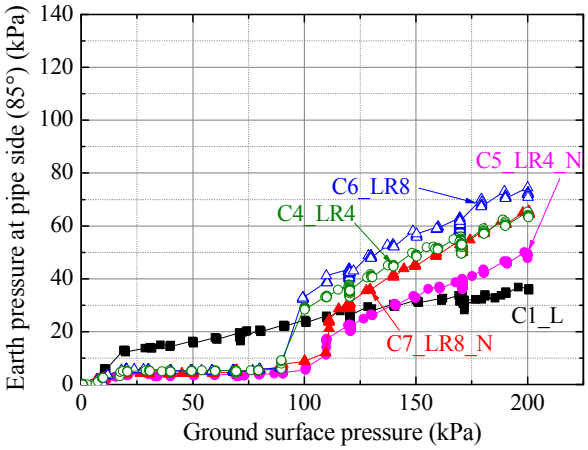

Figure 5.14 Relationship between ground surface pressures and horizontal earth pressures (locally distributed pressure, pipe side).

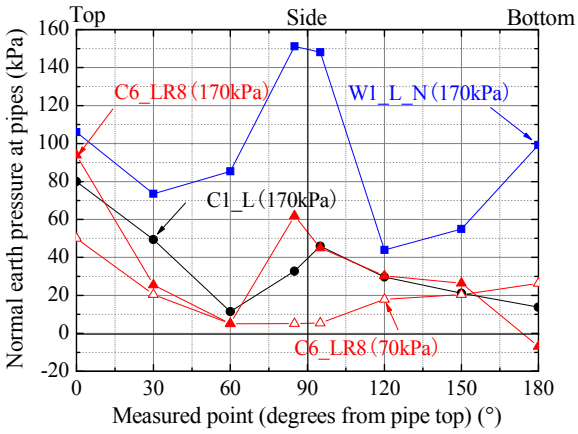

Figure 5.15 Normal earth pressures distribution (locally distributed pressure).

increased more than that before the cracking because the pipe specimen starter to deflect shown in **Figure 5.14** and the deflection generated passive earth pressures.

Figure 5.15 shows that the normal earth pressure acting on the pipe side in case C1 was much smaller than that in case W1 although the deflections in the two cases were almost the same. This may be because the soil stiffness around the pipe sides in case C1, in which the ground surface pressure was applied only to the ground surface above the pipe, was smaller than that in case W1, in which the ground surface pressure was applied to the whole ground surface, due to the different load conditions. The horizontal earth pressure in case C6 increased due to the deflections after the RC pipe cracked.

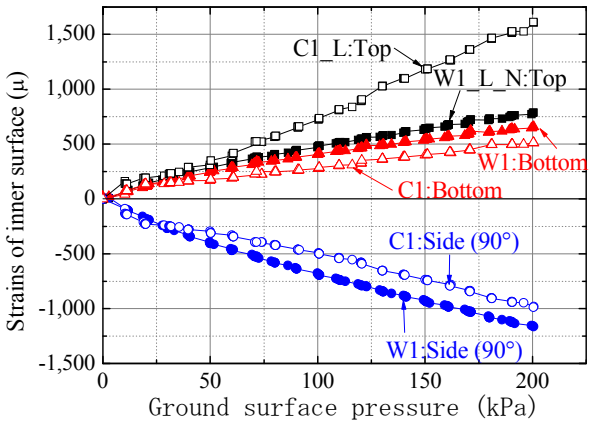

Figure 5.16 Relationship between ground surface pressures and strains of the inner surface (pipe top, bottom, and side).

5.3.3 Strains of the Liner

a) Liner Without RC Pipe

Figure 5.16 shows the relationship between ground surface loads and strains of the liner. The strains, which are elastic, generated by internal pressure were removed, also in the **Figures 5.19–5.21**, because this section is dedicated to the discussion of those generated by external pressure.

Figure 5.16 shows that the strains of the liner were highly dependent on the loading conditions. The strains of the pipe top due to locally distributed pressure (case C1) were larger than those due to uniformly distributed pressure (case W1) because the horizontal earth pressure, which decreased the strains of the pipe top, in C1 was clearly smaller than that in case W1. **Figure 5.17** shows the radial strains in case W1 were larger than those in case C1 because the pressures acting on the overall pipe in case W1 were larger than those in case C1. **Figure 5.18** shows that the strains of the pipe top were more than three times those of the pipe bottom in case C1, although they were almost the same in case W1.

b) Liner Inserted Into the RC Pipe

Figure 5.19 shows that the strains of liner started to increase after the RC pipe cracked (70 kPa) in case W4. The strains of the pipe side, with respect to those of the pipe

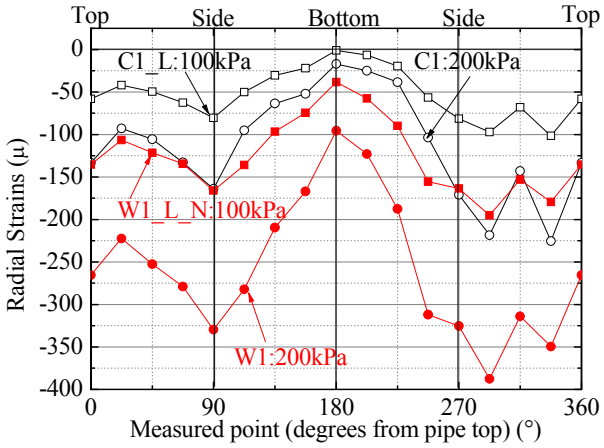

Figure 5.17 Radial strains distribution.

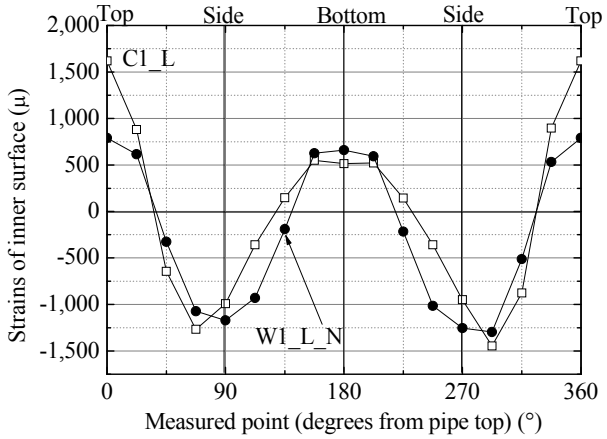

Figure 5.18 Distribution of the circumferential strains of the inner surface

top and bottom in case W4, were smaller than those in case W1. This implies that the earth pressure acting on the liner in case W4 may have been small because the cracked RC pipe could have carried some of the earth pressure, as Takahashi et al. pointed out (Takahashi et al., 2002).

In the cases of locally distributed pressure, the strains of the liner at the pipe top started to increase after the RC pipe cracked as shown in **Figure 5.20**. The strains after the division of the RC pipe in 8 (C6 and C7 cases) tended to increase more than those after the division in 4 (C4 and C5 cases). As described in sections 5.4.3 and 5.4.4, the number of divisions may influence the strains rather than the deflections. The strains of the liner at the pipe top in case C1 increased much more than those in the other cases,

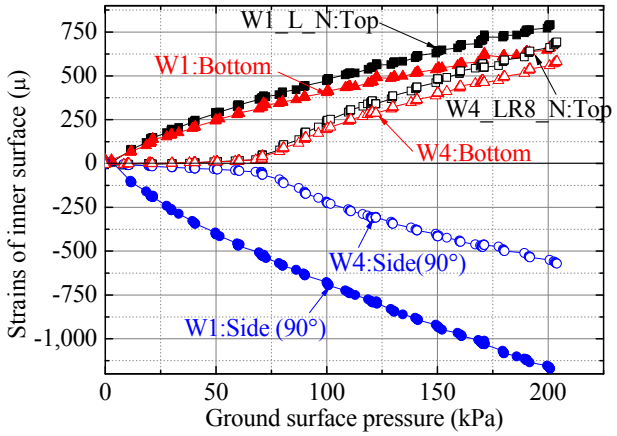

Figure 5.19 Relationship between ground surface pressures and strains of the inner surface (uniformly distributed pressure, pipe top, bottom, and side).

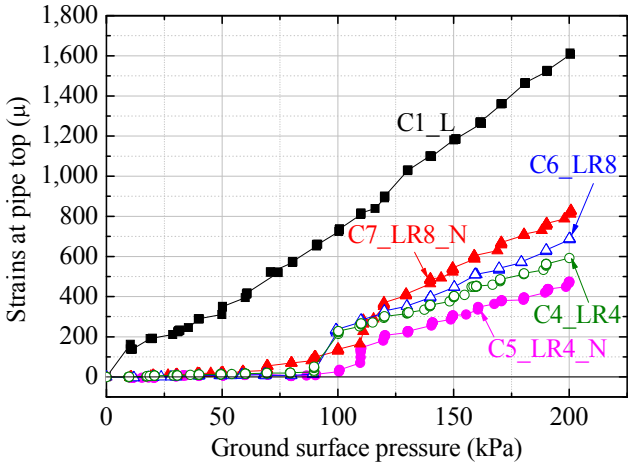

Figure 5.20 Relationship between ground surface pressures and strains at the pipe top (locally distributed pressure).

which means that the RC pipe could carry some of the earth pressures. On the other hand, the strains of the liner at the pipe bottom in case C1 increased less than those in the other cases after the division of the RC pipe as shown in **Figure 5.21**. In the other cases, the earth pressures were transmitted to the liner from the RC pipe through the contact area, which was assumed to be small, between them even if those acting on the liner were smaller than those in case C1.

Figure 5.22 shows the distribution of the strains of the liner under the 200 kPa ground surface pressure. In case C1, the maximum strain in compression occurred at

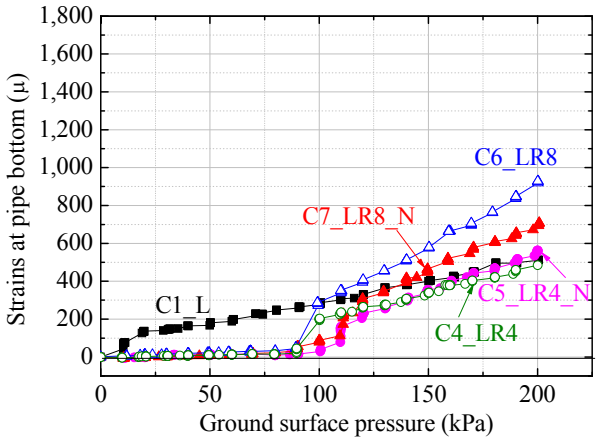

Figure 5.21 Relationship between ground surface pressures and strains at the pipe bottom (locally distributed pressure).

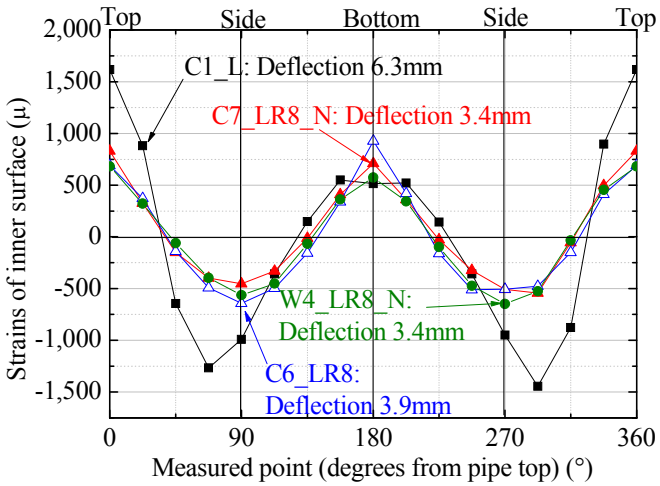

Figure 5.22 Distribution of the circumferential strains of the inner surface (200 kPa).

slightly above the pipe side, and the strain of the pipe top was twice that of the bottom. In cases C6 and C7, the maximum strain in compression also occurred at the pipe side, but the strain of the pipe top was almost the same as that of the bottom. Despite the locally distributed pressure, the strains distribution for the upper part of the pipe was symmetrical to that of the lower part. Similar to the cases C6 and C7, in the case of uniformly distributed pressure (W4), the strain distribution for the upper part was symmetrical to that of the lower one.

In addition, the non-woven fabric did not affect the strains of the liner, as there

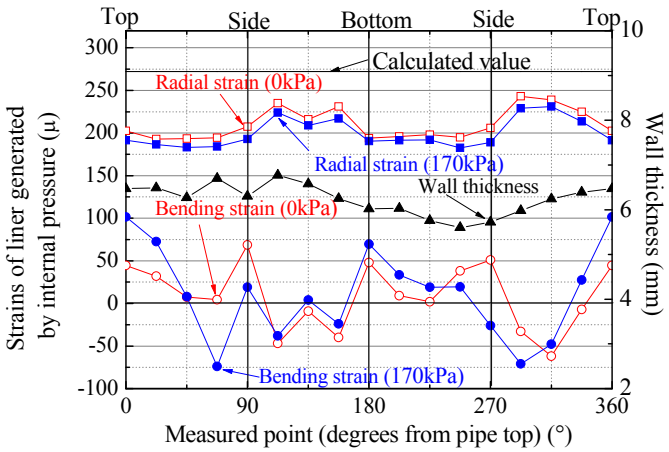

Figure 5.23 Distribution of the strains generated by internal pressure (C1–L cases).

was no clear difference among the C4–C7 cases shown in **Figures 5.20** and **5.21**.

c) Strains Generated by Internal Pressure

Figure 5.23 shows the radial and bending strains generated by an internal pressure of 100 kPa at 0 and 170-kPa ground surface pressures in case C1. The radial strains were calculated to average the circumferential strains of the inner and outer surfaces. The bending strains of the inner surface were calculated to subtract the radial strains from the circumferential ones of the inner surface. **Figure 5.23** also shows the wall thicknesses.

Figure 5.23 shows that the strains due to the internal pressure at the 170 kPa ground surface pressure were slightly lower than those at the 0 kPa one. Earth pressure acting on the pipe may have reduced the strains due to internal pressure. **Figure 5.24** showed that the liner inserted into the RC pipe could have also been inflated due to the internal pressure because there were small gaps between liner and RC pipe due to the shrink after hardening. The division of the RC pipe may have changed the strains distribution because the distribution at 70 kPa, before the RC pipe cracked, was different from that at 120 kPa, after the RC pipe cracked. However, the difference was small and local deformations could not be found.

In addition, the non-woven fabric did not affect the strains of the liner due to internal pressure, as no clear difference attributable to it was observed.

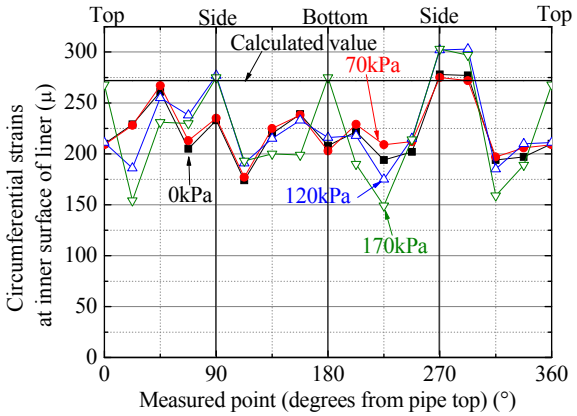

Figure 5.24 Distribution of the strains generated by internal pressure (C6–LR8 cases).

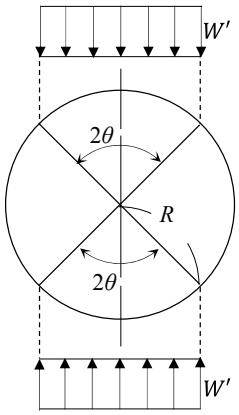

Figure 5.25 Distribution of the vertical earth pressures acting on the liner.

5.4 Design of Liner Considering the Existing Pipe

5.4.1 Vertical Earth Pressure

After the RC pipes are divided, which is assumed to be the worst scenario, earth pressures start acting on the liners. The distribution of the earth pressures acting on the liner may be vertically symmetrical, as shown in **Figure 5.25,** because the strain distribution of the liner is vertically symmetrical even in the case of locally distributed pressure shown in **Figure 5.22**. Earth pressures may be transmitted to the liner from the RC pipe through an area of 2θ, where the contact between them is strong.

A divided RC pipe could carry some of the earth pressures acting on it before

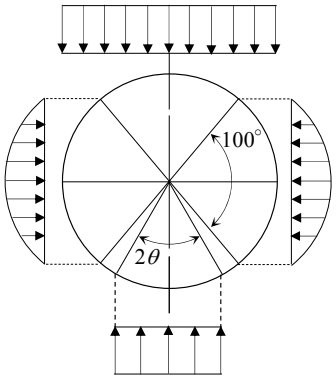

Figure 5.26 Distribution of the earth pressures acting on the flexible pipe in the current design.

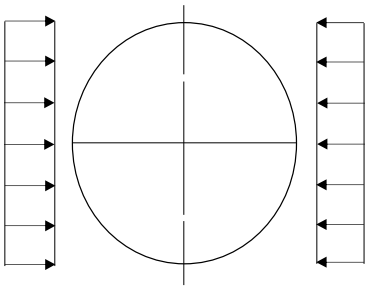

Figure 5.27 Distribution of uniform horizontal earth pressures.

its division shown in **Figures 5.6** and **5.8**, but not the increased ones after it has divided. All the increased pressures may be transmitted to the liner.

5.4.2 Horizontal Earth Pressure

The earth pressures acting on flexible pipes in the conventional design for irrigation pipelines were evaluated as shown in **Figure 5.26** (MAFF, 2009). Horizontal earth pressures assumed to be proportional to the deflection of the pipe, the distribution is parabolic, and the maximum pressure occurs at the pipe side. However, Tohda and Yoshimura (1999) conducted centrifuge tests and numerical analyses on buried pipelines, and proposed that the horizontal earth pressures depend on the buried conditions and that those acting on the pipe side are nearly uniform shown in **Figure 5.27** in the buried conditions that we adopted in our research.

In the strains evaluation in section 5.4.7, in which the maximum strain and

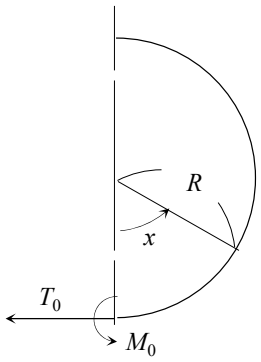

Figure 5.28 Bending moment and radial force acting on the pipe.

deflection were calculated from the earth pressures, the distributions of the horizontal earth pressures are assumed to be parabolic and uniform.

5.4.3 Maximum Stress Calculated from the Vertical Earth Pressure

The maximum stress generated from the proposed vertical earth pressure shown in **Figure 5.25** can be calculated using the Castigliano's theorem. The distribution of the vertical earth pressures is vertically symmetrical, and thus, the maximum stress occurs at the pipe top and bottom.

The moment (M) at the position of the angle x counterclockwise from the pipe bottom generated by the vertical earth pressure shown in **Figure 5.25** can be obtained as follows.

When $x = 0 \sim \theta$ and $x = \pi - \theta \sim \pi$,

$$M = M_0 - T_0 R(1 - \cos x) - \frac{W' R^2}{2} \sin^2 x \tag{5.1}$$

When $x = \theta \sim \pi - \theta$,

$$M = M_0 - T_0 R(1 - \cos x) - W' R^2 \sin\theta \left(\sin x - \frac{\sin\theta}{2} \right) \tag{5.2}$$

where

M_0 moment at the pipe bottom

T_0 radial force at the pipe bottom

R curvature radius

Figure 5.28 shows the moment and the radial force. The strain energy (U) by moment is

$$U = \int_0^{\pi} \frac{M^2}{2EI} R dx \tag{5.3}$$

where

E Young's modulus

I moment of inertia of area

Because the earth pressures acting on the pipe are symmetrical, the pipe does not rotate and move. According to the principle of least work, the rotation angle at the pipe bottom $i = 0$; thus,

$$i = \frac{\partial U}{\partial M_0} = \int_0^{\pi} \frac{M}{EI} \frac{\partial M}{\partial M_0} R dx = \frac{R}{EI} \int_0^{\pi} M dx = 0 \tag{5.4}$$

Since $\int_0^{\pi} M dx = 0$,

$$\int_0^{\theta} \left\{ M_0 - T_0 R(1 - \cos x) - \frac{W' R^2}{2} \sin^2 x \right\} dx +$$

$$\int_{\theta}^{\pi-\theta} \{ M_0 - T_0 R(1 - \cos x) - W' R^2 \sin\theta \left(\sin x - \frac{\sin\theta}{2} \right) \} dx +$$

$$\int_{\pi-\theta}^{\pi} \{ M_0 - T_0 R(1 - \cos x) - \frac{W' R^2}{2} \sin^2 x \} dx = 0 \tag{5.5}$$

Since the horizontal movement of the pipe bottom $\delta_b = 0$

$$\delta_b = \frac{\partial U}{\partial T_0} = \int_0^{\pi} \frac{M}{EI} \frac{\partial M}{\partial T_0} R dx = -\frac{R^2}{EI} \int_0^{\pi} M(1 - \cos x) dx = 0 \tag{5.6}$$

Since $\int_0^{\pi} M(1 - \cos x) dx = 0$,

$$\int_0^{\theta} \left\{ M_0 - T_0 R(1 - \cos x) - \frac{W' R^2}{2} \sin^2 x \right\} (1 - \cos x) dx$$

$$+ \int_{\theta}^{\pi-\theta} \{ M_0 - T_0 R(1 - \cos x) - W' R^2 \sin\theta \left(\sin x - \frac{\sin\theta}{2} \right) \} (1 - \cos x) dx$$

$$+ \int_{\pi-\theta}^{\pi} \{ M_0 - T_0 R(1 - \cos x) - \frac{W' R^2}{2} \sin^2 x \} (1 - \cos x) dx = 0 \tag{5.7}$$

M_0 and T_0 can be derived from the equations 5.5 and 5.7 as follows.

$$M_0 = W' R^2 \frac{1}{\pi}\left(\frac{\theta}{2} + \theta\sin^2\theta + \frac{3}{2}\sin\theta\cos\theta - \frac{\pi\sin^2\theta}{2}\right) \tag{5.8}$$

$$T_0 = 0 \tag{5.9}$$

The moment is the maximum at the pipe top and bottom. From equations 5.1, 5.8, 5.9, and x = 0 or π, we obtain

$$M = W' R^2 \frac{1}{\pi}\left(\frac{\theta}{2} + \theta\sin^2\theta + \frac{3}{2}\sin\theta\cos\theta - \frac{\pi\sin^2\theta}{2}\right) \tag{5.10}$$

When W is assumed to be the earth pressure acting on the existing pipe, we have

$$W' = \frac{W}{\sin\theta} \tag{5.11}$$

where

W' Vertical earth pressure acting on liner

This is because the vertical earth pressure acting on RC pipes is assumed to be transmitted to the liner through the contact area (2θ) between them shown in **Figure 5.25**. By substituting equation 5.11 into equation 5.10, we obtain

$$M = W R^2 \left\{\frac{1}{\pi\sin\theta}\left(\frac{\theta}{2} + \theta\sin^2\theta + \frac{3}{2}\sin\theta\cos\theta - \frac{\pi\sin^2\theta}{2}\right)\right\} = K_1 W R^2 \tag{5.12}$$

where K_1 is the part of { }. Stress can be calculated to divide the moment by the section modulus, and substituting 0–90° to θ provides K_1 shown in **Figure 5.29** and **Table 5.2**; for example, the stress for a 30° contact area is 2.1 times larger than that for a 180° one. **Table 5.2** also shows K_1 obtained from the conventional vertical earth pressure for reference.

5.4.4. Horizontal Deflection Calculated from the Vertical Earth Pressure

Similar to the maximum stress, the horizontal deflection generated by the proposed vertical earth pressure shown in **Figure 5.25** can be calculated using the Castigliano's theorem. The moment at the position of A (M_1) generated by the horizontal load (H) at the pipe side shown in **Figure 5.30** is as follows.

$$M_1 = \frac{HR}{2}\left(\cos x - \frac{2}{\pi}\right) \qquad x = 0 \sim \frac{\pi}{2} \tag{5.13}$$

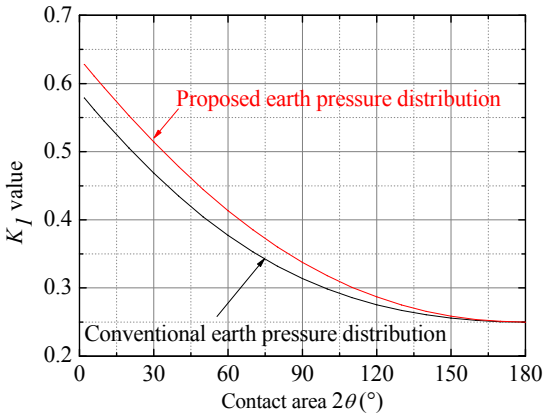

Figure 5.29 K_1 values calculated from the proposed vertical earth pressures (stress).

Table 5.2 K_1 values used for stress calculations.

Bedding angle and contact angle (2θ)	30°	60°	90°	120°	180°
K_1 calculated from the proposed earth pressure distribution	0.514	0.414	0.338	0.287	0.25
K_1 calculated from the conventional earth pressure distribution	0.468	0.377	0.314	0.275	0.25

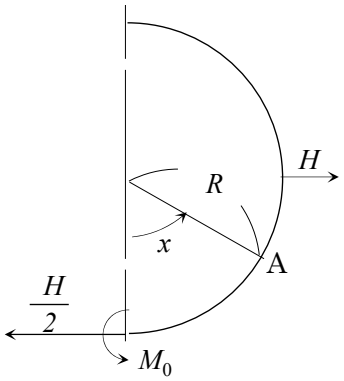

Figure 5.30 Horizontal load, bending moment, and radial load acting on the pipe.

$$M_1 = -\frac{HR}{2}\left(\cos x + \frac{2}{\pi}\right) \qquad x = \frac{\pi}{2} \sim \pi \qquad (5.14)$$

The horizontal movements Δx at the pipe side are calculated from M using the Castigliano's theorem and equation 5.3

$$\Delta x = \frac{\partial U}{\partial H} = \int_0^{\pi} \frac{M}{EI}\frac{\partial M}{\partial H} R dx \tag{5.15}$$

By substituting M obtained 5.1, 5.2, 5.8, 5.9, 5.13, 5.14 into equation 5.15 and $H = 0$, we obtained

$$\Delta x = \frac{W' R^4}{EI}\left\{\frac{1}{2}\left(-\frac{4}{3}\sin^3\theta - \sin\theta\cos^2\theta + \frac{\theta}{\pi} + \frac{3}{\pi}\sin\theta\cos\theta + \frac{2}{\pi}\theta\sin^2\theta\right)\right\} \tag{5.16}$$

By substituting equation 5.11 into equation 5.16, we obtain

$$\Delta x = \frac{WR^4}{EI}\left\{\frac{1}{2\sin\theta}\left(-\frac{4}{3}\sin^3\theta - \sin\theta\cos^2\theta + \frac{\theta}{\pi} + \frac{3}{\pi}\sin\theta\cos\theta + \frac{2}{\pi}\theta\sin^2\theta\right\} = \frac{WR^4}{EI}K\right. \tag{5.17}$$

where K is the part of { }. Substituting 0–90° to θ provides K shown in **Figure 5.31** and **Table 5.3**; for example, the deflection for a 30° contact area is 1.6 times larger than that for a 180° one. The contact area affects the strains more than the deflections.

5.4.5 Maximum Stress Calculated from the Uniformly Horizontal Earth Pressure

The moment of the pipe bottom due to the uniformly earth pressure shown in **Figure 5.27** is the same as that of the pipe side at $\theta = 90°$ in **Figure 5.25**. Thus, by substituting $x = \frac{\pi}{2}$, $\theta = \frac{\pi}{2}$ into equations 5.2, 5.8, and 5.11, the moment M is obtained:

$$M = -0.250 W R^2 \tag{5.18}$$

The value -0.166 is used for the coefficient (-0.250) of the conventional design for irrigation pipelines.

5.4.6 Horizontal Deflection Calculated from the Uniformly Horizontal Earth Pressure

The moment due to the uniformly horizontal pressure is calculated from the moment of $\theta = 90°$ shown in **Figure 5.25** using the equations 5.1, 5.8, and 5.9. In **Figure 5.27**, the pipe bottom and the horizontal earth pressure are assumed as 0° and P, then we obtain

$$M = M_0 - \frac{PR^2}{2}\cos^2 x \tag{5.19}$$

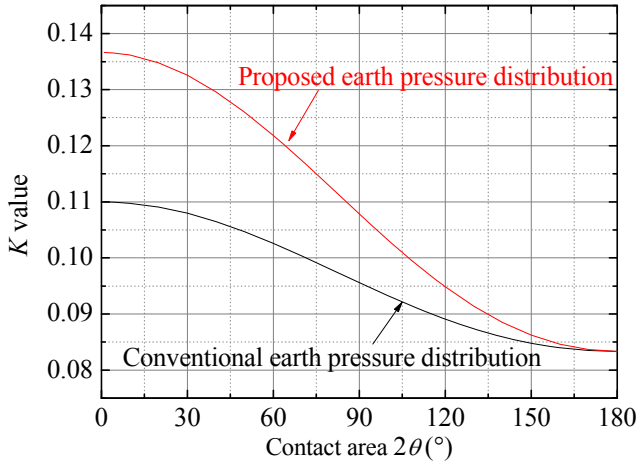

Figure 5.31 *K* values calculated from the proposed vertical earth pressures (deflection).

Table 5.3 *K* values used for deflection calculations.

Bedding angle and contact angle (2θ)	30°	60°	90°	120°	180°
K calculated from the proposed earth pressure distribution	0.133	0.122	0.108	0.095	0.083
K calculated from the conventional earth pressure distribution	0.108	0.103	0.096	0.089	0.083

To calculate the displacement of the load application direction, the direction of H is assumed to reverse in **Figure 5.30**.

$$M_1 = -\frac{HR}{2}\left(\cos x - \frac{2}{\pi}\right) \qquad x = 0 \sim \frac{\pi}{2} \tag{5.20}$$

$$M_1 = \frac{HR}{2}\left(\cos x + \frac{2}{\pi}\right) \qquad x = \frac{\pi}{2} \sim \pi \tag{5.21}$$

By substituting M obtained equations 5.8, 5.19, 5.20, 5.21 into equation 5.15 and $H = 0$, we obtain

$$\Delta x = \frac{PR^4}{EI} 0.0833 \tag{5.22}$$

The relationship between the horizontal displacements at the pipe side Δx_1 is the modulus of the passive resistance of the side fill e as follows.

$$P = e\frac{\Delta x_1}{2} \tag{5.23}$$

By substituting equation 5.23 into equation 5.22, we obtain

$$\Delta x = \frac{0.083}{2}\frac{e\Delta x_1 R^4}{EI} \tag{5.24}$$

This is the horizontal displacement on the half section. Thus, the displacement Δx_2 on both sections is as follows.

$$\Delta x_2 = 0.083\frac{e\Delta x_1 R^4}{EI} \tag{5.25}$$

The value 0.061 is used for the coefficient (0.083) of the conventional design for irrigation pipelines.

5.4.7 Evaluations of the Strains Calculated from the Proposed Earth Pressure

We compared the strains, which were obtained to divide the stress by the Young's modulus, calculated from the proposed earth pressure and those experimentally obtained. The contact area between liner and existing pipe depends mainly on the condition of the existing pipe; thus, 90°, 100°, 110°, 120°, and 180° were assumed as different contact areas. The distribution of the horizontal earth pressures was assumed to be parabolic and uniform.

The strains at the 200 kPa ground surface pressure in case W4 were calculated from the passive resistance of *e*, which was determined so that the horizontal deflection calculated was the same as that experimentally obtained. Because the deflection of the liner increases mainly with the increment of the ground surface load after the division of the existing pipe, the increment of ground surface pressure after the division of the RC pipe (130 kPa, thereby RC pipes crack at 70 kPa) was used for the vertical earth pressure in the calculations. The vertical earth pressure measured at the pipe top using the earth pressure transducers, as shown in **Figure 5.5** (110 kPa), was used in the calculations.

Although the increment of the vertical earth pressure after the division of the RC pipe was used for the vertical earth pressure in the calculations, some of the vertical earth pressure before the pipe division may act to the liner. When the RC pipes divided,

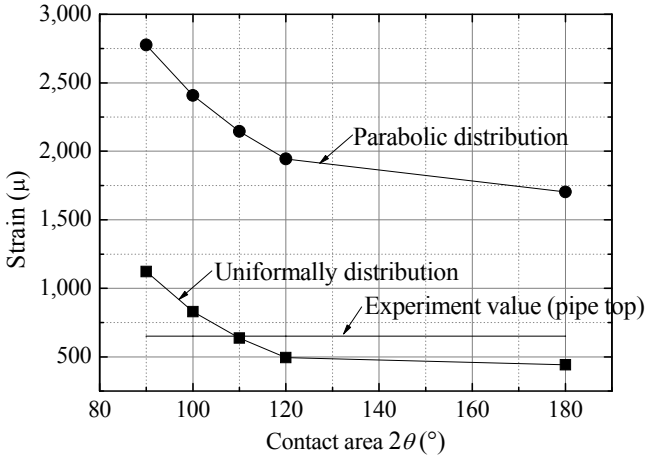

Figure 5.32 Strains calculated from the proposed earth pressures.

the deflections of the liners with existing pipes (cases C4–C7) increased less than half of that of the liner without existing pipes (case C1) as shown in **Figure5.8**. Thus, considering all the vertical earth pressures acting on the RC pipe before its division as the vertical earth pressure acting on the liner is too conservative. Half of the vertical earth pressures acting on the RC pipe before its division may be sufficient for the vertical earth pressure acting on the liner in the design. However, all the vertical earth pressures acting on the RC pipe after its division should be considered as the vertical earth pressure acting on the liner.

Figure 5.32 shows that the strains calculated using the parabolic horizontal earth pressure were much larger than those obtained in the experiments, even when the contact area was 180°. On the other hand, the strains calculated using the uniformly horizontal earth pressure were smaller than those obtained in the experiments when the contact was larger than 110°. The distribution of the horizontal earth pressures acting on the liner may be closer to the uniformly horizontal earth pressure than to the parabolic one.

5.5 Conclusions

RC pipes, liners, and liners inserted into RC pipes were buried in sand, and ground surface pressure and internal pressures were applied to investigate how deteriorated

existing pipes affect the behavior of the liners. Based on the experimental results, we proposed a new design of liners considering the existing pipes. The results led to the following conclusions:

1. A liner inserted into cracked RC pipes does not deform. Liner starts deforming after the reinforcing bars break and the RC pipes is divided. The behavior of the liners inserted into divided RC pipes is close to that of flexible pipes.
2. Divided RC pipes could carry most of the earth pressure acting on them before their division. However, they could not carry the incremented earth pressure acting on them after their division. The most of the increment may be transmitted to the liners.
3. The vertical earth pressure acting on the liner may be vertically symmetrical because the strains of the liner are vertically symmetrical despite the loading conditions.
4. The maximum strain and horizontal deflection were calculated from the proposed earth pressure distribution on the liner for the design of liners considering existing pipes. The comparison of calculated and experimental strains suggested that the horizontal earth pressure may be closer to the uniformly horizontal earth pressure than to the parabolic one.
5. The number of divisions of the RC pipes affect strains more than deflections.
6. The divided RC pipe does not significantly affect the strains of the liner due to internal pressure.
7. The non-woven fabric does not affect the behavior of the liner due to external and internal pressures.

References

Inoue, Y.: A Study on the Structural Behavior and Design of CIPP Liner for Sewerage, Osaka City University, Ph.D. thesis, 2007. (in Japanese)

Japan Sewage Works Association: Manual for Pipe Rehabilitation, 2001. (in Japanese)

Japan Sewage Works Association: Manual of Design and Construction Management for Pipe Rehabilitation, 2008. (in Japanese)

Japan Sewage Works Association: Guideline of Design and Construction Management

for Pipe Rehabilitation, 2011. (in Japanese)

Japanese Society of Irrigation, Drainage and Rural Engineering: Commentary on the design standard for irrigation pipeline. 1978. (in Japanese)

Japan Water Works Association: Guideline of Waterworks Facility Design. 2012. (in Japanese)

Ministry of Agriculture, Forestry and Fisheries; Design standard for Irrigation Pipeline. 2009. (in Japanese)

Mohri, Y., Hazama, M., Makino, T. and Inoue K.: Mechanical Behavior for Renewal pipe, Proceedings of Japan National Conference on Geotechnical Engineering, 40th, pp.1911-1912, 2005. (in Japanese)

Sawada, Y., Sonoda, Y., Ono, K., Inoue, K., Mohri, Y., Ariyoshi, M. and Kawabata, T: Influence of Damage Levels of Outer Aging Pipes on Mechanical Behavior of Rehabilitated Pipes, *Irrigation, Drainage and Rural Engineering Journal*, No.291, pp.157-163. 2014 (in Japanese)

Serpente, R.,F.: Understanding the Modes of Failure for Sewers, *Urban Drainage Rehabilitation Programs and Techniques*, ASCE, 1994.

Takahashi, Y., Li, L., Deguchi, T., Yamada, K. : A Study on the Bedding Effects of the Deteriorated Existing Pipe on the Flexible Rehabilitated Pipe and its Mechanism, *Journal of Japan Sewage Works Association Research journal*, No471, pp.103-113, 2002. (in Japanese)

Tohda J. and Yoshimura H.: Proposal of a Rational Design Method for Buried Flexible Pipes, *Proceedings of Japan Society of Civil Engineerings*, No.617, pp.49-63, 1999. (in Japanese)

CHAPTER 6

The contents of this chapter are based on:

Ariyoshi, M., Izumi A. and Kawabata T.: Evaluation of Circumferential Strain of Low Stiffness Buried Pipe Subjected to Both Internal Pressure and External Load, *Irrigation, drainage and rural engineering journal*, 306, pp. I_95-I_103 (2018) (in Japanese with English Summary)

Chapter 6

Evaluation of Circumferential Strains of Low Stiffness Buried Pipes Subjected to Both External and Internal Pressures

6.1 Introduction

Irrigation pipelines have been widely used since the 1960s in Japan, and the main ones built by the government are longer than 7500 km. Polyvinyl chloride (PVC) pipes, steel pipes, ductile iron pipes (DCIP), fiberglass reinforced plastic mortal (FRPM) pipes, and concrete (RC and PC) pipes are used for irrigation pipelines. The Japanese design standard for irrigation pipelines (MAFF,2009) is based mainly on the works by Marston and Anderson (1930) and Spangler (1941). The ring stiffness is determined so that the stress and deflection, which are calculated from the assumed earth pressure acting on the pipes, are reduced below the allowable values. The design can be applied to the low stiffness PVC pipes (hereafter called VU pipes).

The Japan Institute of Country-ology and Engineering (1980) conducted a research about a buried VU pipe subjected to traffic load. Traffic loads of 8–12 tons were applied to ϕ500 diameter VU pipes buried at cover depths of 1–5 m. The researchers showed that the deflections and strains of the VU pipe generated by external pressure

were less than those calculated using the design. Nakajima and Kawaguchi (1988) measured the deflections and earth pressures for ϕ200 and ϕ500 diameter VU pipes buried at a cover depth of 2 m to investigate how the construction method and the ground conditions affect the modulus of passive resistance of soil. However, they did not examine the detailed behavior of VU pipes because their purpose was to confirm the applicability of the design based on the Marston and Spangler theories. Regarding the strains, only the circumferential ones of the inner surface were measured, while the radial strains were ignored. Izumi et al. (2014) examined the behavior of flexible pipes with same ring stiffness and different wall thicknesses. They showed that the radial stress was larger for thinner wall thicknesses and that uneven radial stress may occur in loose sand when the wall thickness is thin. The behavior of the pipe due to the external pressure was examined in the research, while that due to the internal pressure, which acts on irrigation pipelines, was not clarified.

The objective of our research is to clarify the detailed behavior of low stiffness flexible pipes subjected to external and internal pressures. We buried VU pipes and PVC duct pipes (hereafter called duct pipes), which are commonly used for light drainage, fume and exhaust applications, and measured the strains of the inner and outer surfaces of these pipes to which we applied external and internal pressures.

6.2 Experimental Method

6.2.1 Outline

As shown in **Figure 6.1**, the pipe specimens are buried at a cover depth of 350 mm in Toyoura sand (ρ_s = 2.672 g/cm^3, $\rho_{d\max}$ = 1.685 g/cm^3, $\rho_{d\min}$ = 1.371 g/cm^3) in a soil tank having a length of 1,774 mm, a height of 825 mm, and a depth of 400 mm. **Table 6.1** shows the test cases by changing ring stiffness and soil density. VU and duct pipes shown in **Table 6.2** were used, and the relative densities of the soil were 36–39% (loose sand) and 59–61% (dense sand).

Airbags were placed on the ground surface to apply the external pressure and fixed with steel lids installed above them shown in **Figure 6.2**. H beam steels were placed

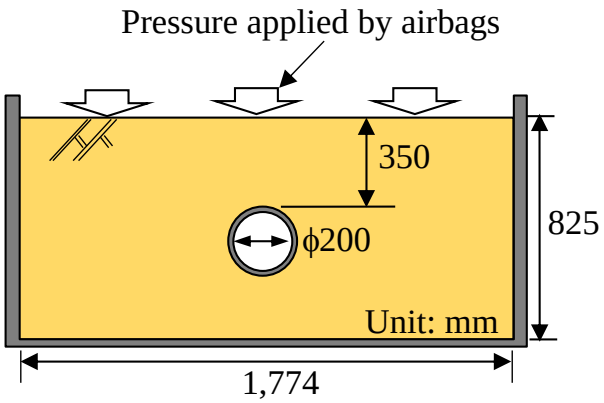

Figure 6.1 Cross section of the model test.

Table 6.1 Experimental conditions.

Case	Testing Pipe	Dry density g/cm^3 (Relative density)
Case1	VU	1.548 (61%)
Case2	VU	1.478 (39%)
Case3	Duct	1.541 (59%)
Case4	Duct	1.471 (36%)

Table 6.2 Characteristics of the pipe specimens.

Type	Wall thickness (mm)	Mean diameter (mm)	Young's modulus (GPa)	Ring stiffness (kPa)
VU	6.75	209.4	2.7	59
Duct	2.43	212.9	2.8	2.8

on the steel lids and fixed to the soil tank with bolts to prevent the displacement of the steel lids due to the expansion of the airbags. A ground surface pressure of 150 kPa was applied with the airbags, and it was gradually increased by 10 kPa every 2 minutes.

Other airbags shown in **Figure 6.3** were placed inside the pipe specimens to apply the internal pressure. For ground surface pressures of 0, 50, 100, and 150 kPa, an internal pressure of 100 kPa was applied to the pipe. The experiment procedure was as follows.

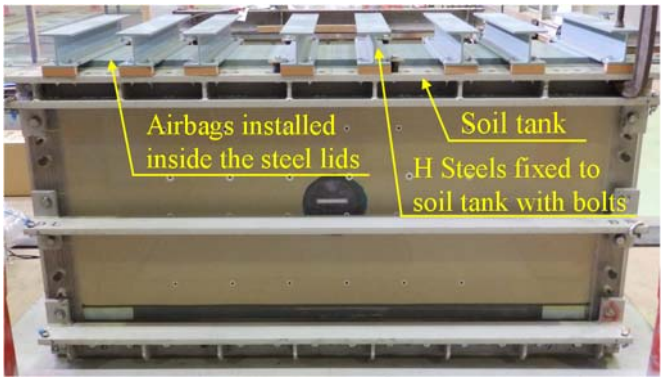

Figure 6.2 Experiment overview.

Figure 6.3 One of the airbag used for tests.

1) An internal pressure of 100 kPa was applied for 2 minutes at ground surface pressure of 0 kPa.

2) The internal pressure was unloaded.

3) The ground surface load was gradually increased to 50 kPa.

4) An internal pressure of 100 kPa was applied for 2 minutes at ground surface pressure of 50kPa.

5) The internal pressure was unloaded.

6) The ground surface load was gradually increased to 100 kPa.

In the same procedure, the ground surface load was increased to 150 kPa and an internal pressure of 100 kPa was applied when the ground surface loads were 100 and 150 kPa.

6.2.2 Pipe Specimens

VU and duct pipes were used for the tests to examine the behavior of low

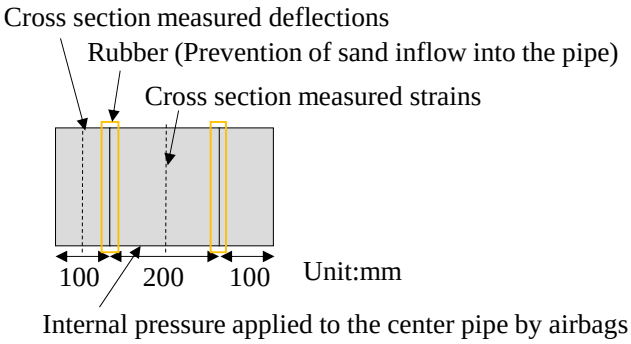

Figure 6.4 Longitudinal section of a pipe specimen.

Figure 6.5 Airbags applying internal pressure.

stiffness pipes. Generally, duct pipes are not used as buried pipes because their ring stiffness is too low. The displacement transducers could not be placed into pipe specimens having the airbags occupying their entire length in the longitudinal direction; thus, the pipe specimens were cut into three pieces and the airbags were placed only in the middle one, while the displacement transducers were placed in the end piece to measure the vertical and horizontal deflections as shown in **Figure 6.4**.

6.2.3 Airbags

AirCarrys manufactured by Hypertech Japan Co., Ltd. were used as airbags to apply internal pressure. A high stiffness PVC (VP) pipe was placed inside the pipe specimen and the airbags were installed between them as shown in **Figure 6.5**. The internal pressure was applied to the pipe specimen by inflating the airbags.

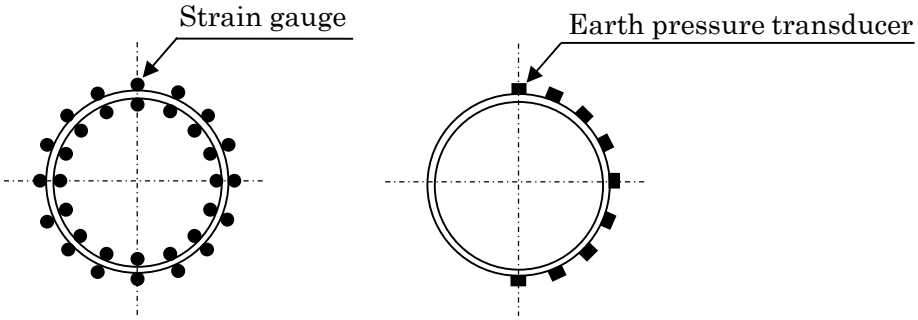

Figure 6.6 Strain gauges and earth pressure transducers attached to a pipe specimen.

6.2.4 Measurements

In the middle pipes, the circumferential strains were measured with strain gauges attached to the inner and outer surfaces of the pipe specimen at every 22.5° as shown in **Figure 6.6**. The radial strains were calculated to average the circumferential strains of the inner and outer surfaces. The bending strains of the inner surface are calculated to subtract the radial strains from circumferential strain of the inner surface. Normal earth pressures acting on the pipes were also measured with earth pressure transducers attached on the outer surface of the pipes at every 22.5° as shown in **Figure 6.6**. In the end pipes, the vertical and horizontal deflections were measured with the displacement transducers.

6.3 Results and Discussion

6.3.1 Deflection and Earth Pressure due to External Pressure

The deflections of the pipes in dense sand were smaller than those in loose sand because the higher stiffness of the soil could decrease the deformation of the pipes. **Figure 6.7** shows that the vertical deflection of the VU pipe in dense sand was 60% (= 1.6 mm/2.6 mm) of that in loose sand at a ground surface pressure of 150 kPa. The vertical deflection of the duct pipe in dense sand was 70% (= 3.1 mm/4.2 mm) of that in loose sand. The ring stiffness of the VU pipe was 21 times larger than that of the duct pipe, which means that the deflection of the duct pipe was 21 times larger than that of the VU pipe for the same load in the parallel plate test. However, in dense sand, the deflection of the duct pipe was 1.9 times (= 3.1 mm/1.6 mm) larger than that of the VU pipe. In loose

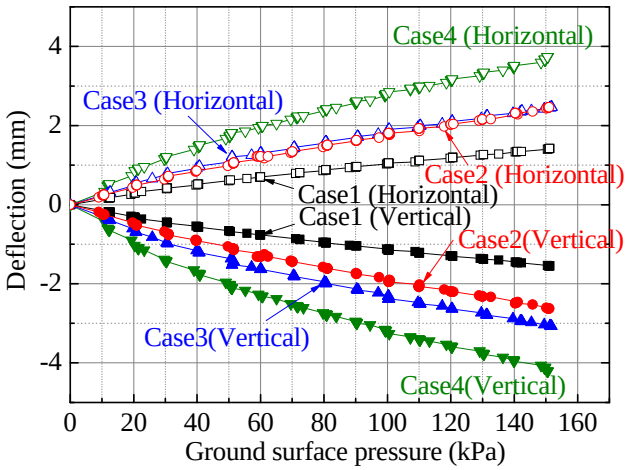

Figure 6.7 Relationship between ground surface pressures and deflections.

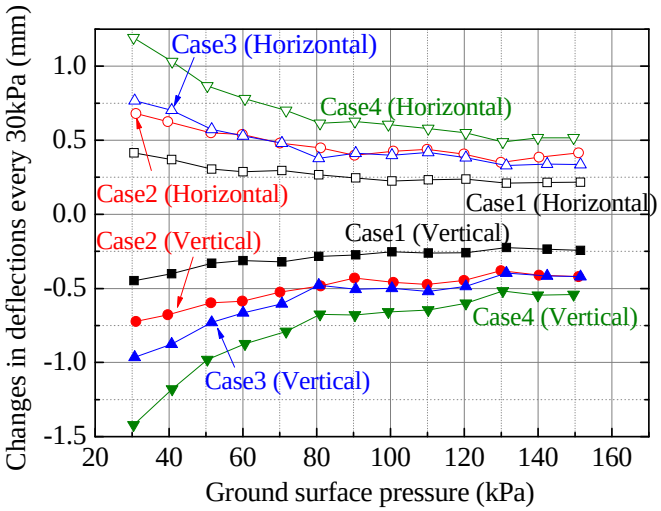

Figure 6.8 Relationship between ground surface pressures and changes in deflections every 30 kPa.

sand, the deflection of the duct pipe was just 1.6 times (= 4.2 mm/2.6 mm) larger than that of the VU pipe. This implies that the deflections of low stiffness pipes are greatly affected by the soil around the pipe rather than ring stiffness.

Figure 6.8 shows the change in the deflections for the 30 kPa increment of ground surface pressure. The horizontal axis shows the maximum value of the ground surface pressure; For example, 30 kPa means the ground surface pressure changed from 0 to 30 kPa, and 40 kPa means from 10 to 40 kPa. The vertical axis reports the change in

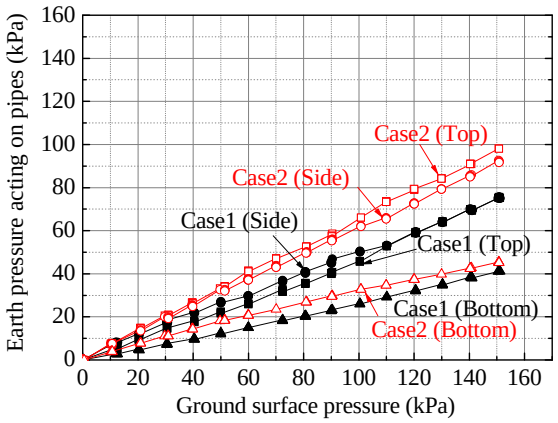

Figure 6.9 Relationship between ground surface pressures and earth pressures acting on the pipes (VU pipe).

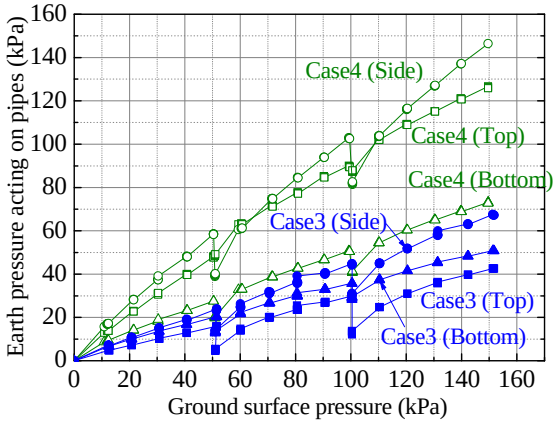

Figure 6.10 Relationship between ground surface pressures and earth pressures acting on the pipes (duct pipe).

the deflection for every 30 kPa increment.

Figure 6.8 shows that the increment of the deflections decreased as the ground surface pressures increased in all cases, although the normal earth pressures acting on the pipe increased linearly as the ground surface pressures increased as shown in **Figures 6.9** and **6.10**. This is because the increment of the ground surface pressure increased the soil stiffness, and thus, reduced the deformation of the pipe. The normal earth pressure generated by internal pressure was removed in **Figures 6.9–6.15** to examine the influence of the ground surface pressure.

Figure 6.10 shows that the normal earth pressure decreased at ground surface

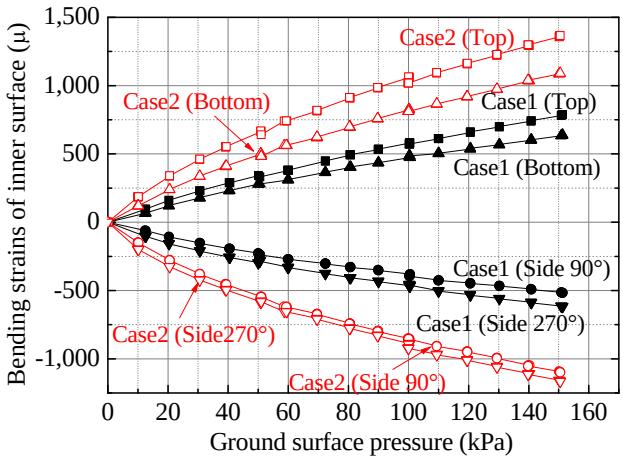

Figure 6.11 Relationship between ground surface pressures and bending strains (VU pipe).

pressures of 50 and 100 kPa due to internal pressures. Right after unloading the internal pressure, the soil density around the pipe partially decreased because the soil may have not returned completely to the position where it was before the pipe inflated due to internal pressure.

The modulus of passive resistance of soil calculated from the deflections based on the design standard for irrigation pipelines was 5100 kPa for ground surface pressures of 0–30 kPa and 9000 kPa for those of 120–150 kPa. The earth pressures measured at the pipe top was used for the vertical earth pressure and that at 180° for the bedding angle in the calculations.

6.3.2 Bending Strains due to External Pressure

The relationship between ground surface pressures and bending strains of the inner surfaces of VU and duct pipes are shown in **Figures 6.11** and **6.12**, respectively. The value 90° and 270° in the figures indicates the angles from the pipe top. The radial strains were calculate to average the circumferential strains of the inner and outer surfaces. The bending strains of the inner surface were calculate to subtract the radial strains from the circumferential strains of the inner surface.

Both in VU and duct pipes, the bending strains in loose sand were larger than

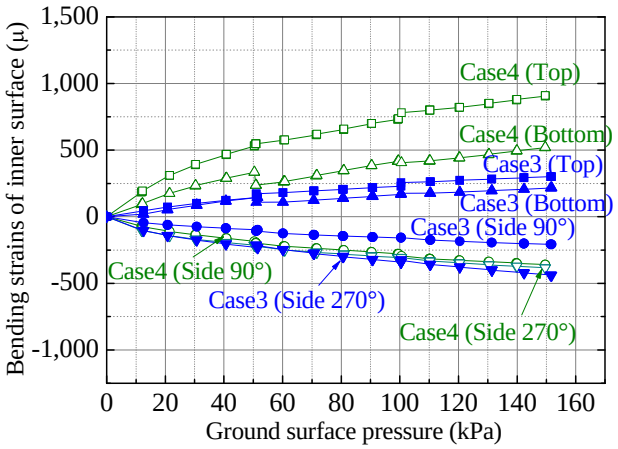

Figure 6.12 Relationship between ground surface pressures and bending strains (duct pipe).

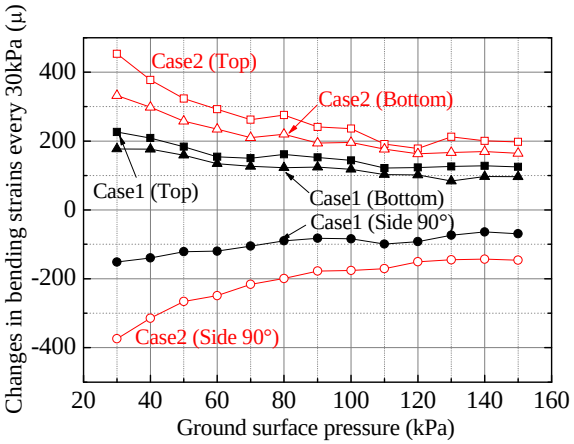

Figure 6.13 Relationship between ground surface pressures and changes in the bending strains every 30 kPa (VU pipe).

those in dense sand, and the maximum bending strains occurred at the pipe top. The maximum bending strain of the VU pipe in loose sand was 1.7 times (= 1366 μ/787 μ) that in dense sand and three times (= 909 μ/301 μ) for the duct pipes. Similar to the deflection, **Figure 6.13** shows that the increment of the bending strains decreased as the ground surface pressure increased.

6.3.3 Radial Strains Due to External Pressure

The relationship between ground surface pressures and radial strains at the pipe bottom and sides of the VU and duct pipes are shown in **Figures 6.14** and **6.15**,

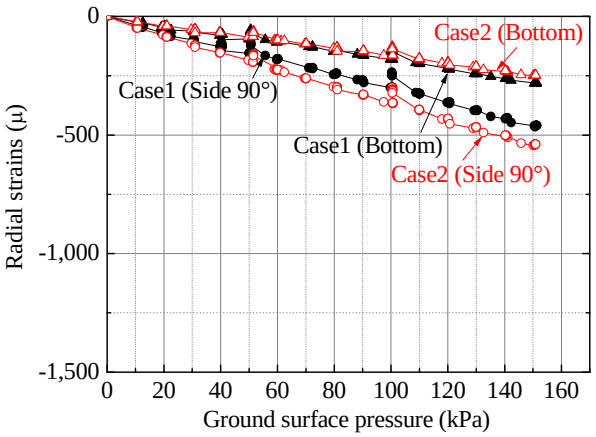

Figure 6.14 Relationship between ground surface pressures and radial strains (VU pipe).

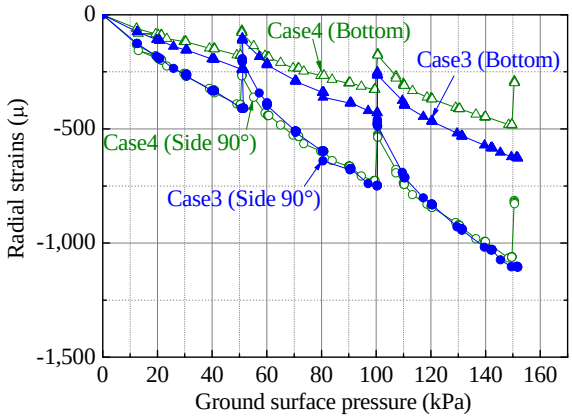

Figure 6.15 Relationship between ground surface pressures and radial strains (duct pipe).

respectively. The strains at the pipe top were omitted because they were almost the same as those at the pipe bottom in all cases. The incremented radial strains at the ground surface pressures of 50, 100, and 150 kPa were circumferential strains generated by internal pressure.

Unlike the bending strains, the radial strains were not affected by the soil density, as the radial strains of Case1 and Case3 were almost the same as those of Case2 and Case4, respectively. The radial strains increased linearly as the ground surface pressures increased. The maximum radial strains, which occurred at the pipe sides, were calculated

Table 6.3 Average vertical earth pressures.

Unit: kPa

Case1	Case2	Case3	Case4
68	69	43	75

from the equilibrium of forces acting on the thin wall circles.

$$\varepsilon_a = \frac{WD}{2tE_p} \tag{6.1}$$

where

ε_a radial strains at the pipe sides

W vertical earth pressure acting on the pipe

D pipe diameter

t wall thickness

E_p Young's modulus of the pipe

We assumed a uniformly distribution for the vertical earth pressures.

In dense sand, the radial strains at the sides of the duct pipes were 2.4 times (=1106 μ/460 μ) larger than those of the VU pipes, and the ratio was about the same as that of the wall thicknesses of VU and duct pipes (2.8 = 6.8 mm/2.4 mm). This indicates that the radial strains were inversely proportional to the wall thickness, as shown in equation (6.1).

The vertical earth pressures W can be calculated from the measured radial strains at the ground surface pressure of 150 kPa using equation 6.1. The vertical earth pressures were 79 kPa for Case1, 92 kPa for Case2, 70 kPa for Case3, and 67 kPa for Case4. The average vertical earth pressures measured using the four earth pressure transducers installed on the upper part of the pipes are shown in **Table 6.3**. The calculated vertical earth pressures tended to be larger than those shown in **Table 6.3** because we measured the earth pressures in the normal direction of the pipe but not those in the tangential direction. The radial strains at the pipe sides may be calculated from the vertical earth pressure using equation (6.1). The measured vertical earth pressures shown in **Table 6.3** were almost the same the calculated values, except for Case3. The real vertical earth

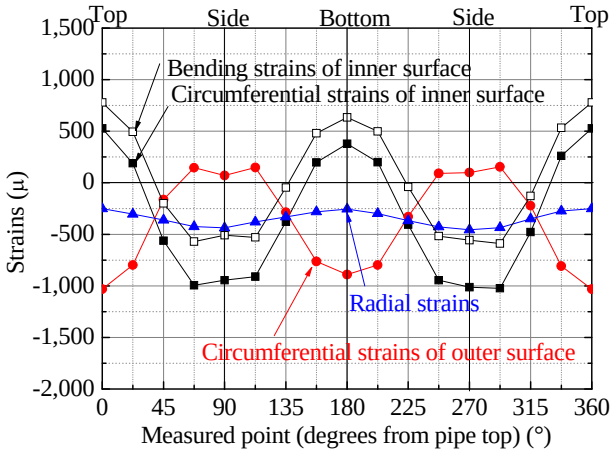

Figure 6.16 Distribution of the strains generated by 150 kPa ground surface pressure (Case1).

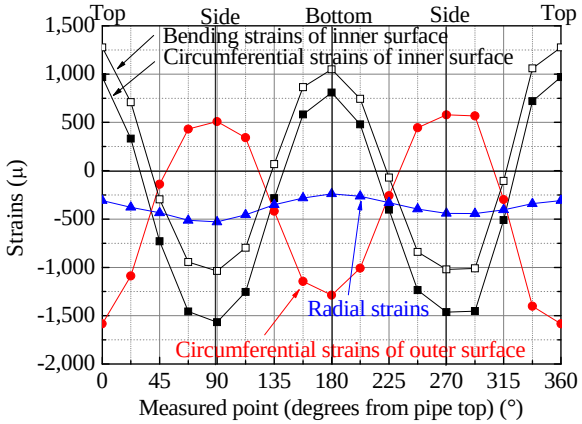

Figure 6.17 Distribution of the strains generated by 150 kPa ground surface pressure (Case2).

pressure acting on the pipe top in Case3 may have been larger than the measured value because the vertical earth pressure at the pipe top was larger than that at the bottom in the other cases.

6.3.4 Strains Distribution

The radial strains of low stiffness pipelines are not small with respect to the bending strains, although they were not considered in the design standard for irrigation pipelines as shown in **Figures 6.16** and **6.17**. At the bottom of the pipes buried in dense

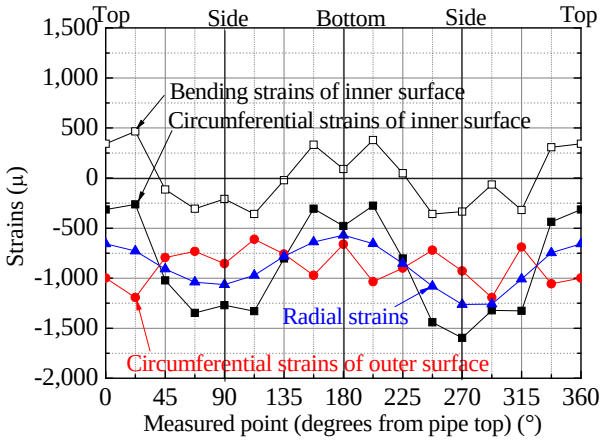

Figure 6.18 Distribution of the strains generated by 150 kPa ground surface pressure (Case3).

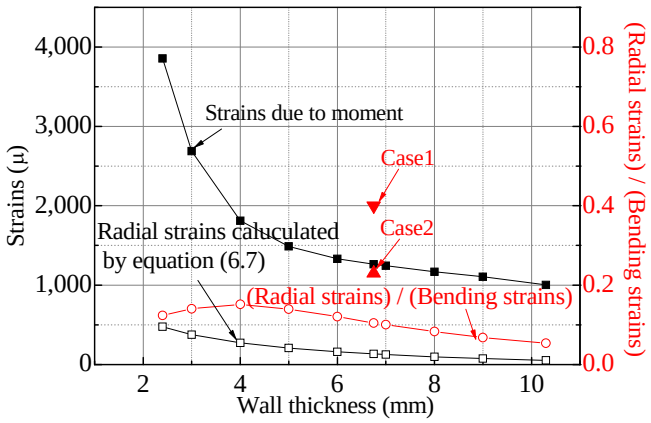

Figure 6.19 Relationship between wall thickness and strains.

sand (Case1), the absolute value of radial strain was 40% of that of the bending strain.

The radial strains of duct pipes would be large with respect to the bending strains because they are inversely proportional to the pipe thickness. Thus, the inner and outer strains of duct pipes were in compression at all positions because the radial strains were larger than the bending strains as shown in **Figure 6.18**. At the bottom of the pipes buried in dense sand (Case3), the radial strain (570 μ) was six times the bending strain (92 μ). The pipe may be broken by the buckling shown in the experiment by Ariyoshi et al. (2009). In **Figure 6.18**, Case4 was omitted because it showed the same tendency of Case3.

Figure 6.19 shows the ratio between the bending and the radial strains calculated

from the assumed earth pressure acting on the pipe in the design. The bending and the radial strains were calculated using the equations 6.2–6.6 and equation 6.7, respectively. The calculations were made under the following conditions: pipe material PVC; pipe diameter 200mm; cover depth (H_s) 2 m; modulus of passive resistance of soil (e') 4000 kPa; bedding angle (θ) 180°; soil density (γ) 18 kN/m^3; Young's modulus of the pipe (E) 3 GPa.

$$M = M_V + M_H \tag{6.2}$$

$$M_V = \beta\gamma H_s R^2 \tag{6.3}$$

$$M_H = -0.166 P_V R^2 \tag{6.4}$$

$$P_V = \frac{e'\Delta X}{2FR} \tag{6.5}$$

$$\Delta X = \frac{2FKW R^4}{EI + 0.061 e' R^3} \tag{6.6}$$

where

M moment at the pipe bottom

M_V moment generated by the vertical earth pressure

M_H moment generated by thr horizontal earth pressure

β coefficient determined by the bedding angle (0.25)

γ unit weight of soil

H_s cover depth

R mean radius of the pipe

P_V horizontal earth pressure

F deflection lag factor (1)

e' modulus of passive resistance of soil

ΔX horizontal deflection

K coefficient determined by the bedding angle (0.083)

W vertical earth pressure

I moment of inertia of pipe thickness for ring bending

The bending stress was calculated to divide the moment at the pipe bottom by the section modulus. The bending strains were calculated to divide the bending stress by the Young's

modulus in the elastic range, which was <15000 μ as obtained by the tensile yielding strength (45 MPa) and the Young's modulus (3 GPa).

The radial strains at the pipe bottom (ε_b) were calculated using the following equation (Saruwatari, 1978).

$$\varepsilon_b = \frac{2P_V R}{3tE} \tag{6.7}$$

Figure 6.19 shows that the radial strains were less than 15% of the bending strains in the calculations, regardless the wall thickness.The ratio between bending and radial strains at the 150 kPa ground surface pressure in Case1 and Case2 are also shown in **Figure 6.19**. The ratios of the experimental values were larger than those of the calculated ones. The ratios of the experimental values were 23% in dense sand (Case2) and 40% in loose sand (Case1), although those of the calculated values were 10% at the same wall thickness as in the experiments. Hence, the earth pressure distribution may be greatly different from that assumed in the design.

The lower the ring stiffness, the larger the ratio of radial and bending strains. At the pipe bottom of the duct pipe in Case3, the ratio was more than six, which largely exceeds the range shown in **Figure 6.19**.

6.3.5 The Behavior of the Pipe due to Internal Pressure

An internal pressure of 100 kPa was applied to the pipe specimens when the ground surface pressures were 0, 50, 100, and 150 kPa. For the VU pipe buried in dense sand, the radial strains (377 μ) at the ground surface pressure of 150 kPa decreased by more than 10% from those at 0 kPa (435 μ) as shown in **Figure 6.20** and **Table 6.4**. **Figure 6.21** shows that the change in the earth pressure increased with the ground surface pressure because the soil stiffness may also increase with it. Thus, the larger the ground surface pressure, the smaller the circumferential strains.

In the duct pipe buried in dense sand, the average circumferential strains (880 μ) at the ground surface pressure of 150 kPa decreased by 26% from those at 0 kPa (1185 μ) as shown in **Table 6.4** and **Figure 6.22**. Because the behavior of the pipes with smaller ring stiffness may be more susceptible to the stiffness of the ground, the decrement in the

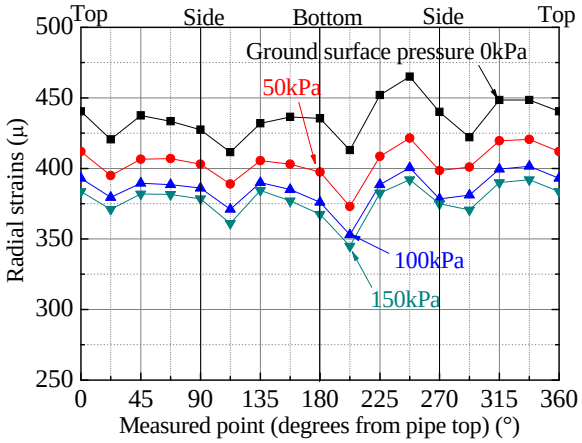

Figure 6.20 Distribution of radial strains generated by 100k Pa internal pressures (Case1).

Table 6.4 Average radial strains generated by 100 kPa internal pressure.

Unit: μ

Ground surface pressure	Case1	Case2	Case3	Case4
0kPa	435	434	1,185	1,196
50kPa	404	416	1,059	1,116
100kPa	385	415	956	1,038
150kPa	377	408	880	981

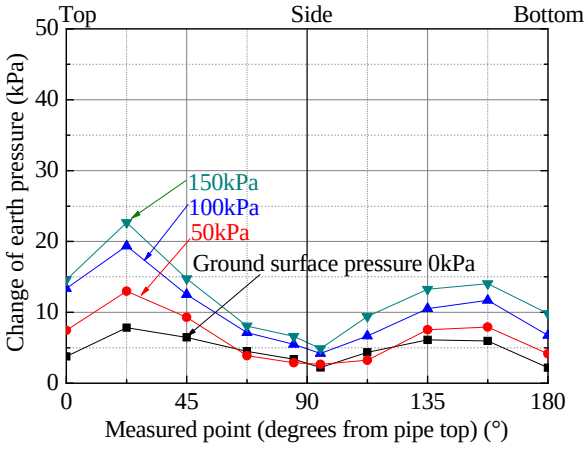

Figure 6.21 Earth pressures acting on the pipe generated by 100 kPa internal pressure (Case1).

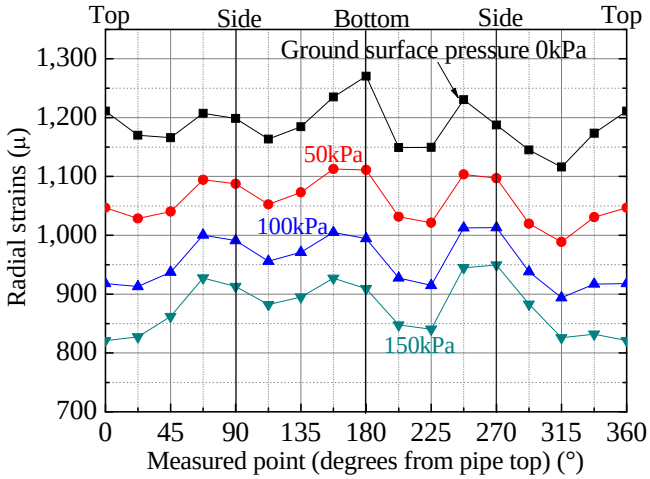

Figure 6.22 Distribution of radial strains generated by 100 kPa internal pressures (Case3).

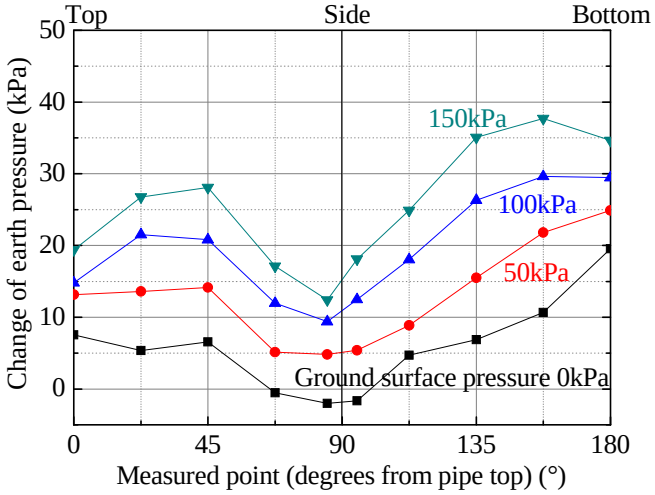

Figure 6.23 Earth pressures acting on the pipe generated by 100 kPa internal pressure (Case3).

duct pipe was larger than that in the VU pipe.

The increase of the earth pressure due to the internal pressure of the duct pipe was larger than that of the VU pipe because the duct pipe inflates more than VU pipe as shown in **Figure 6.21** and **Figure 6.23**. For both duct and VU pipes, the circumferential strains in dense sand at the ground surface pressure of 150 kPa were about 10 % smaller than those in loose sand as shown in **Table 6.4**. This also indicates that the higher the soil

stiffness, the smaller the increment of the circumferential strains due to internal pressure.

6.4 Conclusions

External and internal pressures were applied to VU and duct pipes buried in sand to examine the behavior of low ring stiffness buried pipes. The result led to the following conclusions:

1. The increments of deflections and bending strains decrease gradually as the ground surface pressures increase because the increment of the ground surface pressure increases the soil stiffness, and thus reduces the deformation of the pipe.
2. Radial strains generated by external pressure are not greatly affected by soil stiffness.
3. For the pipes having low ring stiffness, the radial strains are large with respect to the bending strains. In the VU pipe buried in dense sand at a ground surface pressure of 150 kPa, the radial strains were 40% of the bending strains. Further, in the duct pipe, the radial strains were six times the bending strains.
4. The radial strains due to internal pressure decrease as the ground surface pressure increases. In the VU pipe buried in dense sand, the radial strains at a ground surface pressure of 150 kPa decreased by more than 10% from those at 0 kPa. In a similar way, for the duct pipe, the radial strains decreased by 26%.
5. The pipes having a low ring stiffness largely inflates when internal pressure is applied. Thus, the earth pressure acting on the pipe also increases due to internal pressure.

References

Ariyoshi, M., Mohri, Y., Hori, T., Matsushima, K. and Kawabata K.: Model Test for Behavior of Buried Thin Wall Pipe, *Drainage and Rural Engineering Conference*, pp.614-615, 2009. (in Japanese)

Izumi, A., Sawada, Y., Hinobayashi, J., Mohri, Y., Ariyoshi, M. and Kawabata, T.: Characteristic Mechanical Behavior for Flexible Pipes Having Different

Thickness and Equivalent Bending Ring Stiffness, Irrigation, Drainage and Rural Engineering Jorunal, No.292, pp.231-239, 2014. (in Japanese)

Japan Institute of Agriculture and Engineering: Report of the Behavior of PVC Pipe for Sewerage Subjected to Traffic Load, 37-75. 1980. (in Japanese)

Marston, A.: The Theory of External Loads on Closed Conduits in the Light of the Latest Experiments, Bulletin 96, Iowa Engineering Experiment Station. 1930.

Ministry of Agriculture, Forestry and Fisheries; Design standard for Irrigation Pipeline. 2009. (in Japanese)

Nakajima, K. and Kawaguchi, N.: Results of Test to Ascertain Actual Properties of Pipe Made of Hard Vinyl Chloride by Laying it Underground, *Water and Land*, No.72, pp.57-70, 1988. (in Japanese)

Saruwatari, R.: Handbook of irrigation pipeline, Sankaido Publishing Co., Ltd., pp.85. 1978. (in Japanese)

Spangler, M.G.: The Structural Design of Flexible Pipe Culverts, Bulletin 153, Iowa Engineering Experiment Station, 1941.

CHAPTER 7

The contents of this chapter are based on:

Ariyoshi, M., Tanaka, Y., Izumi A. and Kawabata, T.: In Situ and Laboratory Testing of Small Diameter PVC Irrigation Pipes for Investigation of Fatigue Failure, *Transportation Infrastructure Geotechnology*, No.5, pp.59-74 (2018)

Chapter 7

In-situ and Laboratory Testing of Small Diameter PVC Irrigation Pipes for Investigation of Fatigue Failure

7.1 Introduction

Polyvinyl chloride (PVC) pipes are widely used in irrigation in Japan. PVC pipes are particularly used in small diameter and occupy approximately 30% of the irrigation pipes with a dimeter less than 300 mm.

Yamaguchi (2017) reported that in Japan, PVC pipes failed more often than other types of irrigation pipe. Tanaka (2016) conducted a field survey on the failure of PVC pipes and the causes of their failures. Two hundred and eighteen leakage accidents occurred between 2005 and 2013 in the survey area. He conducted fracture analysis and fluorescent X-ray analysis on the failed PVC pipes and revealed fatigue as the main type of failure. He pointed out that such fatigue may be attributed both to traffic load and to internal pressure caused by the water hammer phenomenon, which occured either if valves are rapidly opened and closed or from the mutual interference of pressure reducing valves.

However, it has not been clarified to what extent the traffic load or internal pressure contributed to the fatigue in the field. The purpose of this research is to investigate the principle cause of fatigue. Identifying the cause of the fatigue could make it possible to take appropriate countermeasures and lead to prevention fatigue in the future.

It could also contribute to the improvement of the Japanese design standard for irrigation pipeline (MAFF, 2009), which does not consider fatigue at all. Previous studies in Europe and North America have proposed several methods to predict fatigue failure cycles. Vinson (1981) ran tests on 6-inch PVC pipes, which were exposed to large repetitive surge pressures until fatigue failure occurred. Vinson then developed an equation to predict fatigue failure cycles as a function of peak stress. Jared et al. (2004) also ran fatigue tests on 6 inch pipes under four different pressure cycling conditions and proposed an equation that included average stress and stress amplitude. Reference on the design of fatigue in North America should be made to the Handbook of PVC Pipe Design and Construction, as published by PVC Pipe Association (2012).

In this research, strains of pipes caused by construction, traffic loads and internal pressures were measured in the field. The measurement and design values are compared to investigate the responses of buried PVC pipes to various stresses. The Japanese design standard for irrigation pipeline is based on the theories of Marston (1913) and Spangler (1941). The traffic load induced earth pressure for design of pipeline is evaluated as shown in **Figure 7.1**. Surface load on a rectangular area spreads to truncated pyramid through soil cover at an angle of 45°. The pressure on the pipe is determined to be the traffic load divided by the base area of the pyramid. Furthermore, a flattening test and a cyclic load test were conducted on an excavated pipe to examine a long term response of the PVC pipe used in the field.

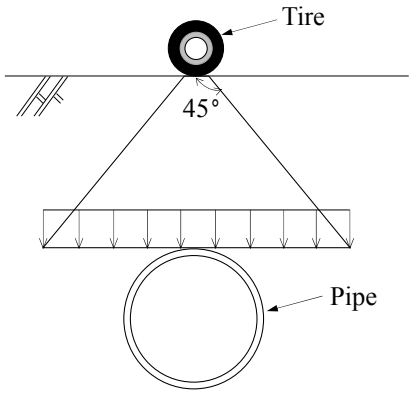

Figure 7.1 The traffic load induced earth pressure for design of the irrigation pipeline in Japan

7.2 Outline of Experiment

7.2.1 Field Measurements

The cross-sections of installed pipes used in this experiment are shown in **Figures 7.2** and **7.3**. The shallower the cover, the greater the earth pressure acting on the pipe because of traffic loads. The Japanese design standard for irrigation pipeline recommends that pipelines under agricultural roads should be at least 1m deep in order to protect the pipeline from traffic loads. The depths of cover in **Figures 7.2** and **7.3** are routinely used in practice. **Figure 7.2** and **Figure 7.3** show cross sections that evaluated the pipes exposed to construction stress and traffic load respectively.

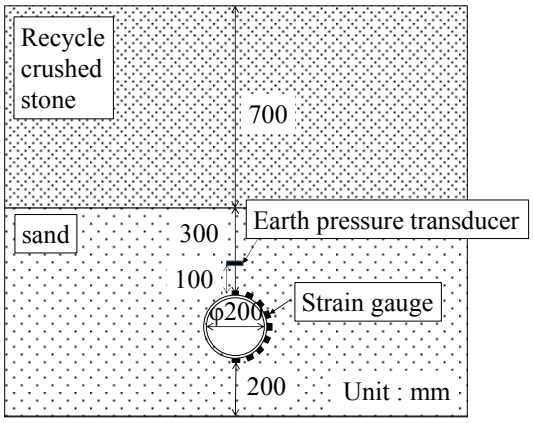

Figure 7.2 Cross section A for construction.

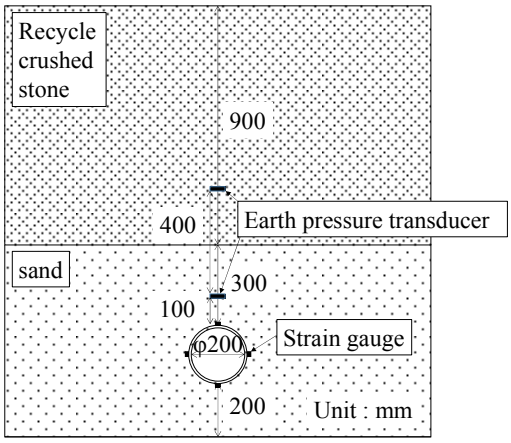

Figure 7.3 Cross section B for the traffic loading test.

The test pipes were made of PVC and had diameters of 200 mm and thickness of 10 mm. Sand was used for the embedment soil, and the particle size distribution of the soil is shown in **Figure 7.4**. Recycled crushed stone was used for the backfill material and it was placed 300 mm above the pipe top. The particle size distribution of the recycled crushed stone is shown in **Figure 7.5**. The sand and recycled crushed stone were placed in layers of approximately 300 mm thick and compacted by a plate compactor and a tamping rammer, respectively, to achieve a Proctor compaction of more than 90%, which is the value required by the Japanese design standard for irrigation pipelines. The ground surrounding the pipe trench is limestone and its uniaxial compressive strength is 20-30 MPa (Imaizumi et al., 1989).

The traffic loading test was carried out 11 months after the construction project

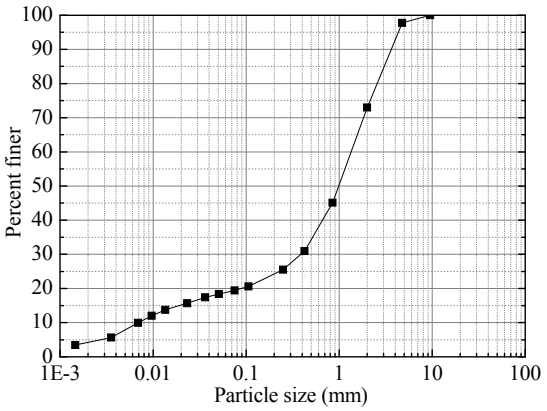

Figure 7.4 Gradation curve of the backfill sand.

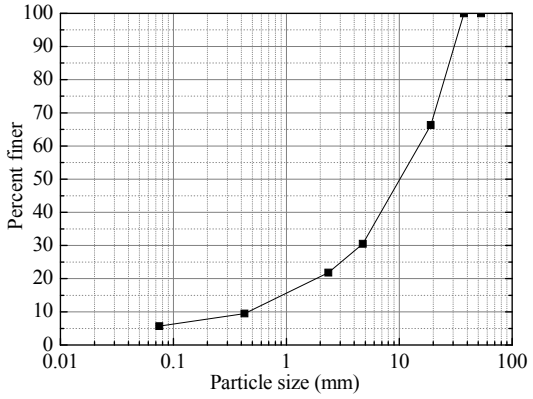

Figure 7.5 Gradation curve of the backfill sand.

was completed. The truck used in the test is shown in **Figure 7.6**. The truck weighed 203 kN, which corresponds to the maximum load expected in the field. The front wheel had a single axle and the rear wheel had two axles. The test sequence is listed below;

1. The truck passed above the pipe 5 times at a speed of 10-20 km/h (first truck loading test)
2. The first axle of the rear wheel was stopped above the pipe 5 separate times for a time period of 2 or 5 min each time. (truck stop test)
3. The truck passed above the pipe 5 times at a speed of 10-20 km/h (second truck loading test).

Strain gauges were attached to the outer surface of the pipes. In cross section A, the strains were measured every 22.5° in a half section from the pipe top to the pipe bottom. In cross section B, the strains were measured at the pipe top, the pipe bottom and the pipe sides. Earth pressure transducers were installed in the soil, as shown in **Figures 7.2** and **7.3**. The pipe water pressures at the manholes 2.5 m away from cross section A and 2 m away from cross section B were measured with water pressure gauges. The measurement sampling rate was 1 Hz at cross section A, and 100 Hz at cross section B.

Figure 7.6 Truck used in the traffic loading test.

7.2.2 Flattening Test and Cyclic Load Test for an Excavated Pipe

A flattening test and a cyclic load test were conducted on an excavated PVC pipe. The excavated pipe was used for 11 years in the field and small crack was observed. The pipe was installed in 2005 and excavated in 2016. Two pipe sections were taken from locations away from the small crack. The longitudinal length of the pipe is 50 mm for the

flattening test and 300 mm for the cyclic load test. The pipe is called a VH pipe in Japan, and the design value of the internal pressure is 1.25 MPa. The pipe's internal diameter was 143.1 mm with a thickness of 11.0 mm.

A flattening test was carried out to confirm the rigidity and cracking of the pipe. The test was conducted according to JIS (Japanese Industrial Standard) K 6742, which is corresponding to ISO 1452. The test used a two-edge bearing method, as shown in **Figure 7.7**. The loading speed was 10 mm/min. The test ended when the deflection ratio reached 50%. The vertical deflection and the load were measured.

A cyclic load test was carried out to examine the possibility of fatigue failure. The test apparatus is shown in **Figure 7.8**. The pipe was repeatedly loaded with the strain of the pipe top ranging from 1500 μ and 3800 μ, which corresponded to stress values ranging from 4.1 MPa to 10.4 MPa. Note that the elastic modulus was 2.7 GPa, which

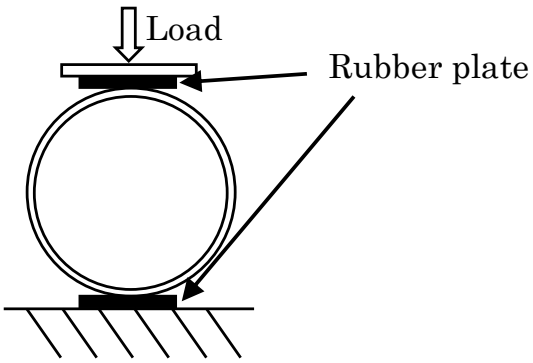

Figure 7.7 Flattening test.

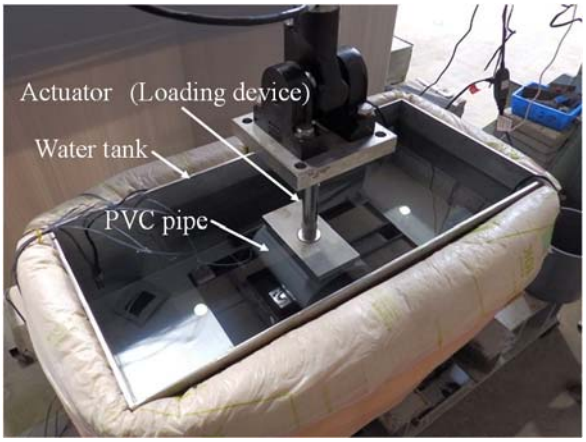

Figure 7.8 Cyclic load test.

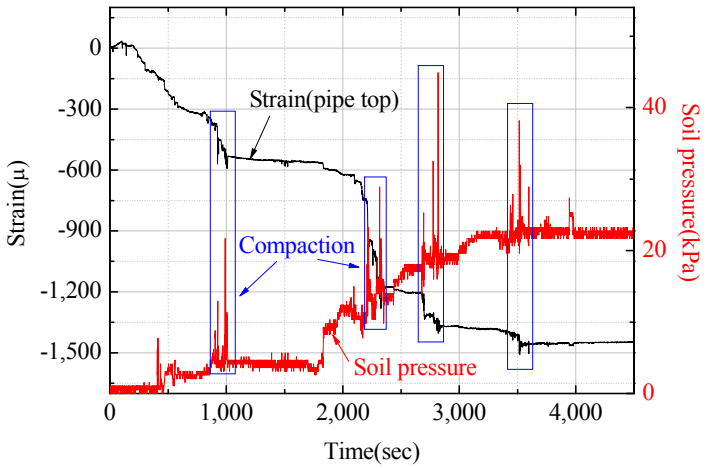

Figure 7.9 Strain on the pipe top and soil pressure as functions of time during the Backfill.

was calculated by the flattening test. The deflection ratio was measured and it ranged from 0.6% to 1.5%. The rate of cyclic load was 2 Hz. The pipe was immersed in water and the temperature was held at 22±1 °C. The vertical deflection and the load were measured.

7.3 Results and Discussion

7.3.1 Field Measurement

(a) Construction

The earth pressure and strain at the pipe top under construction are shown in **Figure 7.9**. The earth pressure increased rapidly during compactions. The strain also increased with the increase in earth pressure and the incremental strains caused by the compactions remained after that. The ground was plastically deformed by the compactions and the pipe deformed accordingly.

The strain distribution on the pipe after construction is shown in **Figure 7.10**. The pipe was deformed horizontally by earth pressure. The maximum strain occurred at the pipe top because the upper part of the pipe was more susceptible to the effects of compactions than the lower part. The strain at the pipe top was 1448 μ, which is 2.4 times

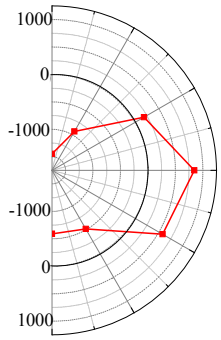

Figure 7.10 Strain distribution of the pipe after construction.

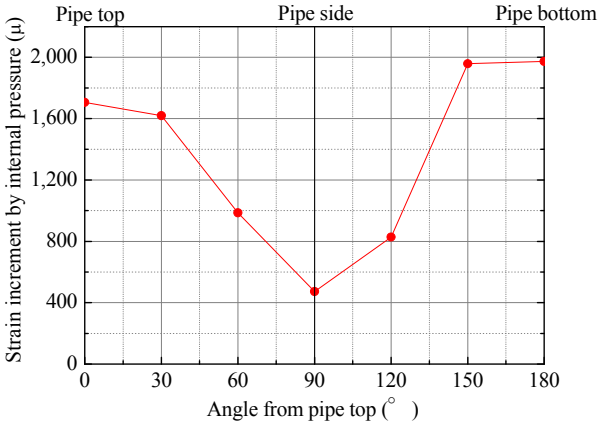

Figure 7.11 Change in strain due to internal water pressure.

that of the pipe bottom. The maximum strain estimated by the Japanese design standard for irrigation pipeline, which is based on the theories of Marston and Spangler, is 590 μ under the assumption that the modulus of passive resistance of soil e=4000 kPa and the bedding angle θ=120°. Technically, stress is used in the design, not strain. Stress and strain are determined uniquely in the elastic range, and the strain was calculated from the stress. This is much smaller than the measured maximum value obtained in this experiment.

(b) Internal Pressure

The valve on the upstream of cross section A was opened after the construction and the pipe was filled with water. The internal pressure acting on the pipe was 440 kPa. The change in strains caused by the internal pressure is shown in **Figure 7.11**. The

circumferential strain (ε_t) was estimated to be 1513 μ by the following equation, which represents the circumferential strain of a thin wall pipe by internal pressure;

$$\varepsilon_t = \frac{P_i D_m}{2tE}$$

Where:

P_i internal pressure (440 kPa)

t wall thickness (10 mm)

E elastic modulus (3 GPa)

D_m mean diameter (206 mm)

Figure 7.11 shows that the strain increment at the pipe top and bottom were larger than that of the estimated value. On the other hand, the strain increment at the pipe side was smaller than that of the estimated value. The change of circumferential strain included changes in radial strain and bending strain. These results implied that deformation of the pipe caused by internal pressure did not only inflate uniformly, but it also deformed to the shape of a true circle.

(c) Traffic Load

Internal pressure and strains of the pipe during the traffic loading test are shown in **Figures 7.11** and **7.12**. In **Figure 7.13**, the value of strain is set to be 0 three minutes before the truck passes. The water pressure fluctuated during the traffic loading test

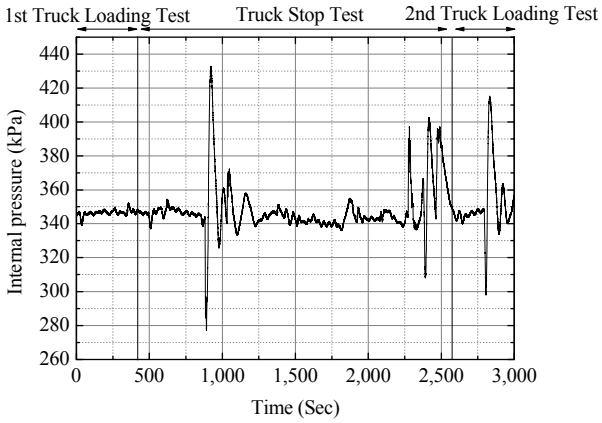

Figure 7.12 Time history of internal pressure during the traffic loading.

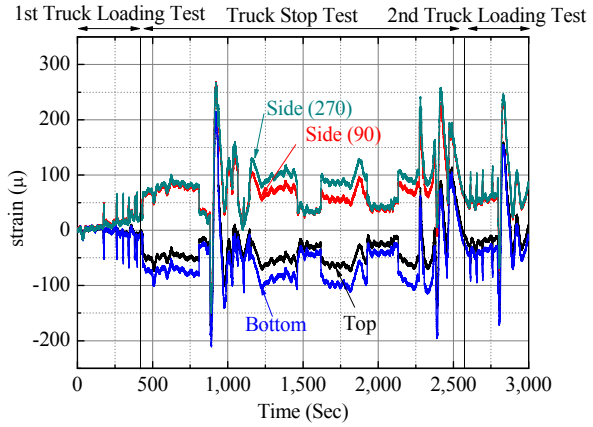

Figure 7.13 Time history of strains during the traffic loading.

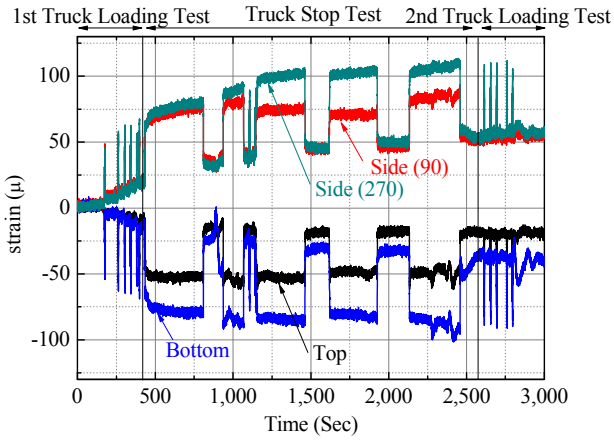

Figure 7.14 Time history of strains estimated by traffic load.

because it is in operation. The maximum internal pressure was 433 kPa, and the minimum water pressure was 277 kPa. Fluctuations in internal pressure occurred frequently in the field. The fluctuations are due to both the opening and closing of valves and the mutual interference of pressure reducing valves. Many water fluctuations have magnitudes of 10-20 m. The number of water fluctuations depends on water use, but occasionally there are more than 20 per day. **Figures 7.11** and **7.12** show that the strains were increased or decreased with the accompanied fluctuations in internal pressure.

To examine the influence of only the traffic load on the pipe, the strains that excluded the strains caused by internal pressure are shown in **Figure 7.14**. The strains caused by internal pressure, with the assumption that there was a linear relationship

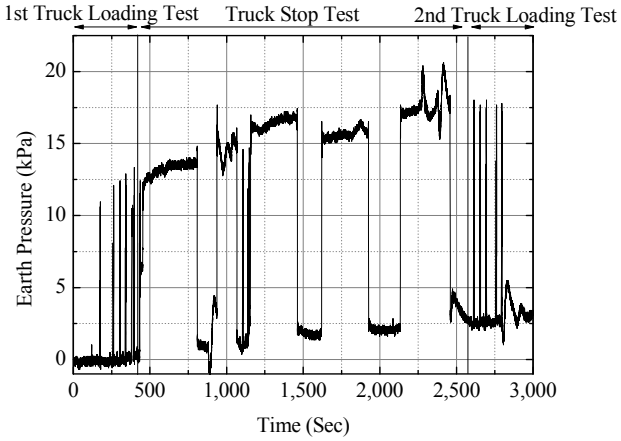

Figure 7.15 Time history of earth pressure from lower soil pressure gauges during the traffic loading test.

between internal pressure and strain, were estimated from a measured value of strains caused by an internal pressure of 345 kPa. The results were the following: pipe top was 896 μ, pipe bottom was 1049 μ and pipe sides were 904 μ and 913 μ. The earth pressure measured from the lower pressure cell is shown in **Figure 7.15**. They both increased when the truck passed or stopped above the pipe. **Figure 7.14** shows that small residual strains occurred due to traffic loads. A residual strain of approximately 50 μ occurred in the pipe sides after the traffic loading test. Although it had been 11 months since the construction project has been completed, the ground had not been subjected to loads of the same magnitude as those used in the traffic loading test. Therefore, the truck stop test deformed the ground plastically and residual strains of the pipe were induced. Additional residual strains did not occur during the second truck loading test, which implied that the ground would remain stable for the traffic load used in the first truck loading test and the truck stop test.

The strain and earth pressure measurements taken during the first pass of the second truck loading test are shown in **Figures 7.16** and **7.17**, respectively. Each strain and earth pressure value had three peaks, likely due to the front wheel having only one axle and the rear wheel having two axles, as shown in **Figure 7.6**. The ratio of the load of the front wheel to that of the rear wheel was 1:4, in accordance with the design for irrigation pipeline in Japan. However, in the measured value, the ratio of the maximum

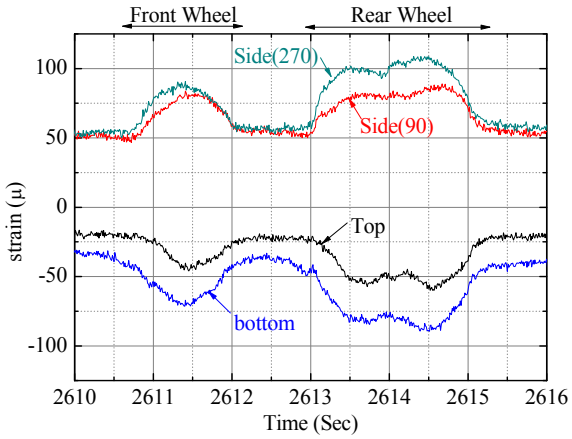

Figure 7.16 Time history of strains caused by traffic load during the first pass of the second truck loading test.

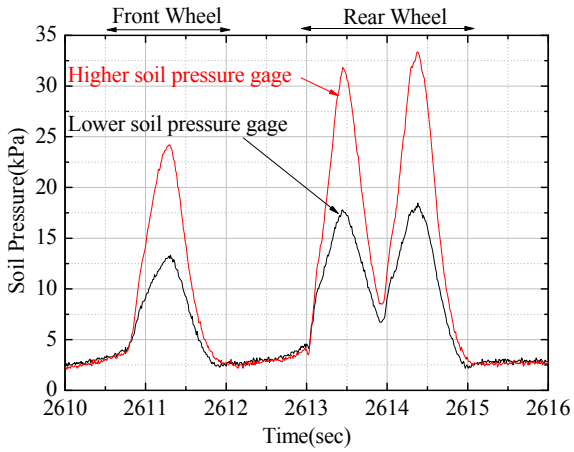

Figure 7.17 Time history of earth pressure caused by traffic load at the first pass of the second truck loading test.

earth pressures caused by the front wheel to that by the rear wheels was 1:1.4 or less as shown in **Figure 7.17**. The contact areas between the rear wheels and ground are larger than that between the front wheel and ground and pressures of the rear wheels became small because the rear wheel has two axles.

The maximum earth pressure measured at the lower position (18.4 kPa) was about 55% of that at the higher position (33.4 kPa). Because earth pressure decreased about 45% (=100-55%) through 300 mm of soil thickness, the earth pressure at the pipe top, which was 100 mm below the lower earth pressure transducers, was presumed to be

approximately 15 kPa.

Strain increments from residual strains caused by the traffic loading test were less than 70 μ, which is much smaller than the strains caused by internal pressure, as shown in **Figure 7.11**. Water fluctuations occur frequently in the field, as shown in **Figure 7.12**. The strain is estimated to change by approximately 500 to 600 μ when the water pressure changes by 200 kPa. This indicated that the fatigue that occurred in the field was mainly due to water fluctuations, rather than traffic loads.

The maximum strain caused by a T-20 truck load was estimated to be 954 μ by the design method for irrigation pipeline in Japan (under the assumption that the modulus of passive resistance of soil e=4000 kPa and the bedding angle θ=120°), which is much larger than the measured value of 70 μ. One reason for the large difference between design value and the measured value was due to the possibility that the earth pressure that actually acted on the pipe top was about half that of the design value (30 kPa).

7.3.2 Tests on Excavated Pipe

(a) Flattening Test

The load-deflection curve is given in **Figure 7.18**. Flexural rigidity (EI) was calculated to be 257.0 N·m^2 using data at a deflection ratio of 5%. This value is slightly less than 289.4 N·m^2, which is a standard value calculated using a nominal minimum thickness of 10.5 mm, an external diameter of 165 mm and an elastic modulus of 3 GPa.

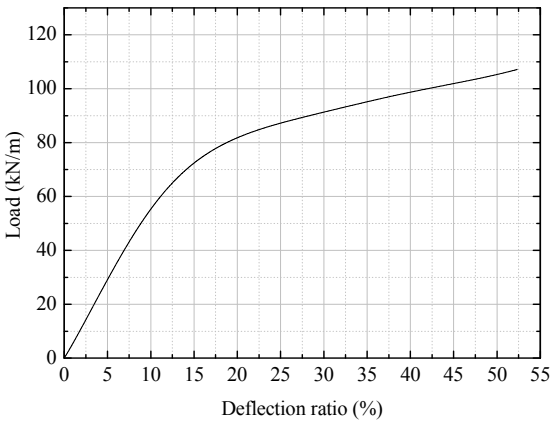

Figure 7.18 Relation between deflection ratio and load.

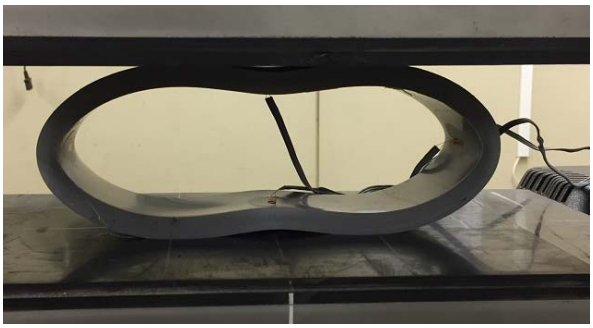

Figure 7.19 PVC pipe at the end of the flattening test.

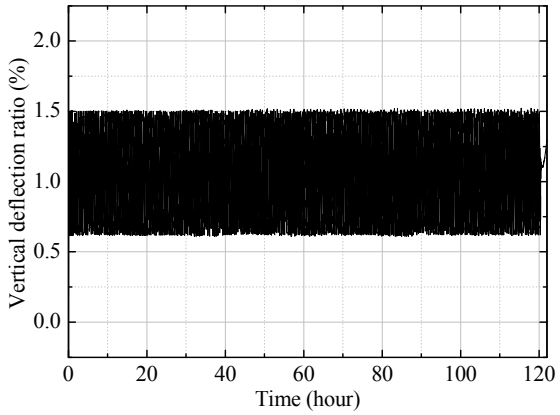

Figure 7.20 Time history of vertical deflection ratio during the cyclic load test.

The pipe did not show any cracking and breaking even when the deflection ratio reached 50% shown in **Figure 7.19**. This implied that pipe failures in the field were not caused by the exceedance of the allowable stress. The result was similar to several past researches (Alferink, 1996: Folkman, 2014), which concluded that ageing was not a significant factor influencing the performance of PVC pipe.

(b) Cyclic Load Test

The change in the vertical deflection ratio over time is shown in **Figure 7.20**. **Figure 7.20** illustrates that the pipe was accurately deflected according to the setting value until the end of the test. The test was finished after 120.4 hours. This was when the cyclic load repetition reached approximately 870,000 times. The test was demonstrated by a crack that occurred from end to end in the pipe top, as shown in **Figure 7.21**. In

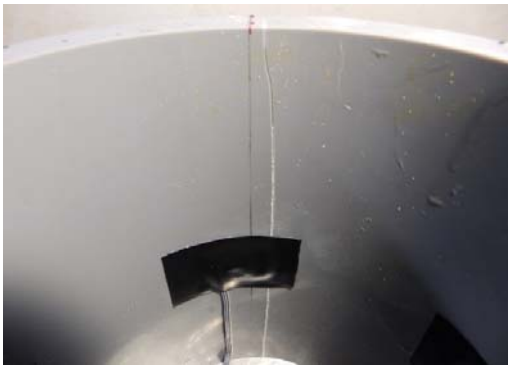

Figure 7.21 A crack in the pipe top after the cyclic load test.

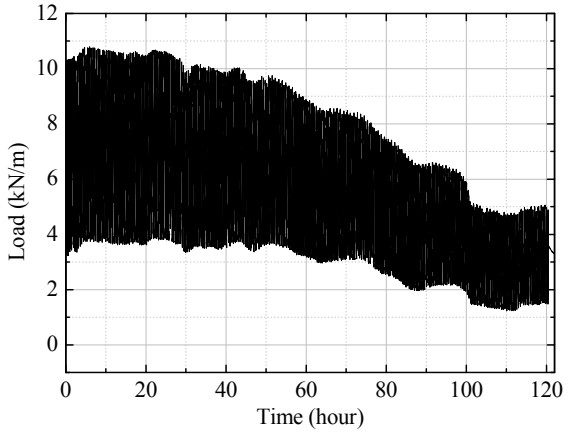

Figure 7.22 Time history of load during the cyclic.

addition, the pipe could not be loaded any further. The load was gradually reduced during the cyclic load test because the stiffness of the pipe had decreased due to the crack as shown in **Figure 7.22**.

The exact number of cycles that were required to generate a crack could not be determined. A crack was confirmed visually when the crack reached the pipe end as shown in **Figure 7.23** and the number of cycles was approximately 22,000. Cracks occurred only in the pipe top. A photograph of the crack surface is shown in **Figure 7.24**. There was a small black lump detected at the origin of fatigue.

Although a crack did not occur at the deflection ratio of 50% in the flattening test, a crack did occur at a deflection ratio of only 1.5% in the cyclic load test. The results

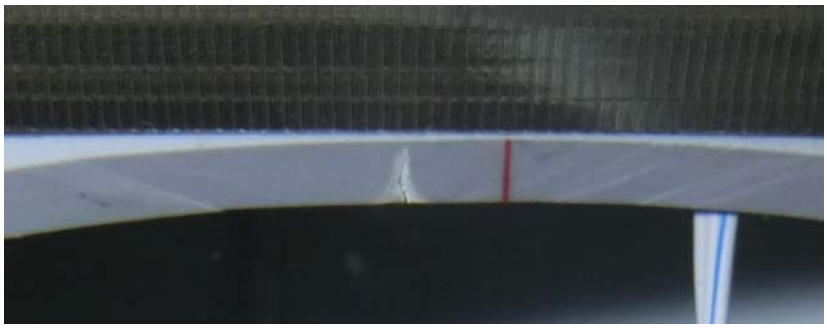

Figure 7.23 Crack on the edge during the cyclic load test.

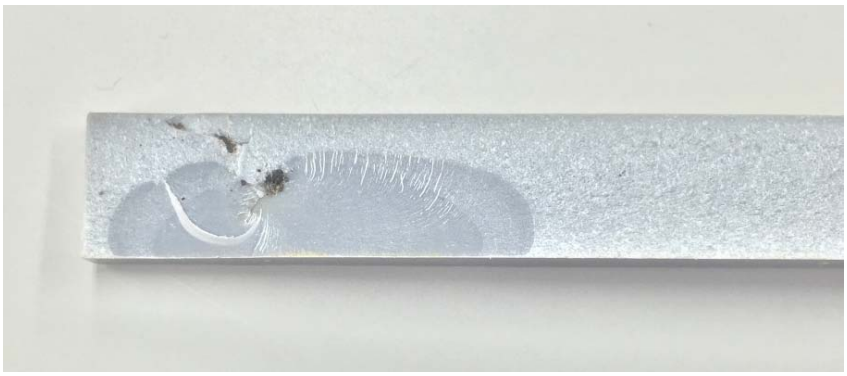

Figure 7.24 Fatigue fracture on the surface of the PVC pipe.

reinforced the idea that PVC pipes in the field failed mainly due to fatigue.

7.4 Conclusions

Field measurements in small diameter PVC pipes under construction, traffic load and internal pressure from water were carried out. A flattening test and a cyclic load test for an excavated pipe were also conducted. The results indicated the followings;

1. The strain in the pipe top increased rapidly under compaction and it remained after that. The strain in the pipe top after the construction was 1448 μ, which is about 2.4 times that of the strain calculated at the pipe bottom and 2.4 times that of the estimated value stated in the Japanese design standard for irrigation pipelines.
2. The strains in the pipe top and pipe bottom caused by internal pressure after the construction were larger than that of the pipe sides. This implied that deformation of the

pipe caused by internal pressure did not only inflate uniformly, but it also deformed to the shape of a true circle.

3. Strain increments caused by the 203 kN truck load were 70 μ or less, which was much smaller than the estimated design value.

4. The pipe strain increased or decreased with fluctuations in the internal pressure. The strain caused by internal pressure in the field was much larger than that caused by traffic load and this likely caused fatigue in the pipe.

5. The pipe showed no cracking and breaking when the deflection ratio reached 50% in the flattening test.

6. In the cyclic load test, a crack was confirmed visually when the number of cycles was approximately 22,000. The crack did occur at a deflection ratio of only 1.5% in the cyclic load test although a crack did not occur at a deflection ratio of 50% in the flattening test. These results reinforced the idea that PVC pipes in the field failed by fatigue.

References

Alferink, F., Janson, L. E., Holloway, L.: Old PVC-U Water Pressure Pipes: Inve stigation into Design and Durability. *PVC 1996 Conference Proceedings*, 42 C382 Institute of Materials, Brighton, England, pp.87-96, 1996.

Folkman, S.: Validation of the long life of PVC pipes. *Proceedings of the 17th Plastic Pipes Conference*, Chicago, Illinois, USA, pp.1-9, 2014.

Imaizumi, M., Tomita, T., Zaha, Y.: Engineering Properties of The Ryukyu Limes tone by Schmidt-Rock-Hammer in South-East part of Miyakojima, the Ryuk yu Islands. *Journal of the Japan Society of Engineering Geology*, Vol.30, N o.1, pp.1-13, 1989 (in Japanese)

Jeffrey, J. D., Moser, A. P., Folkman, S.: New Design Guidelines for Fatigue Fai lure in PVC Pipe, *Plastics Pipes XII Conference Proceedings*, Milan, Italy, 2004.

Marston, A., Anderson, A.O.: The Theory of Loads on Pipes in Ditches and Tes ts of Cement and Clay Drain Tile and Sewer Pipe. Bulletin 31. Ames: Iow

a Engineering Experiment Station, 1913.

Ministry of Agriculture, Forestry and Fisheries of Japan: Design standards for irri gation pipeline. 2009. (in Japanese)

PVC pipe association: The Handbook of PVC Pipe Design and Construction, fift h edition, Industrial press, INC. pp.5.14-5.25, 2012.

Spangler, M. G.: The Structural design of Flexible Pipe Culverts. Bulletin 153. Ames: Iowa Engineering Experiment Station, 1941.

Tanaka, Y., Tsuda, T.: Field Study on Small Diameter PVC Pipe and Leak Detec tion Technology, 11th Pipeline Technology Conference, Berlin, Germany, 11 3-125, 2016.

Vinson, H. W.: Response of PVC pipe to large, repetitive pressure surges. Procee dings of the international conference on underground plastic pipe, ASCE, N ew York, USA, 485-494. 1981.

Yamaguchi, Y.: Example Analysis about Accident Factors and Measures of Irrigat ion Pipeline. Water, Land and Environmental Engineering, Vol.85, No.8, 767 -769, 2017. (in Japanese)

CHAPTER 8

Chapter 8

Conclusions

In this thesis, Chapters 2 and 3 introduced a novel method for evaluating the structural safety of flexible buried pipes from measurements of the bending strain. The behavior of flexible pipes when subjected to external or internal pressures was discussed in Chapters 4–7. The following summarizes the conclusions that follow from these tests.

In the tests discussed in Chapter 2, the bending strain estimation method, which calculates bending strains from changes of the curvature radius, was verified its applicability for steel pipes. The larger the bending strains, the better the accuracy of their values estimated with the proposed method. Appropriate base lengths for each diameter are also proposed.

During the tests discussed in Chapter 3, the applicability of the proposed method to FRPM pipes was examined. The bending strains of FRPM pipes can be estimated accurately even if the nominal values of wall thickness and curvature radius are used in

the calculations. Base length in terms of the diameter of the FRPM pipe was proposed on the basis of calculations on how errors in the measurement length affect the accuracy of the method.

Chapter 4 discussed the behavior of the flexible pipe used as a CIPP liner when subjected to internal pressure. This investigation involved tests with ϕ1,000 pipe specimens. After the liner contacts the sound existing pipe, the circumferential strain caused by internal pressure increases only a little. Filling the annular gap between the sound existing pipe and liner greatly reduces the circumferential strains at straight portion and longitudinal strains at bend in the liner.

Chapter 5 discussed the behavior of CIPP liners under external pressure, as studied in scale-model tests with ϕ300 pipe specimens. The liner only deforms when the existing pipe is divided. The behavior of the liners inserted into divided RC pipe is close to that of flexible pipe. The strains of the liner are vertically symmetrical despite the loading conditions. This indicates that the vertical earth pressure acting on the liner may be vertically symmetrical. The maximum strain and horizontal deflection are calculated from the predicted earth pressure acting on the liner to propose a new liner design considering a deteriorated existing pipe.

In Chapter 6, the behavior of flexible pipe having low ring stiffness subjected to external and internal pressures was examined through tests using ϕ200 VU pipe (wall thickness of 6.8mm) and very thin pipe (wall thickness of 2.4mm). For the PVC pipes having low ring stiffness, the radial strains are large with respect to the bending strains. Unlike the bending strain, the radial strains generated by external pressure are not affected greatly by the soil stiffness. The internal pressure increase the earth pressure acting on the pipes having low ring stiffness because the pipes tend to inflate largely.

In Chapter 7, the responses of small PVC pipes to traffic loads and internal pressure were measured in the field to examine the causes of PVC pipe failure. The strain increment caused by a 203 kN truck was only 70μ, which is much smaller than the strain increment caused by water pressure fluctuations. In addition, cyclic load testing and flattening testing were conducted on a pipe excavated after 11 years of service. A crack occurred at the deflection ratio of only 1.5% during the cyclic load test, although no crack

occurred at a deflection ratio of 50% in the flattening test. These results indicate that PVC pipes used in irrigation systems likely fail because of fatigue caused by water pressure fluctuations.